

## ABSTRACT

FENG, CHENGCHENG. Qualitative and Quantitative Degradation Studies of C.I. Reactive Blue 19 in Soil: A Mass Spectrometry Approach. (Under the direction of Dr. Nelson R. Vinueza).

As one of the most dominant fibers in textiles, cotton fiber has attracted lots of attention and grown extensively throughout the world. Textile dyeing or other auxiliary processing chemicals are usually incorporated into the fibers, yarns, or fabrics to achieve a uniform depth of color and color fastness properties suitable for the end use. Reactive dyes based on azo and anthraquinone functional groups are the most commonly used textile dyes and have an excellent affinity to cotton fibers, considering their consumed tonnage and amount.

Nowadays, landfilling is the common disposal route for textile fabrics (natural or synthetic); However, landfills will generate numerous environmental contamination problems. Different types of dyes and finishes on textile fabrics can become important sources of pollution during the degradation process because these chemicals can leach into soil. Currently, the biodegradation of dyes from dyed fabrics in soil is not fully understood, and what can leach into the ground can be more toxic than the dye itself. In this research, dyed cotton fabrics with reactive dyes are chosen as the subject of this experimental approach to understand their potential harm to the environment and determine the possible degradation products in soil.

The changes of the chemical structures of reactive dyes on the cotton fabrics under a composting process, following the ASTM D 5988-18, and their leach to soil were monitored using liquid chromatography, high-resolution mass spectrometry, and tandem mass spectrometry.

Modifications were made to the original QuEChERS (Quick, Easy, Cheap, Effective, Rugged, and Safe) extraction method to extract Reactive Blue 19 from blank soils. These include the selectivities of extraction solvents, QuEChERS contents (salts), and agitation modes. Then a simulated composting process on cotton fabrics dyed with Reactive Blue 19 was performed for 90

days. The soil samples were then analyzed using the combination of the modified QuEChERS method and tandem mass spectrometry. The degradation product of Reactive Blue 19 was extracted by the QuEChERS method and identified to be Acid Blue 25, based on QTOF mass spectrometry and tandem mass spectrometry. After detecting and elucidating the degradation product, a quantitative method aiming to measure the concentration of Reactive Blue 19 degradation product in soil. The developed quantitative method for the degradation product from soil showed excellent linearity ( $R^2 > 0.9990$ ), good accuracy (mean % error less than 12%), good precision (mean % CV less than 9%), good sensitivity (the LLOQ of this quantification method was  $1.2949 \pm 0.4770 \mu\text{g/mL}$  and LOD was  $0.3884 \pm 0.1431 \mu\text{g/mL}$ ), and good recovery rate.

© Copyright 2021 by Chengcheng Feng

All Rights Reserved

Qualitative and Quantitative Degradation Studies of C.I. Reactive Blue 19 in Soil: A Mass Spectrometry Approach

by  
Chengcheng Feng

A dissertation submitted to the Graduate Faculty of  
North Carolina State University  
in partial fulfillment of the  
requirements for the degree of  
Doctor of Philosophy

Fiber and Polymer Science

Raleigh, North Carolina  
2021

APPROVED BY:

---

Nelson R. Vinueza  
Committee Chair

---

Melissa Pasquinelli

---

Ericka Ford

---

Stephen Michielsen

## **DEDICATION**

This dissertation is dedicated to my dear families and myself.

## **BIOGRAPHY**

Chengcheng Feng was born in Jingzhou, Hubei Province, China. She was admitted to Donghua University in Shanghai, one of the best-known universities in China. She earned her bachelor's degree in Textile Engineering from Donghua University in 2015. Then she continued to pursue the Master of Science Degree in Textile Engineering under the direction of Dr. Stephen Michielsen at NC State University. In fall 2017, she started the Ph.D. Program in Fiber and Polymer Science under the direction of Dr. Nelson Vinueza at NC State University.

## ACKNOWLEDGMENTS

I express my sincere gratitude to my advisor, Dr. Nelson R. Vinueza, for his visionary guidance, insightful advice, and genuine support in my Ph.D. program, without which this work would not have been accomplished to its least content. I also want to express my thanks to Dr. Stephen Michielsen and my committee members, Dr. Melissa Pasquinelli and Dr. Ericka Ford.

I would also like to thank Vinueza Labs group members, Dr. Xinyi Sui, Julio Teran, Dr. Yufei Chen, Dr. Nadia Sultana, Dr. Emily Lichtenberger, all of whom have always been so supportive, helpful, and collaborative to the research work described here. In addition, I appreciate the kindness, care, and helpful experience offered by WCOT staff Traci Figura, Judy Elson, and Joyce Cole. Finally, I would like to thank my parents for their consistent support on my studies at NC State and all those lovely close friends I have made here in Raleigh. Thanks for all their generous supports whenever and wherever I needed it.

## TABLE OF CONTENTS

LIST OF TABLES .....	ix
LIST OF FIGURES .....	x
<b>CHAPTER 1. Research Objectives</b> .....	<b>1</b>
1.1. Modifications of QuEChERS Extraction Method and its Applications to the Extraction of Reactive Dyes from Blank Soil.....	3
1.2. Detection and Elucidation of Reactive Blue 19 Degradation Products from Soil .....	3
1.3. Quantitative Analysis of Reactive Blue 19 Degradation Products from Soil .....	3
<b>CHAPTER 2. Introduction to Mass Spectrometry</b> .....	<b>5</b>
2.1. Brief History of Mass Spectrometry (MS).....	5
2.2. Components of Mass Spectrometry (MS).....	6
2.3. High-Performance Liquid Chromatography (HPLC) .....	7
2.3.1. Diode-Array Detection (DAD) .....	9
2.4. Ionization Methods .....	10
2.4.1. Electrospray Ionization (ESI) .....	11
2.4.1.1. Charge Residue Model (CRM) .....	14
2.4.1.2. Ion evaporation model (IEM) .....	15
2.5. Mass Analyzers .....	15
2.5.1. Main Terminologies.....	15
2.5.1.1. Mass Measurement Accuracy (MMA) .....	15
2.5.1.2. Mass Resolution.....	16
2.5.1.3. Resolving Power .....	17
2.5.2. Time-of-Flight (TOF) Mass Analyzer .....	18
2.5.3. Quadrupole Mass analyzer.....	22
2.5.4. Tandem Mass Spectrometry (MS/MS) by Triple Quadrupole Mass Spectrometers ..	25
2.5.4.1. Collision-Induced Dissociation (CID) .....	26
2.5.5. Ion Trap Mass Analyzer.....	28
<b>CHAPTER 3. Cotton Fibers and Dyes</b> .....	<b>31</b>
3.1. Textile Fibers .....	31
3.1.1. Cotton Fibers.....	32
3.2. Basis of Colorants, Dyes, and Pigments .....	33
3.2.1. Planck’s Relationship.....	35
3.2.2. Beer–Lambert Law .....	35

3.3. Azo and Carbonyl Dyes .....	37
3.3.1. Azo Dyes.....	37
3.3.2. Carbonyl Dyes .....	38
3.4. Reactive Dyes .....	38
3.4.1. Characteristic Structural Features of Reactive Dyes .....	40
3.4.1.1. Chromophoric Groups/ Chromogen (D).....	42
3.4.1.2. Reactive Groups (Re).....	43
3.5. Dye-Fiber Chemical Reactions .....	45
3.5.1. Ionization of Cellulose Fibers .....	47
3.5.2. Nucleophilic Substitution Reaction Between a Reactive Dye and a Fiber .....	47
3.5.3. Nucleophilic Addition by Conjugate Addition .....	49
3.5.4. Hydrolysis of Reactive Dyes .....	51
3.5.4.1. Hydrolysis of RB19 .....	54
3.6. Acid Dyes.....	55
<b>CHAPTER 4. Soil and QuEChERS Method.....</b>	<b>59</b>
4.1. Main Compositions of Soil .....	59
4.2. Textile Wastes to Landfills .....	60
4.3. Separation Practicalities .....	62
4.3.1. Liquid-Liquid Extraction (LLE) .....	62
4.3.2. Solid Phase Extraction (SPE).....	64
4.4. Quick, Easy, Cheap, Effective, Rugged, and Safe (QuEChERS) Method .....	66
<b>CHAPTER 5. Modifications of QuEChERS Extraction Method and its Application to the Extraction of Reactive Dyes from Blank Soil.....</b>	<b>68</b>
5.1. Introduction.....	68
5.2. Materials .....	69
5.2.1. Solvents.....	69
5.2.2. Chemicals and Dyes.....	70
5.2.3. Other Supplies.....	71
5.2.4. Blank Compost Soil for Analysis .....	71
5.3. Experimental and Instrumentation .....	71
5.3.1. Sample Preparation .....	71
5.3.2. Modifications to Original QuEChERS Extraction Method .....	72
5.3.2.1. Modifications to Extraction Solvents.....	73

5.3.2.2. Modifications to QuEChERS Contents .....	74
5.3.2.3. Modifications to Agitation Modes .....	75
5.3.3. The Final Decision of Modified QuEChERS Method and Its Application to the Extraction of RB19 from Blank Soils .....	76
5.3.4. Instrumentation .....	77
5.3.4.1. Q-TOF MS .....	77
5.3.4.2. Linear Ion Trap MS (LTQ) .....	78
5.4. Results and Discussion .....	79
5.4.1. Detection of Standard Dye RB19 Solutions .....	79
5.4.2. Detection of Reactive Dyes Extracted from Blank Soils .....	81
5.4.3. Validation of Quantification Method .....	84
5.5. Summary .....	86
<b>CHAPTER 6. Detection and Structural Elucidation of C.I. Reactive Blue 19</b>	
<b>Degradation Products from soil .....</b>	<b>88</b>
6.1. Introduction .....	88
6.2. Materials .....	89
6.2.1. Solvents and Chemicals .....	89
6.2.2. Dyes .....	89
6.2.3. Other Supplies .....	90
6.2.4. RB19 Dyed Cotton Fabrics .....	90
6.3. Experimental .....	91
6.3.1. Simulated Compost Degradation and Sample Preparation .....	91
6.3.2. QuEChERS Extraction of RB19 Degradation Products from Soil Samples After Simulated Compost Soil Degradation .....	92
6.3.3. Detection and Structural Elucidation of RB19 Degradation Products from Degraded Soil using LC-MS .....	93
6.3.3.1. Detection of RB19 Degradation Products from Soil (Linear Ion Trap MS) .....	93
6.3.3.2. Structural Elucidation of RB19 Degradation Products from Soil (Q-TOF MS) ..	94
6.4. Results and Discussion .....	95
6.4.1. Detection of RB19 Degradation Products from Degraded Soil .....	95
6.4.2. Structural Elucidation of RB19 Degradation Products from Degraded Soil .....	97
6.5. Summary .....	101
<b>CHAPTER 7. Quantification of C.I. Reactive Blue 19 Degradation Products from Soil ..</b>	<b>102</b>
7.1. Introduction .....	102

7.2. Materials .....	103
7.2.1. Solvents and Chemicals .....	103
7.2.2. Dyes .....	103
7.2.3. Other Supplies.....	104
7.3. Experimental .....	104
7.3.1. Sample Preparation of Stock Solution for Standard AB25 Dye Solutions.....	104
7.3.2. Extraction of Standard AB25 from Blank Soil Using Modified QuEChERS Extraction Method and Establishment of Calibration Curve .....	104
7.3.3. Method Validation for the Quantification System.....	105
7.3.4. Instrumentation – Linear Ion Trap MS (LTQ).....	106
7.4. Results and Discussion .....	107
7.4.1. Detection of Standard AB25 Dye Solutions using LC-DAD-MS .....	107
7.4.2. Extraction of AB25 from Blank Soil and Establishment of Calibration System.....	108
7.4.3. Validation of Calibration Curve.....	109
7.5. Summary .....	114
<b>CHAPTER 8. Conclusion and Future Aspects.....</b>	<b>115</b>
8.1. Conclusions.....	115
8.2. Recommendations for Future Works .....	116

## LIST OF TABLES

<b>Table 1.</b> Ionization Methods, Timeline, and Ionizing Agents.....	11
<b>Table 2.</b> Resolving Powers of Different Mass Spectrometers .....	18
<b>Table 3.</b> Three Types of Vacuums Regimes used in TOF-MS .....	19
<b>Table 4.</b> Merits of Mass Analyzers .....	30
<b>Table 5.</b> Classifications of Textiles Fibers .....	32
<b>Table 6.</b> Approximate Relative Strengths of Bonding Between Dye and Fiber .....	46
<b>Table 7.</b> Some H-bond Donors and Acceptors.....	46
<b>Table 8.</b> Different Sample Extraction Procedures Commonly Used .....	62
<b>Table 9.</b> The Properties of Common Solvents used in Extractions.....	63
<b>Table 10.</b> Molecular Weight, Topological Polar Surface Area and XlogP for Typical Samples (Pesticides, Ibuprofen and Dyes) used in QuEChERS Extraction Method ...	73
<b>Table 11.</b> Solvents Used in Modified QuEChERS Extraction Method .....	74
<b>Table 12.</b> Modifications to QuEChERS Extraction Method.....	82
<b>Table 13.</b> Experimental Parameters for Standard Dye RB19 Solutions and RB19 Extracted from Blank Soil (ions generated, mass-to-charge ratios of theoretical and experimental, ppm error).....	83
<b>Table 14.</b> Overall Validation Parameters .....	85
<b>Table 15.</b> The Results of Inter-day Precision and Accuracy of Each Concentration Points of RB19 Extracted from Blank Soils.....	86
<b>Table 16.</b> Linear Regression Data from MS/MS Calibration Curves for AB25 Extracted from Blank Soils.....	111
<b>Table 17.</b> Summary of Validation Parameters on AB25 QuEChERS Quantification Method..	112
<b>Table 18.</b> Results of Intra-day and Inter-day Accuracy and Precision of Each Concentration Point of Standard AB25 Dye Solutions Evaluated by the LC-DAD-MS Method.....	113

## LIST OF FIGURES

<b>Figure 1.</b> Consumptions of Cotton Fibers in Natural Fibers Market .....	1
<b>Figure 2.</b> Main Components of Mass Spectrometry .....	7
<b>Figure 3.</b> Configuration of HPLC System .....	9
<b>Figure 4.</b> Schematic of Major Processes Occurring in the Atmospheric Pressure Region of Electrospray Ionization .....	12
<b>Figure 5.</b> Main Theory of Ion Evaporation Model (CRM) and Charge Residue Model (IEM) ..	14
<b>Figure 6.</b> Illustration of Mass Resolution (a) and Resolving Power (b) .....	17
<b>Figure 7.</b> Basic Components of the Early Linear TOF Mass Spectrometer .....	20
<b>Figure 8.</b> Principle of Operation of Reflectron in TOF-MS .....	21
<b>Figure 9.</b> Scheme of an Agilent 6520 Quadrupole-Time-of-Flight Mass Spectrometer .....	22
<b>Figure 10.</b> Schematic of a Quadrupole Consisting of Four Metal Rods Parallel to Each Other..	23
<b>Figure 11.</b> Examples of how varying DC and RF voltages affect quadrupole mass analyzers ...	23
<b>Figure 12.</b> Mathieu Stability Diagrams for Different Ions.....	24
<b>Figure 13.</b> Schematic of a Triple Quadrupole (QqQ) System for MS/MS .....	26
<b>Figure 14.</b> Two Discrete Fragmentation Processes in CID.....	27
<b>Figure 15.</b> Schematic of Thermo Scientific™ LTQ XL™ Linear Ion Trap Mass Spectrometer	29
<b>Figure 16.</b> Angled Schematic of Linear Ion Trap Mass Analyzer .....	30
<b>Figure 17.</b> The Basic Structure of Cellulose .....	33
<b>Figure 18.</b> Example of an Azo Group Attached to Two Different Groups (a) and an Anthraquinone-1-sulfonic Acid Group (b) .....	37
<b>Figure 19.</b> Structures of C. I. Reactive Blue 19 (RB19) and its Derivatives (D in red, S in blue, B in green, and Re in purple). R: -CH <sub>2</sub> -CH <sub>2</sub> -SO <sub>3</sub> Na, dye; R: -CH=CH <sub>2</sub> , vinyl sulfone; R: -CH <sub>2</sub> -CH <sub>2</sub> OH, hydroxylate.....	41
<b>Figure 20.</b> An Example of Chromogen with Chromophore and Auxochrome .....	43

<b>Figure 21.</b> Three Basic Types of Reactive Groups .....	44
<b>Figure 22.</b> General Structures of Different Kinds of Basic Reactive Dyes Based on Reaction Activities.....	45
<b>Figure 23.</b> Diagram of the Nucleophilic Substitution Mechanism on Triazine Reactive Groups (a: X = Cl; b: X = -NHR.) .....	48
<b>Figure 24.</b> An Example of Nucleophilic Addition Reaction.....	49
<b>Figure 25.</b> Diagram of the Nucleophilic Addition Mechanism on Vinyl Sulfone Reactive Dyes with Cellulose Fibers .....	50
<b>Figure 26.</b> Different Reaction Products of Dichlorotriazine Reactive Groups under Different Alkaline Solutions .....	52
<b>Figure 27.</b> Typical Examples of Homo-bifunctional (a) and Hetero-bifunctional (b) Reactive Dyes .....	53
<b>Figure 28.</b> Hydrolysis Route of RB19 .....	54
<b>Figure 29.</b> Three basic acid dyes types and typical examples. (a) Azo, C.I. Acid Orange 7; (b) Anthraquinone, C.I. Acid Blue 25; (c) Triphenylmethane, C.I. Acid Blue 1. ....	57
<b>Figure 30.</b> Affinity Mechanism Between AB25 and Protein Fiber .....	58
<b>Figure 31.</b> Components in "Ideal" Soil with 50% Solid Material and 50% Pore Space .....	60
<b>Figure 32.</b> Main Steps in QuEChERS Extraction Method for Pesticides Extractions .....	67
<b>Figure 33.</b> Structures of C.I. Reactive Blue 19 in SES Form (a) and VS Form (b).....	70
<b>Figure 34.</b> C.I. Reactive Blue 19 Solutions for Analysis (seven concentrations ranging from 1, 3, 5, 10, 30, 50, to 70 $\mu\text{g/mL}$ ).....	72
<b>Figure 35.</b> Original QuEChERS Extraction Method (a) and Modified QuEChERS Extraction Method (b) for Extractions of Reactive Blue 19 from Blank Soils (QuEChERS content was 80 mg $\text{MgSO}_4$ , extraction solvent was made up by HPLC Grade ACN and MeOH with the ratio of 9:1) .....	77
<b>Figure 36.</b> Response from DAD, EIC, and Mass Spectra of Standard Dye RB19 Solutions Detected by LC-DAD-MS .....	80
<b>Figure 37.</b> Calibration Curve for Pure Dye RB19 Solutions (Standard deviations were calculated based on three repeated runs).....	81

<b>Figure 38.</b> Mass Spectra of RB19 Extracted from Blank Soils .....	83
<b>Figure 39.</b> Calibration Curve for RB19 Extracted from Blank Soils .....	84
<b>Figure 40.</b> Chemical Structures of RB19 in SES Form (a) and AB25 (b).....	90
<b>Figure 41.</b> Diagrams of QuEChERS Extraction on the Soil Samples after Simulated Compost 90-Day Degradation .....	92
<b>Figure 42.</b> Gradient Method used in Software “XCalibur” for Ion Trap MS (water as solvent A and acetonitrile as solvent B).....	94
<b>Figure 43.</b> TIC Chromatogram and Response from DAD for Degraded Soil Samples Detected with no Signals.....	96
<b>Figure 44.</b> EIC and DAD Response of the Unknown Signal from Degraded Soil Samples .....	97
<b>Figure 45.</b> Mass Spectra of the Unknown Signal from Degraded Soil Samples .....	97
<b>Figure 46.</b> Q-TOF MS Spectrum (Relative Abundance (%) vs. Mass-to-Charge Ratio) Showing the Detection of RB19 Degradation Product from Soil with 90-Day Interval .....	99
<b>Figure 47.</b> MS/MS of RB19 Degradation Product from Soils with 90-Day Interval .....	99
<b>Figure 48.</b> MS/MS Spectra from QTOF-MS of RB19 Degradation Product from Soil with 90-Day Interval and AB25 Standard Dye .....	100
<b>Figure 49.</b> Chemical Structure of C.I. Acid Blue 25.....	103
<b>Figure 50.</b> Modified QuEChERS Extraction Method SOP for Extraction of AB25 from Blank Soil.....	105
<b>Figure 51.</b> Response from DAD and Mass Spectra of Standard AB25 Dye Solutions .....	107
<b>Figure 52.</b> Calibration Curve for Standard AB25 Dye Solutions .....	108
<b>Figure 53.</b> Response from DAD and Mass Spectra of AB25 Extracted from Blank Soil .....	109
<b>Figure 54.</b> The Linearity Assessments for Quantitative Analysis of Pure AB25 Standard Dye Solutions (blue line) and AB25 Extracted from Blank Soils (red line), respectively, via LC-DAD-MS. Each point in the calibration curve shows the average across all runs (n=9). .....	110

## CHAPTER 1. Research Objectives

As one of the most dominant natural fibers in textiles, cotton fiber has attracted lots of attention and grown extensively throughout the world. It is reported that the worldwide production of cotton fibers reached 26 million metric tons in 2018, accounting for 81.1 percent in natural fiber markets (Figure 1) [1].

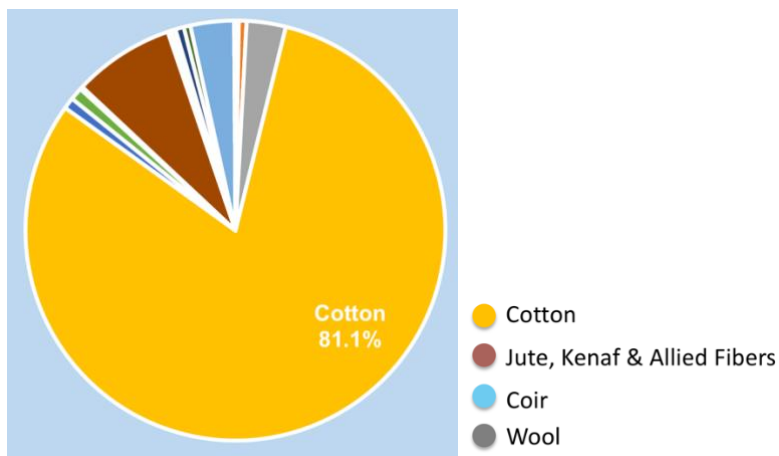


**Figure 1.** Consumptions of Cotton Fibers in Natural Fibers Market [1]

Reactive dyes are highly successful modern synthetic dyes. They are widely used with cotton and rayon, flax, wool, and nylon fibers in the textile industry because of good stability, good diffusivity and dye permeability, and good color fastness [2]. However, reactive dyes are non-degradable under the typical aerobic conditions found in conventional, biological treatment systems and adsorb very poorly to biological solids, resulting in water and soil pollutants [3,4]. In addition, they also represent a large group of organic compounds that could have undesirable effects on the environment, and some of them can pose risks to humans.

Textile production is a burden for the environment worldwide, using significant amounts of natural resources and toxic chemicals. However, despite this considerable cost, millions of tons of textile products are still disposed of every year to the environment. Let us imagine what is going to happen if all of those dyed fabrics go to landfills? The presence of those dyes and finishing on

the fabrics can be an important source of pollution due to those chemicals which can leach into the soil, where they can be very toxic, affecting the environment and human health. Thus, textile waste pollution can be a severe and inevitable problem for both the environment and waste management.

Based on The Guardian's data in 2019, globally, 87% of all disposed textiles are sent to landfill or incinerated; 12% is mechanically recycled by cutting it or shredding it into a fiber insulation material or rags. Also, less than 1% of the textiles are chemically recycled back to reusable raw materials [5]. Furthermore, based on the United States Environmental Protection Agency (US EPA), it is reported that the total amount of textiles in municipal solid waste (MSW, the primary source is discarded clothing) combusted in 2017 was 3.2 million tons, accounting for 66% of the total generated textiles wastes [6]. However, the disposal of fabric materials in textiles is also a complex phenomenon when considering the complex properties of soil and a serious challenge to waste management [7], in which options include recycled and reused clothes, conversion to new products, wiping, and polishing, landfill, and incineration for energy [8].

Even though there are lots of studies working on the effects of dyes on water systems, based on the biodegradation of synthetic dyes via different fungi, bacteria, yeasts, and algae, it has become a promising approach for the treatment of dye waste-water pollutions [9]; in those cases, they just remove the color of the effluents, and some toxic chemicals are still there after the water treatment.

Less work has been carried out concerning the effects of dyed textiles and dye pollution in soil [7,10]. The extraction and study of reactive dyes and cotton fabrics in soil are not fully understood yet; thus, conducting these investigations are meaningful and significant. This proposed work is undertaken to understand how the cotton fabrics and reactive dyes that we

normally use in daily life can become sources of pollution to nature; and the fundamentals of what is happening.

### **1.1. Modifications of QuEChERS Extraction Method and its Applications to the Extraction of Reactive Dyes from Blank Soil**

Based on the original QuEChERS (Quick, Easy, Cheap, Effective, Rugged, and Safe) extraction method, several modifications were made to develop a modified method for the extractions of reactive dyes from soil, including the selectivities of extraction solvents, QuEChERS contents (salts), and agitation modes.

### **1.2. Detection and Elucidation of Reactive Blue 19 Degradation Products from Soil**

Firstly, the simulated biodegradation of the dyed cotton fabrics was performed in the soil for 90 days at the Department of Fiber Science and Apparel Design, Cornell University, under controlled laboratory conditions according to standard ASTM D 5988-18. These soil samples were analyzed using the modified QuEChERS extraction method and liquid chromatography - mass spectrometry (LC-MS) approach. Furthermore, the structure of the unknown degradation product was elucidated as well.

### **1.3. Quantitative Analysis of Reactive Blue 19 Degradation Products from Soil**

After the detection and elucidation of the unknown degradation products from the 90-day degraded soil samples, quantification analysis is performed in a wide range of concentrations by using LC-diode-array detection (DAD)-MS and tandem MS (MS/MS), in which DAD was used for the gathering of any spectral absorption for the reactive dye. At the same time, a mass spectrometer detects the mass-to-charge ratio ( $m/z$ ) of degradation products. The quantification method was validated, such as linearity, sensitivity, precision, and accuracy. The fundamentals of

MS, dyes, and QuEChERS method will be introduced in Chapters 2, 3, and 4, and the experimental results will be discussed in Chapters 5, 6, and 7.

## CHAPTER 2. Introduction to Mass Spectrometry

### 2.1. Brief History of Mass Spectrometry (MS)

Originally, in the early 20th century, MS was used to measure the masses of atoms, and one of its first contributions to science was to demonstrate the existence of isotopes. In October 1913, Sir Joseph John Thomson (J. J. Thomson), named as “the father of mass spectrometry,” published “Rays of Positive Electricity and Their Application to Chemical Analyses,” in which Thomson tried to bring MS to the attention of chemists with this book [11]. It is also said that the first mass spectrometric experiment was arguably conducted by J.J. Thomson in the late 19th century when he measured mass-to-charge ratio ( $m/z$ ) in experiments, where he announced the results of his four months’ experiments on cathode rays, which suggested that the rays were negatively charged subatomic particles. His work had resolved the cathode ray’s controversy [12], which eventually lead to the electron discovery [13].

During the 1940s, chemists in the petroleum industry used MS to measure small hydrocarbons' abundance in process streams [14]. When the petroleum industry recognized the tool’s ability to determine chemical compositions, MS made the jump from physics to chemistry. By the 1960s, MS had become a standard analytical tool in analyzing organic compounds [15]. Nearly a century of MS research has established that it is one of the most powerful probes into the structure and composition of matter [16].

However, due primarily to the lack of suitable ionization techniques for fragile and nonvolatile compounds, MS applications in biological fields were largely restricted. Several developments in ionization changed the situation [15]. The new inventions of ionization techniques, such as plasma desorption (PD, developed in the 1970s), and fast atom bombardment (FAB, developed in 1981) [15], gave mass spectrometers the ability to analyze large molecules

such as proteins, carbohydrates, and nucleic acids. In addition, later ionization methods such as matrix-assisted laser desorption/ionization (MALDI, developed in 1988) and electrospray ionization (ESI, developed between 1984 and 1988) enhanced the analysis of biological samples [11]. With the continuous development of MS, its capabilities have spread from physics to chemistry to biology; furthermore, more new isotopes and their accurate masses and relative abundances have been discovered over several decades [17].

## **2.2. Components of Mass Spectrometry (MS)**

MS is a leading analytical technique in compound identification and characterization. In the easiest way, MS can be summarized by three main parts: ionization source, the mass analyzer, and detector (Figure 2).

In the analysis of liquid chromatography-mass spectrometry (LC/MS), a sample is injected into an LC column. The components are eluted and separated from the LC column and passed into the MS detector, where they are analyzed. However, analysis by direct infusion or flow injection provides no chromatographic separation of components in the sample before it passes into the mass spectrometer detector. The MS detector data are then stored and processed by the data system, which is vendor dependent. The final output is the mass spectrum, which is a plot of the relative abundance of ions vs. mass-to-charge ratio ( $m/z$ ) for a given mass range.

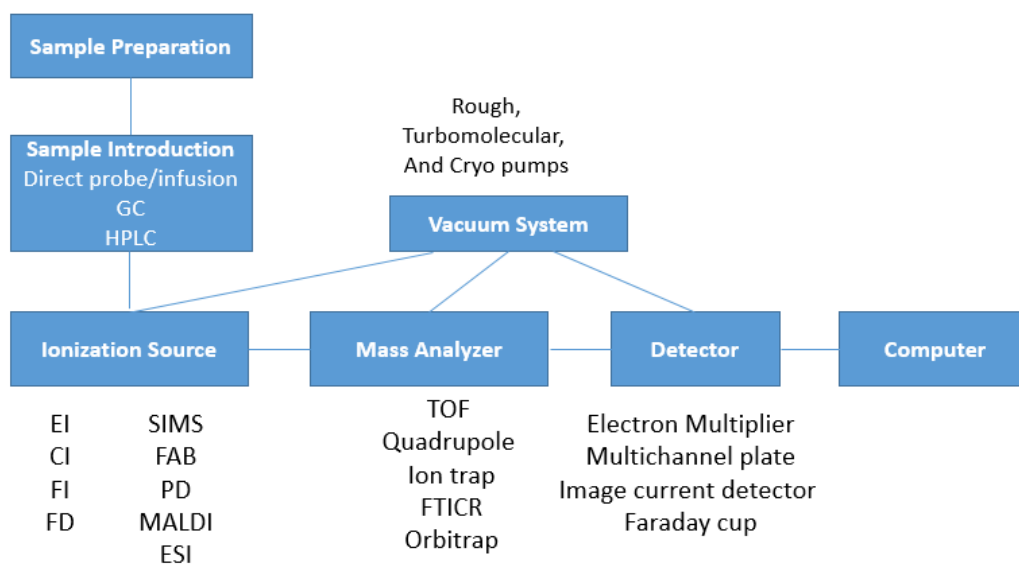


**Figure 2.** Main Components of Mass Spectrometry

The mass of atoms and molecules is expressed in terms of the unified atomic mass unit (u). By international agreement, the mass of one atom of the  $^{12}\text{C}$  isotope is assigned the exact value of 12. One unified atomic mass unit is defined as equal to 1/12 the mass of a single atom of the  $^{12}\text{C}$  isotope [15]. The Dalton (Da) is used in place of u, especially when expressing large biomolecules' mass (Equation 1). The mass of other atoms is expressed relative to the mass of the  $^{12}\text{C}$  isotope. Thus,

$$1 \text{ u} = 1 \text{ Da} = 1.660542 \times 10^{-27} \text{ kg} \quad (1)$$

As presented above, the MS data are presented as m/z, which is the mass of the ion (m) is divided by the number of charges (z) the ion carries [15]. Thus, the m/z values are different if the ion carries different numbers of charges.

### 2.3. High-Performance Liquid Chromatography (HPLC)

Mass spectrometry is usually coupled with analytical techniques such as HPLC, which is an important component for the analysis of analytes of a mixture, and different methods can be

chosen based on the analytes' differences in the chemical properties such as polarity, size, and H-bonding.

Chromatography is the most commonly used technique for separating the different components in a liquid mixture. Tswett firstly introduced this term in his first paper in 1906 [18,19], who is known as the "Father of Chromatography" [20]. There had some suspicion that Tswett named the technique after himself literally as "Tswett's writing" due to that "color" means "Tswett" in Russian and "graphein" means "writing" [19]. Chromatography involves the sample being dissolved in a particular solvent called the mobile phase. The mobile phase carries the analyte through another phase named the stationary phase, where the sample mixtures will be separated based on their different properties.

There are different chromatography techniques, such as paper chromatography, thin-layer chromatography (TLC), gas chromatography (GC), and LC. The mobile phase and stationary phase will depend on the chromatographic method used. The development of HPLC is connected closely with Professor Csaba Horváth [21], who built up the fundamental work of HPLC between 1964 and 1966 [21]. HPLC is one of the most widespread analytical and preparative scale separation techniques used for scientific research and industrial analysis.

HPLC is used to separate and analyze compounds through the mass-transfer of analytes between the mobile phase (MP, liquid solvents) and stationary phase (SP, column packing). The sample components are first dissolved in the solvents and then forced to flow through a column under high pressure. The system configuration of HPLC consists of a pumping unit, sample injection unit, separation unit (column), detector, and data processing unit (Figure 3). It is necessary to monitor the eluents at a constant flow rate and pressure pumps, especially when performing the qualitative and quantitative analysis. Constant flow rate pumps have been the

standard approach since the debut of the first commercial HPLC system in the 1960s [22], because the study of complex mixtures and component identification becomes difficult due to flow rate changes. Furthermore, as the pressure drop changes, the flow rate would also be uncontrollable, leading to unpredictable retention times.

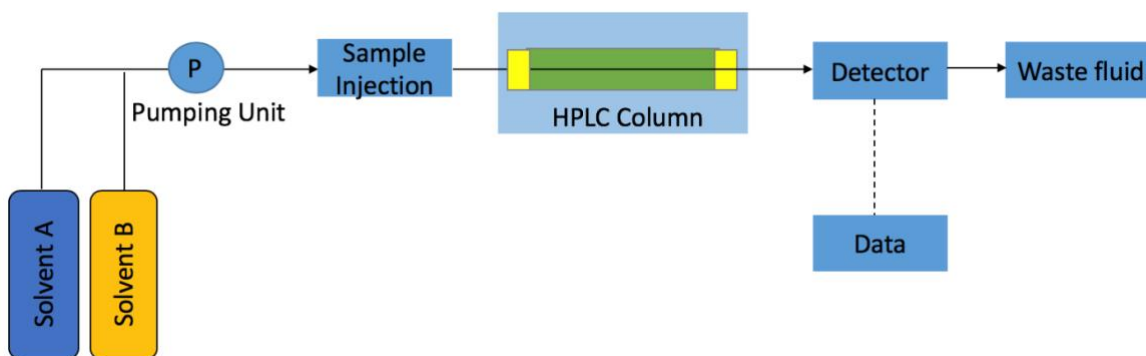


**Figure 3.** Configuration of HPLC System

Each component interacts slightly differently with the adsorbent material because of different affinities (polarities, ionic interactions), leading to the separation of those components as they flow out of the column at different times [23]. Currently, the most commonly used HPLC is reverse-phase chromatography, where the mobile phase is polar, and the stationary phase is non-polar.

### **2.3.1. Diode-Array Detection (DAD)**

Diode-array detection (DAD) is an analytical technique that can record the ultraviolet and visible (UV-VIS) absorption spectra of samples passing through HPLC. The DAD enables simultaneous acquisition across various wavelengths, rather than just a single one, for selecting the best wavelength for analysis [24]. Spectral acquisition used in conjunction with a chromatographic separation is a technique that allows the analyst to collect multiple spectra across

a chromatographic peak. Once these spectra have been collected from an HPLC analysis, they can be used to assess spectral peak purity and possible identification [24].

Based on the structures of the components, the lamp was employed for specific wavelengths in detectors. For example, the benzene rings that existed in most components can absorb light at a wavelength of 254 nm; hence, the detection wavelength of 254 nm is often used [25]. In this research, DAD is an extremely useful dye analysis technique because it helps determine when the dye is coming out from the column and perform its quantification.

## **2.4. Ionization Methods**

A compound must be charged or ionized to be manipulated by electric or magnetic fields inside the mass spectrometer. Thus, ionization is a process by which an atom or a molecule acquires a negative or positive charge by gaining or losing electrons to form ions. It often occurs whenever sufficiently energetic charged particles or radiant energy travel through gases, liquids, or solids.

In the ionization source, the samples can be in the gas or condensed phase. For gas-phase methods, the most common ionization methods are electron ionization (EI, the earliest ionization method that was developed in 1918), chemical ionization (CI), and field ionization (FI), because these methods can ionize volatile and thermally stable samples typically below 1kDa. For condensed phase sample, the ionization methods used are field desorption (FD, the first ionization method that can be applied to non-volatile and thermally unstable samples), secondary ionization mass spec (SIMS), fast atom bombardment (FAB), plasma desorption (PD), matrix-assisted laser desorption ionization (MALDI), electrospray ionization (ESI), atmospheric pressure chemical

ionization (APCI), and atmospheric pressure photoionization (APPI). The introductory dates and ionizing agents for different ionization methods are listed in Table 1.

**Table 1.** Ionization Methods, Timeline, and Ionizing Agents

Basic Types	Names and Acronyms	Dates of First Introduction	Ionizing Agents
Gas Phase	EI	1918	Energetic Electrons
	CI	1966	Reagent Gaseous Ions
	FI	1953	High-Potential Electrode
Desorption/ Desolvation	FD	1969	High-Potential Electrode
	SIMS	1940	Energetic Ion Beam
	FAB	1980	Energetic Atom Beam
	PD	1974	Fission Fragment from $^{252}\text{Cf}$
	MALDI	1983	Laser Beam
	<b>ESI</b>	<b>1968/1984</b>	<b>High Electric Field</b>

#### 2.4.1. Electrospray Ionization (ESI)

Electrospray ionization (ESI) is the most widely used ionization technique in MS. It was firstly introduced in 1968 by Malcolm Dole [26], but some problems were not solved until 1984 by John Fenn [13], who was awarded the 2002 Nobel Prize in Chemistry for the development of ESI-MS. ESI is known for the softest ionization characterization, which allows the analysis of both small (< 1000 Da) and large molecules (up to 100,000 Da) with very little fragmentation and enables the direct coupling of the mass spectrometers to other instruments such as high-performance liquid chromatography. Moreover, it primarily produces multi-charged ions, such as

$[M + nH]^{n+}$  and  $[M - nH]^{n-}$ , sometimes it can be up to 25 charge states; thus, the multi-charging also extends the mass range of an analyzer by a factor of  $z$ . However, it is not suitable for low polarity and has a limited transfer of ions into MS.

ESI is a method by which solutes present in a solution can be transferred into the gas phase as ions. The gas-phase ions can then be detected by mass spectrometric means (ESI-MS). A high electric field is used to produce/desolvate analyte ions. High voltage is applied to create an aerosol. Different solutions and voltages also affect the different spray morphologies: dripping, cone jet, dijet, and multijet.

During the ESI process, there are three significant steps in the production of gas-phase ions from electrolyte ions in solution (Figure 4): (1) production of charged droplets at the electrospray capillary tip; (2) shrinkage of the charged droplets due to solvent evaporation and Rayleigh fissions (also called Coulomb fission); (3) the actual mechanism by which gas-phase ions are produced from these droplets. The stages (1) to (3) occur in the atmospheric pressure region of the apparatus [27, 28].

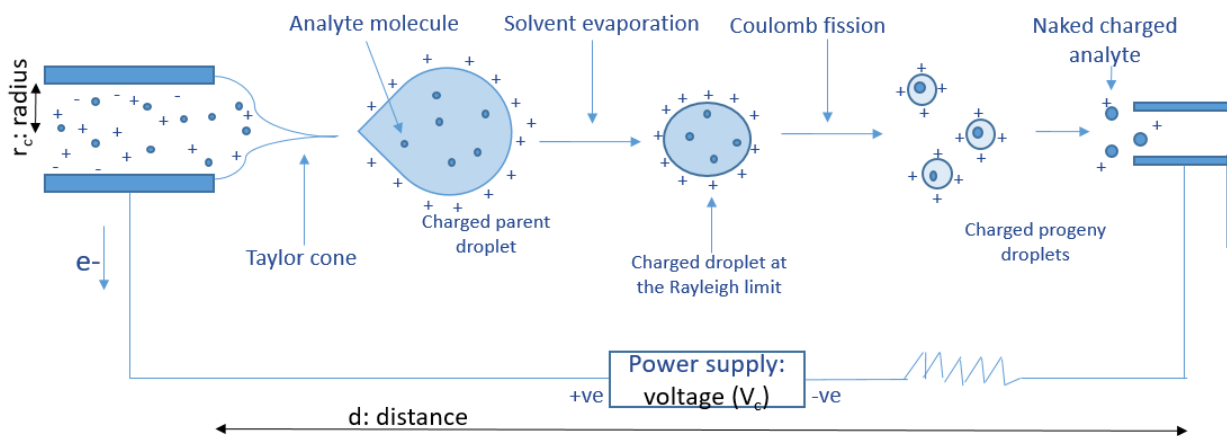


**Figure 4.** Schematic of Major Processes Occurring in the Atmospheric Pressure Region of Electro Spray Ionization

In the first step, the electrical field interacts with the solution and the charged species present inside the solution move in the field direction, leading to the formation of a liquid cone tip, which is so called “Taylor Cone”. This liquid cone tip becomes unstable if the electric field is high enough. Therefore, a fine jet emerges from the cone tip. The surface of the jet is charged by an excess of cations. The repulsion between the charges on the jet causes the jet to break up into small charged droplets.

There also is the generation of the charged droplets at the capillary tip. Typically, the capillary is 1 mm o.d. and located 1-3 cm from the counter electrode. As shown in Figure 4, because a high voltage  $V_c$  is applied to the conductive capillary and the spray capillary tip is very thin, so the electric field  $E_c$  at the capillary tip is very high ( $E_c \sim 10^6$  V/m), the relationship is shown in Equation 2 [27]:

$$E_c = \frac{2V_c}{r_c \ln\left(\frac{4d}{r_c}\right)} \quad (2)$$

As all of the parameters are labeled in Figure 4,  $V_c$  is the applied potential,  $r_c$  is the capillary outer radius, and  $d$  is the distance from the capillary tip to the counter electrode.  $E_c$  is essentially inversely proportional to  $r_c$ , while  $E_c$  decreases very slowly with the electrode separation due to the logarithmic dependence on  $d$  [27].

In the second step, this charged droplet will then shrink due to solvent evaporation while the charge remains constant. As the droplet gets smaller, the repulsion between the charges at the surface increases, and at a particular droplet radius, this repulsion overcomes the cohesive force of the surface tension. This will lead to droplet fissions, which will release smaller charged progeny droplets. The condition for this instability is called Rayleigh fission or Coulomb fission.

Last, having repeated Rayleigh fission, the droplets become smaller and smaller. Eventually, it will convert to tiny charged droplets, which are the precursors of gas-phase ions. However, the mechanisms by which the gas phase ions are produced from the progeny droplets vary. Two theories can explain the real mechanism in which the gas phase ions are generated from the charged progeny droplets. Both models involve droplets being released from the Taylor cone and decreasing in size as the solvent evaporates. However, they differ in how the ions can be generated from charged progeny droplets.

#### 2.4.1.1. Charge Residue Model (CRM)

The first model is the charge residue model, developed by Malcolm Dole in 1968. In the charge residue model, with repeated Rayleigh fission, the offspring droplets formed from the parent droplet further reduce in size. Each offspring droplet contains one analyte molecule. As the solvent molecules evaporate from the offspring droplets, the charge is deposited onto the analyte's surface, thus producing gas-phase ions (Figure 5). CRM mainly applies to macromolecules such as proteins because each droplet is only able to contain one molecule.

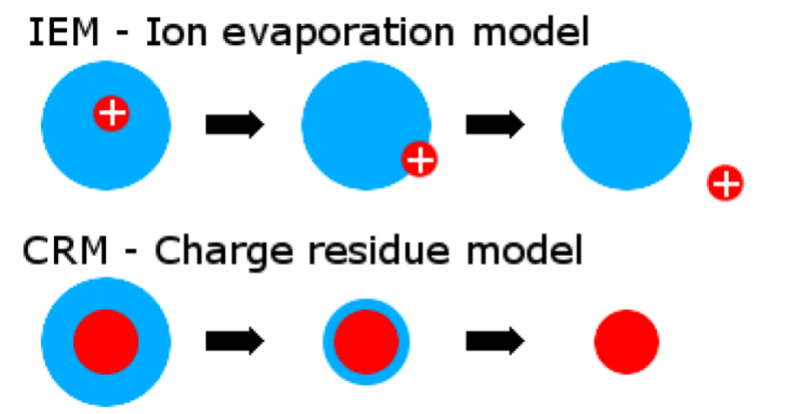


**Figure 5.** Main Theory of Ion Evaporation Model (CRM) and Charge Residue Model (IEM)

#### ***2.4.1.2. Ion evaporation model (IEM)***

The second model is the ion evaporation model (IEM), proposed by Iribarne and Thomson in 1976. As the radius of the offspring droplet continues to decrease, the charge density and electric field increase. The surface charge density is sufficiently lower than the Rayleigh limit, which causes the ejection of an ion from the offspring droplet instead of droplet dissociation. The IEM schematic is illustrated in Figure 5. This model is a supported one for small molecules.

### **2.5. Mass Analyzers**

Mass analyzers are critical in MS. Overall, mass analyzers can be divided into two main types: scanning and pulsed. Scanning mass analyzers include magnetic sector (B), linear quadrupole (Q), linear quadrupole ion trap (LIT), and quadrupole ion trap (QIT), for which the detection of ions with different  $m/z$  values is successively along the time scale. Pulsed mass analyzers include Time-of-Flight (TOF), Fourier transform ion cyclotron resonance (FTICR) and Orbitrap, for which all ions are detected simultaneously. To evaluate different mass analyzers' performances, some parameters are used, such as mass measurement accuracy, mass resolution, and resolving power.

#### ***2.5.1. Main Terminologies***

##### ***2.5.1.1. Mass Measurement Accuracy (MMA)***

Mass measurement accuracy (MMA,  $\Delta(m/z)$ ) is evaluated based on the difference between experimental and theoretical exact masses - divided by the ion's exact theoretical mass, namely the  $m/z$  measurement error. It is usually expressed in terms of parts per million (ppm).

$$MMA (ppm) = \frac{|M_{exp} - M_{theo}|}{M_{theo}} \times 10^6 \quad (3)$$

Where  $M_{exp}$  is the experimentally measured mass and  $M_{theo}$  is the theoretical exact mass expected for the compound. The MMA helps determine how well the mass spectrometer is performing in identifying the correct mass value per ion. There is an allowable ppm error per mass analyzer where a compound's composition can still be identified.

### **2.5.1.2. Mass Resolution**

The mass resolution, expressed in  $\Delta m_x$ , with a dimensionless ratio unit, shows the separation of two adjacent peaks observed in the MS spectrum (Figure 6a). It is a measure of the ability to separate ions with closely adjacent similar  $m/z$  values. If just a single peak is present with no overlapping peaks, a single method is used: the resolution is expressed as the mass of the peak divided by the peak width at either 5% or 50% of the peak height. However, if more than one peak is present and the peaks overlap, this makes the peak width measurement at 5% difficult. In this case, a doublet method can be applied, where mass resolution is measured using two overlapping peaks of approximately equal height, where the valley between the two peaks is at a given value, typically 10%. The less the overlap is, the higher the mass resolution is [29].

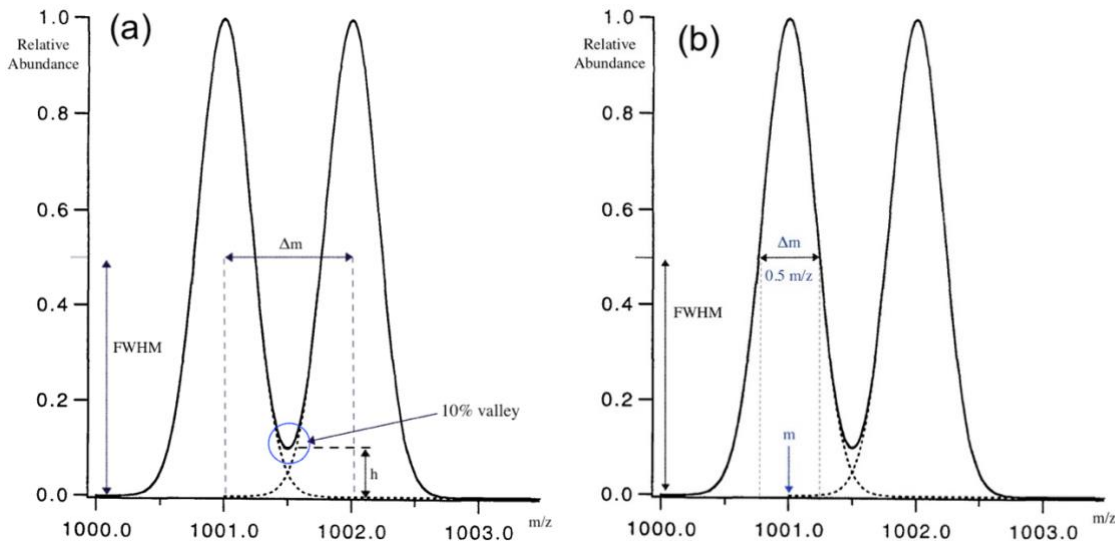


**Figure 6.** Illustration of Mass Resolution (a) and Resolving Power (b)

### 2.5.1.3. Resolving Power

Resolving power (RP) is the ability of an instrument or measurement procedure to distinguish between two peaks at  $m/z$  values differing by a small amount and expressed as the peak width in mass units [29]. Low RP is often defined as mass spectrometers with RP smaller than 3000. High RP is often defined as mass spectrometers with RP higher than 5000. The definition of RP can be expressed as follows:

$$RP = \frac{m}{\Delta m} \quad (4)$$

Where  $M$  refers to the mass of singly charged ions that make a single peak, and  $\Delta m$  refers to the width of this peak at a height that is a specific fraction (50%, 5%, or 0.5%) of the maximum peak height, in Figure 6b [30]. The 50% peak height case is frequently referred to as RP based on the FWHM (full-width-half-maximum) of a specified peak.

In summary, resolution refers to the separation between similar  $m/z$  values actually achieved in a real mass spectrum, while resolving power is referred to as an instrument's property

to resolve neighboring peaks [20]. The resolving powers of different types of instruments vary, which are listed in Table 2. Unlike low-resolving power instruments that can only reach several thousand resolving power units, the resolving powers of high-end instruments such as Orbitrap and FT-ICR can reach millions of levels. In this research, three mass analyzers were used, the TOF, the quadrupole and the linear ion trap.

**Table 2.** Resolving Powers of Different Mass Spectrometers

Type	Resolving Power (FWHM)
Quadrupole/ Ion Trap	1,000 - 10,000
TOF	10,000
High-Resolution-TOF	60,000
FT-Orbitrap	100,000
FT-ICR-MS	1,000,000

### ***2.5.2. Time-of-Flight (TOF) Mass Analyzer***

TOF mass analyzer was firstly developed in 1946 by W. E. Stephens and later firstly commercialized by Bendix Corporation in 1950 [31].

It is a kind of a fancy clock, the ion arrival times are in the function of  $m/z$ . By giving the same kinetic energy to all of the ions and allowing them to “fly” for a fixed distance, the lighter ion travels faster than heavier ones. In addition, by giving the same kinetic energy, the longer the flight time is, the larger the  $m/z$  the ion has. Usually, there are three standard vacuum operational conditions: rough, high, and ultra-high, whose differences are listed in Table 3.

**Table 3.** Three Types of Vacuums Regimes used in TOF-MS

Vacuum Regimes	Pressure Range (Torr)	Composition	Mean Free Path (cm)
Rough	760 to $10^{-3}$	80% N <sub>2</sub> and 20% O <sub>2</sub>	~ 5
High	$10^{-3}$ to $10^{-8}$	80% H <sub>2</sub> O, 10% N <sub>2</sub> and 10% CO	~ $5 \times 10^{3-6}$
Ultra-high	$10^{-8}$ to $10^{-12}$	H <sub>2</sub>	~ $5 \times 10^{6-9}$

In principle, TOF is based on the energy uptake  $E_{el}$ , which is equal to kinetic energy KE:

$$E_{el} = KE \quad (5)$$

$$E_{el} = qU = ezU \quad (6)$$

$$KE = \frac{1}{2}m_i v^2 \quad (7)$$

Where  $q$  is an electric charge,  $e$  is the electron charge,  $z$  is integer charge number,  $U$  is voltage,  $m_i$  is ion mass,  $t$  is time,  $x$  is flight distance, and  $v$  is velocity. The formula of velocity and traveling time can be combined to give Equations 8 and 9.

$$v = \sqrt{\frac{2ezU}{m_i}} \quad (8)$$

$$t = \frac{\Delta x}{v} = \Delta x \sqrt{\frac{m_i}{2ezU}} \quad (9)$$

Based on these two equations, velocity is inversely proportional to the square root of  $m/z$ , and traveling time is proportional to the square root of  $m/z$ .

Early TOFs were linear, as shown in Figure 7 [32]. Ions are formed in a short source region (s) in the presence of an electrical field (E) that accelerates the ions into a longer, field-free drift

region (D). Linear TOF mass spectrometers are the simplest instruments because the ions move in a straight line through the flight tube to the detector.

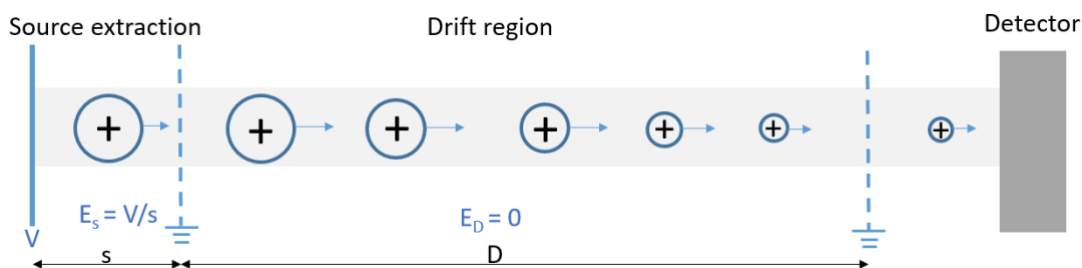


**Figure 7.** Basic Components of the Early Linear TOF Mass Spectrometer

However, for the linear TOF, the resolving power is not optimized because of the effects of initial time, space, and kinetic energy distributions [32] have on the different arrival times of ions of the same  $m/z$  value to the detector. To improve the resolving power of TOF, Boris Mamyrin developed reflectron in 1994 [33], which is also the most successful energy focusing method to date. It is a component of the ion optics and acts as an “ion mirror” that focuses ions of different kinetic energies in time, as shown in Figure 8. Ions with the same  $m/z$  value but different initial kinetic energies will have different momentum. The ions with more momentum will penetrate more the ion mirror to exit at the same velocity as ions with less momentum. This makes the ions with the same  $m/z$  value arrive at the same time to the detector, improving resolution.

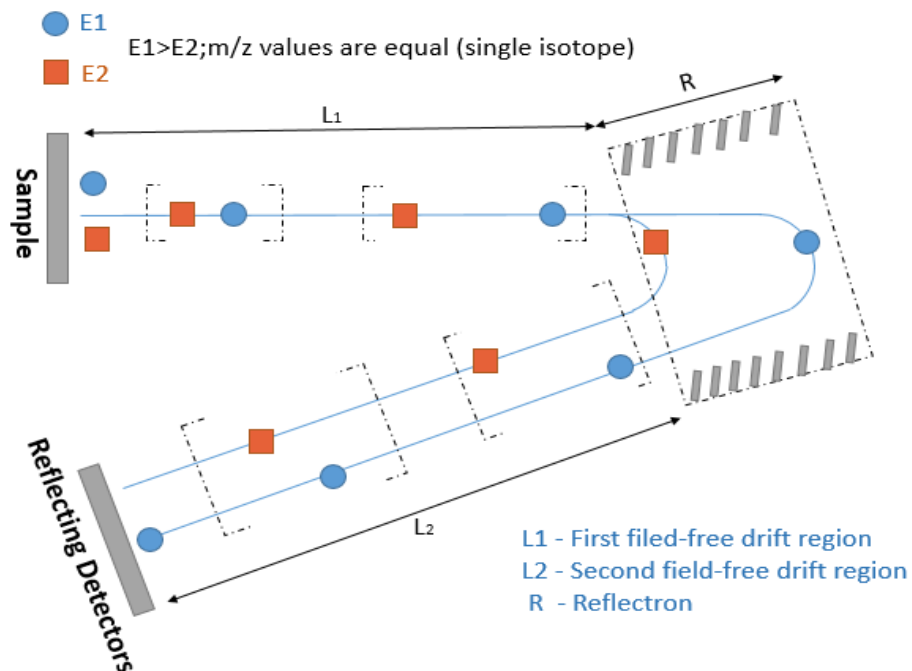


**Figure 8.** Principle of Operation of Reflectron in TOF-MS

In practice, a reflectron is comprised of a series of ring-shaped electrodes of increasing potential. The reflection voltage  $U_r$  is set to about 1.05–1.10 times the acceleration voltage  $U_a$  to ensure that all ions are reflected within the homogeneous portion of the device's electric field. The ions penetrate the reflectron until they reach zero kinetic energy and are then expelled from the reflectron in the opposite direction. The leaving ions' kinetic energy remains unaffected; however, their flight paths vary according to their kinetic energy differences. Ions carrying more kinetic energy (E1 in Figure 8) will fly deeper into the decelerating field and thus spend more time within the reflectron than less energetic ions (E2 in Figure 8). Thereby, the reflectron affects a correction in time-of-flight that substantially improves the TOF analyzer's resolving power [16,33]. Also, the reflectron provides (imperfect) focusing with respect to the angular spread of the ions leaving the source, and it corrects for their spatial distribution. It has the advantage that it increases the drift-length without increasing the size of the instrument. Thus, the reflectron's ability to compensate for the initial energy spread of ions largely increases the resolving power of TOF [32,33].

As mentioned earlier, the TOF is a pulsed mass analyzer, so it can efficiently couple with the MALDI source, which is a pulsed ionization source method. Orthogonal acceleration (oaTOF) was also developed in 1967 to eliminate coupling difficulties with continuous ionization sources such as ESI [34]. The detector for TOF is commonly a microchannel plate detector.

One of the instruments employed for this research is a quadrupole-time-of-flight (QTOF), a hybrid mass spectrometer consisting of octopole ion guides and quadrupoles for mass filtering, a collision cell, and a time-of-flight section (see Figure 9). The QTOF can provide high resolving power. After the ion travels through the quadrupole, it enters into the collision cell, which can be used to fragment ions to gain structural information via tandem mass spectrometry.

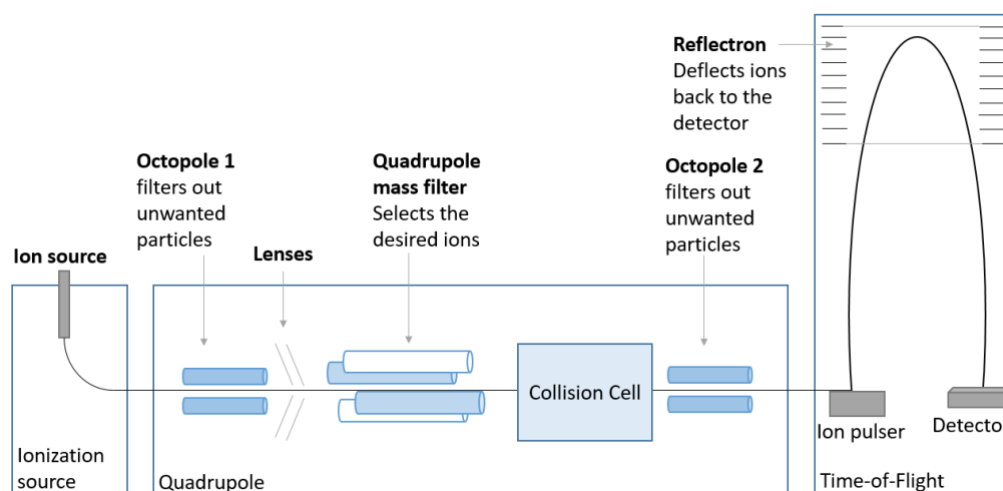


**Figure 9.** Scheme of an Agilent 6520 Quadrupole-Time-of-Flight Mass Spectrometer

### 2.5.3. Quadrupole Mass analyzer

A quadrupole mass analyzer is composed of four parallel opposite hyperbolically or cylindrically shaped rod electrodes extending in the z-direction and mounted in a fixed and square configuration [35]. It has two pairs of opposite rods on which a potential of the type  $U \pm V \cos \omega t$  is applied, where  $U$  is the direct current potential (DC), and  $V \cos \omega t$  is the radio frequency potential

(RF). The ions ejected (accelerated along the z-axis, green line in Figure 10) from an ion source will oscillate in both x and y directions by this field's action.

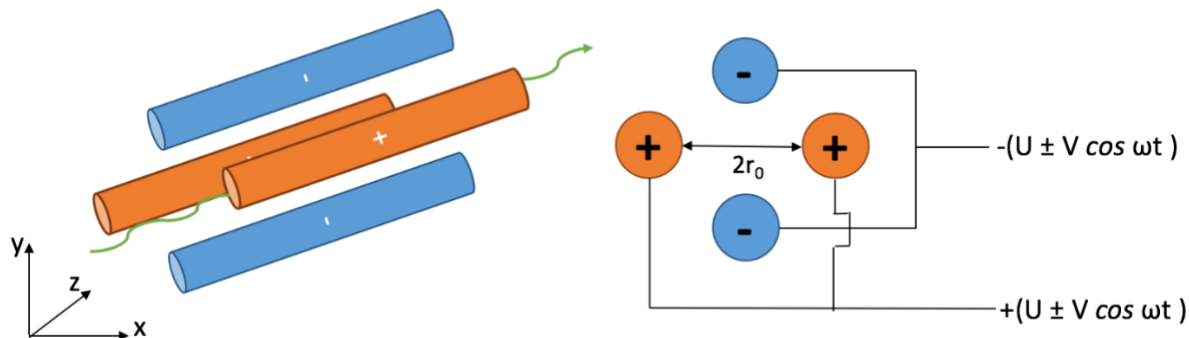


**Figure 10.** Schematic of a Quadrupole Consisting of Four Metal Rods Parallel to Each Other

The quadrupole mass analyzer also has the mass filter's function, which has been the most widely used mass analyzer since the 1970s. When RF is zero, the DC-only quadrupoles enable all ions to pass or hit the rods; when both RF and DC are applied, the function of mass filtering is shown in Figure 11.

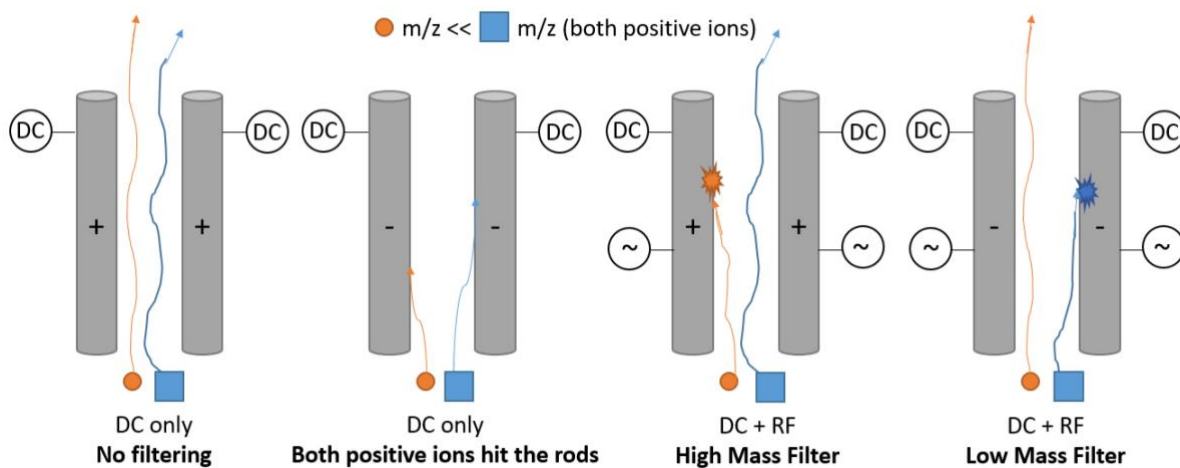


**Figure 11.** Examples of how varying DC and RF voltages affect quadrupole mass analyzers

The parameters that affect the motion include the ion  $m/z$  value, the  $U$ ,  $V$ ,  $\omega$  values, and  $r$  (the mass filter dimension). For an ion of a given  $m/z$ , to define the parameters “ $a$ ” related to DC ( $U$ ) voltage and “ $q$ ” related to RF ( $V$ ) voltage as follows:

$$a = \frac{4eU}{(m/z) r_0^2 \omega^2} \quad (10)$$

$$q = \frac{2eV}{(m/z)r_0^2\omega^2} \quad (11)$$

$$\frac{a}{q} = \frac{2U}{V} = \text{constant} \quad (12)$$

By plotting “a” vs. “q” parameters [36], a “Mathieu Stability Diagram” for a given ion in a quadrupole field can be obtained (see Figure 12). The “Scan line” in red color also indicates that, even though the U and V values would change, but the a/q ratio will remain the same. If the V and U values are increased, keeping the U/V ratio constant, ions will increase their a, q values, and when the straight-line portion inside the apex of the stability diagram is reached, they will follow stable trajectories, thus passing through the rods and reaching the detector placed after the rods themselves [36], finally, all the ions can be selectively detected.

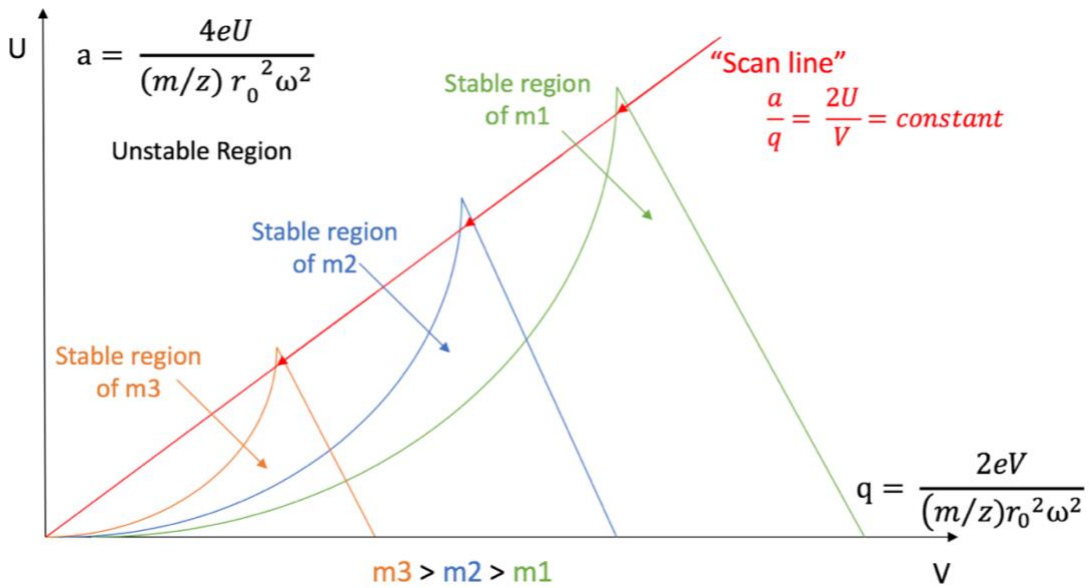


**Figure 12.** Mathieu Stability Diagrams for Different Ions

The inability to maximize mass range, mass resolving power, or mass accuracy without compromising the quadrupole performance has ensured that these performance characteristics

remain modest when operating quadrupole mass filters under standard conditions. Despite these disadvantages, quadrupole mass filters are still capable of enhancing sensitivity and excellent linear dynamic ranges. Also, because of the low cost, small physical sizes, ease of automation, and low ion acceleration voltages have contributed to these instruments' popularity [13].

#### ***2.5.4. Tandem Mass Spectrometry (MS/MS) by Triple Quadrupole Mass Spectrometers***

MS/MS is based on the use of a first quadrupole mass analyzer, employed to select ions of interest, and a second mass analyzer devoted to the analysis of the decomposition products of the preselected ions. Generally, for the tandem mass spectrometry experiment, there are three quadrupoles set up in a linear position, often called “triple-quad” (QqQ-MS), as shown in Figure 13.

The ions of interest ( $M^+$ ) produced by the suitable ionization method are selected by the first quadrupole (Q1, the mass filter with the function of  $m/z$  selection). The second quadrupole (q2) is an RF-only collision cell, where the precursor ions are activated by collisions and undergo further fragmentation, where a process called collision-induced dissociation (CID) happens in the second quadrupole. The specific fragmentation ions resulting from CID are related to the ions' molecular structure and can be selected by the third quadrupole (Q3) mass analyzer.

In the collision cell (q2), where DC is zero, it becomes an RF-only quadrupole, and it does not have the function of mass filtering. Triple-quad MS has increased sensitivity and specificity versus other mass spectrometers, and its fragmentation information can provide structure characterization.

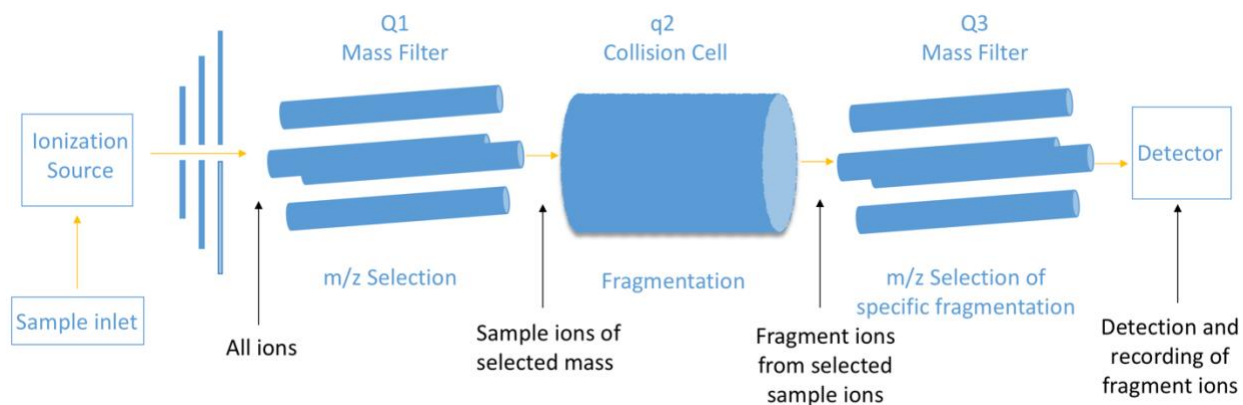


**Figure 13.** Schematic of a Triple Quadrupole (QqQ) System for MS/MS

#### 2.5.4.1. Collision-Induced Dissociation (CID) / Collision-Activated Dissociation (CAD)

As mentioned in tandem MS, q2 is a fragmentation chamber, which breaks ions via CID, a technique to induce fragmentation of molecular ions in the gas phase. Thompson firstly observed CID in 1913, but not explained until 1919 when Aston identified the process, which we now call CID or CAD [37]. CID began as a structural tool that began in the 1960s in the laboratory of Fred McLafferty. To gain structural information on an unknown over the molecular formula afforded by an accurate mass measurement. CID is often employed to fragment the molecule and interrogate its constitutive parts.

Two discrete fragmentation processes can explain CID's theory: collisional activation and unimolecular dissociation (Figure 14). As previously described in the schematic of MS/MS (Figure 13), the CID process happens in the collision cell (q2), molecule ions accelerate to high kinetic energy and then are allowed to collide with gas atoms or molecules, usually nitrogen, argon, or helium. In the collision process, part of the kinetic energy is converted into the vibrational/rotational energy of the parent ions. If the internal energy gained is high enough, the

precursor ions will fragment fast enough for the fragment ions to be observed in MS. Thus, it becomes one of the most commonly used fragmentation techniques in use nowadays.

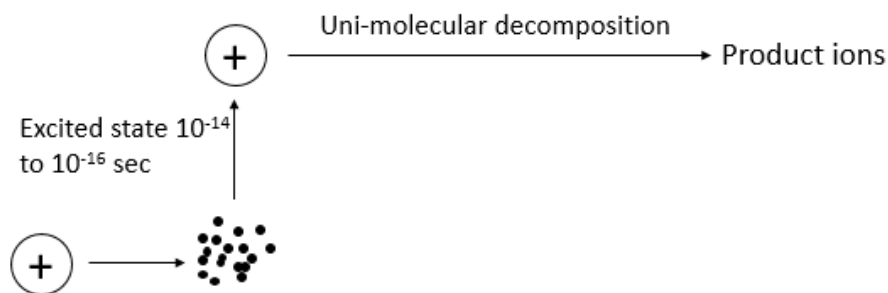


**Figure 14.** Two Discrete Fragmentation Processes in CID

The relationship between the kinetic energy of ions and converted internal energy can be expressed in equation 13:

$$E_{cm} = E_{TR} \frac{m_N}{m_N + m_i} \quad (13)$$

$E_{cm}$  identifies the center-of-mass collisional energy (internal energy available),  $E_{TR}$  is the kinetic energy of ions,  $m_N$  is the mass of the gaseous target (nitrogen, argon, or helium), and  $m_i$  is the mass of the ion. With the increase of ion mass  $m_i$ ,  $E_{cm}$  decreases; with the increase of target mass  $m_N$  or  $E_{TR}$ , the amount of energy available for conversion into internal energy  $E_{cm}$  increases.

It is the type of instrument and the mass analyzer that sets the initial kinetic energy  $E_{TR}$ , according to which the CID can be classified as “low or high energy” [30]. Typically, high-energy CID (kiloelectronvolt collision energy) is for TOF instruments that contain magnetic and electric sectors [38]. Usually, each precursor ion experiences on average 1-10 collisions that deposit high enough energy to cause electronic excitation [30]. Low-energy CID (much lower initial kinetic energy, usually  $\leq 200$  eV) is common in quadrupole and ion trap instruments for efficient precursor ion selection and fragment ion dispersion [30]. However, for low-energy CID, the internal energy transferred during one collision is not enough to cause fragmentation. Thus, multiple collisions are

needed, which can be achieved by increasing the pressure of collision gas or the time of excitation in (ITs) [30].

#### ***2.5.5. Ion Trap Mass Analyzer***

Another instrument used in this research is the Thermo Scientific™ LTQ XL™ linear ion trap mass spectrometer (represented by LTQ), as shown in Figure 15. The left part is HPLC, and the right part is a mass spectrometer.

In LTQ, a single quadrupole offers selected ion monitoring (SIM); a linear ion trap goes further by enabling consecutive reaction monitoring where a selected ion is fragmented into a product ion. The resulting product ion can also be fragmented in additional successive steps. Each additional fragmentation step makes compound identification more certain and facilitates structural characterization. LTQ has the following advantages: tandem MS capabilities, good sensitivity, adequate mass range, ease requirements of vacuum, fast, and the operational parameters can be changed at very high rates. It also extends the legendary MS<sup>n</sup> performance of the LTQ ion trap, incorporating more techniques to generate structural elucidation using multiple dissociation techniques such as CID and high-energy collisional dissociation (HCD).

When using ESI source in LTQ, the recommended flow rate for ESI is 3 µL/min – 1 mL/min, the optimal flow rate is 200 µL/min. Generally, higher LC flow rates require higher heated capillary temperatures and higher gas flow rates. The temperature of the tray can be kept at 5 °C, which prevents the solution from evaporating.

Upon entering the ion source, sample molecules are ionized by the ESI probe and then passed through the heated capillary. The ion optics focus and accelerate the resulting sample ions into the mass analyzer, where they are analyzed based on the values of m/z. The ion current signal

from the ion detection systems is then received and amplified by the system electronics, and it is then passed on to the data system for further processing, storage, and display. The schematic of the process in LTQ is shown in Figure 15.

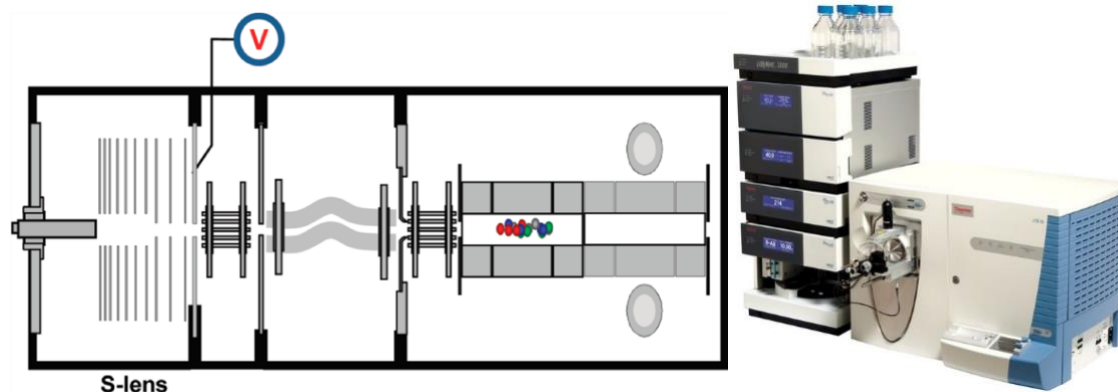


**Figure 15.** Schematic of Thermo Scientific™ LTQ XL™ Linear Ion Trap Mass Spectrometer

Unlike the 3D quadrupole ion trap, the linear ion trap has higher injection efficiencies and ion storage capabilities. “Linear” is used because the field between the electrodes is desired essentially by 2D multipoles [39]. A linear ion trap mass spectrometer uses dynamic electric fields (an appropriate static DC and RF voltages) to trap charged particles [18]. The radial confinement of ions is affected by RF trapping potentials (1MHz) in the center section (Figure 16). In contrast, the axial confinement is affected by the auxiliary DC potentials in the front and rear lenses (Figure 16) [40]. Generally, the length of the center section is longer than that of the front and rear sections. In the linear ion trap mass spectrometer, mass selective ion ejection is accomplished by radial resonant excitation of the stored ions from the center section [40].

For the ions to impinge upon an external detector, a 0.25-mm-high slot was cut along the middle 30 mm of the center section of one rod, and a detection system can be mounted in front of the slot, shown in Figure 16. The comparisons between the three mentioned mass analyzers are summarized in Table 4.

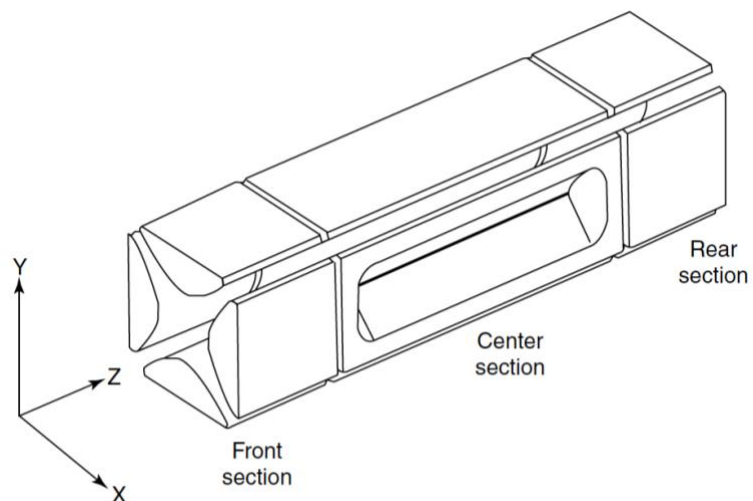


**Figure 16.** Angled Schematic of Linear Ion Trap Mass Analyzer

**Table 4.** Merits of Mass Analyzers

Mass analyzers	TOF	Quadrupole	Linear Ion Trap
m/z limit	Unlimited	4000	15 - 4000
Resolving power ( $RP_{FWHM}$ )	30,000 is routine (range: 10k-60k)	1000 - 3000 is routine	15,000 - 30,000 (depending on scan speed)
Mass measurement accuracy (ppm)	ESI-TOF: 1-5, MALDI-TOF: 10-100.	100	50 - 100

## CHAPTER 3. Cotton Fibers and Dyes

### 3.1. Textile Fibers

There is a wide range of textile fibers available in the textile market. In general, there have two main types of fibers, natural (protein, cellulosic) and human-made (regenerated, synthetic) fibers (see Table 5) [41].

Most man-made fibers were developed in the first half of the twentieth century and, from that time onwards, tremendous advances have been made in this fiber industry [42]. In man-made fibers, regenerated fibers are derived from natural sources, where their production involves chemical processing to form another polymer. The most representative regenerated fibers are viscose rayon, Lyocell, and Modal, derived from cellulosic fibers [43]. Viscose rayon, known as artificial silk, was first produced in filament length until the early 1930s [42], which can be manufactured by reacting cellulose (cotton pulp and wood pulp) carbon disulfide in alkali to give its water-soluble xanthate derivative. This derivative then follows the regeneration of the cellulose in fibrous form using sulfuric acid [43]. Lyocell, introduced in 1994, is a more recently developed regenerated cellulosic fiber with strong environmental credentials and commercialized under the trade name Tencel<sup>®</sup> [44]. Lyocell is manufactured from wood pulp, from sustainably farmed eucalyptus, dissolved in an organic nontoxic solvent, N-methylmorpholine N-oxide (NMMO) [44].

Among man-made fibers, synthetic fibers comprise those fibers produced from polymers that are chemically synthesized from monomeric starting compounds. They account for well over 50% of the total worldwide demand for textile fibers. Specifically, polyamides (nylon) fibers were the first synthetic fibers to achieve commercial prominence, and polyester fibers dominate in current synthetic fiber markets [45].

**Table 5.** Classifications of Textiles Fibers [2,43]

Natural fibers		Man-made fibers	
Cellulose	Protein	Regenerated	Synthetic
Cotton	Wool	Viscose rayon	Polyesters
Hemp	Silk	Lyocell	Polyamides
Bamboo	Mohair	Modal	Polypropylene

### **3.1.1. Cotton Fibers**

Natural fibers have 4000 to 5000 years of history for making clothes, far away before the first man-made fiber that was produced commercially in 1885 [42]. In the early 1990s, the amount of natural fibers is roughly equal to that of the synthetic fibers produced. However, due to a rapid increase in polyester demand, the worldwide productions of man-made fibers (58.5 million metric tonnes, over 75% were polyester) is almost twice that of natural fibers in 2013 [45]. The coexistence and competition between man-made and natural fibers are currently stabilized, especially in the areas of quality, sustainability, and economy of their production [42].

In natural fibers, cotton is the most dominant and important fiber in textile applications and is grown extensively throughout the world. As mentioned in Chapter 1, it is reported that the worldwide production of cotton fibers can reach up to 26 million metric tonnes in 2018 [1], which accounts for almost 81.1 percent of natural fibers markets.

In natural fibers, cellulose is a renewable polymer that grows in plants (trees, grass). After chemical purification, it can be used for the production of man-made textiles fibers [46]. Cellulose is a polysaccharide, a high molecular weight polymer consisting of long chains of repeating glucose units, with up to around 1300 such units in each molecule [43]. Cellulose has a fairly open

structure (Figure 17), which allows large dye molecules to penetrate more easily into the fiber. Each glucose unit contains three hydroxyl (OH) groups, one primary and two secondaries.

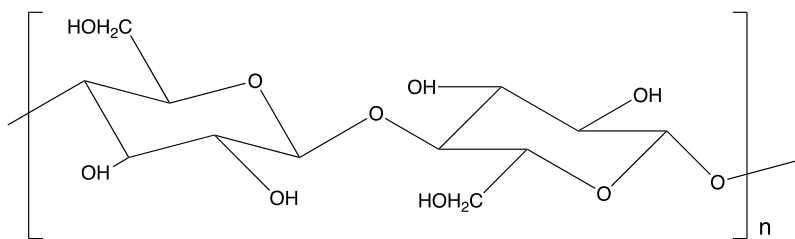


**Figure 17.** The Basic Structure of Cellulose

The reactivity and presence of the hydroxyl groups are of considerable importance in the dyeing of cellulose with reactive dyes [43]. The dyes are commonly induced to react with the cellulose in aqueous alkali, where the deprotonation of the hydroxyl groups (Cell-OH, section 2.5.1) takes place. This produces a stronger nucleophilic cellulose anions (Cell-O<sup>-</sup>), which are generally regarded as the active nucleophiles in the reactive dyeing of cellulose. The typical dye exhaustion of cotton is in the 50–90% range but is strongly affected by the dye and the dyeing conditions [46]. More importantly, effective dye exhaustion will vastly improve the dyeing process's economic and ecological aspects.

The most common types of fiber-reactive dyes for cellulosic fibers react either by aromatic nucleophilic substitution or by nucleophilic addition to activated alkenes [43], more details of which will be explained in section 3.5.

### 3.2. Basis of Colorants, Dyes, and Pigments

Color is one of the elements of nature that makes human life more fascinating in the world. Before synthetic dyes were discovered, plants (roots, berries, leaves, and wood), animals, and minerals have been used as primary sources for dyes or pigments since ancient times [47]. Both dyes and pigments are the most important colorants used to add color to all sorts of substances,

which have wide ranges of applications, such as textiles, coatings, plastics, paper, construction, glass, cosmetics, automotive, and food [47].

The differences between dyes and pigments are that dyes are soluble in water or an organic solvent and provide brighter color than conventional pigments. However, it is not true for all application classes of textile dyes. For example, disperse dyes for polyester fibers are only sparingly soluble in water and are applied as a fine aqueous dispersion; vat dyes for cellulosic fibers are completely insoluble materials, but they can be converted into a water-soluble form that may then be applied to the fiber via a chemical reduction process [43]. Differently, pigments are coloring materials that need to be insoluble in both liquid media types and are dispersed as particles, and more light-stable and permanent [47].

In the actual applications, an appropriate color is an obvious requirement for a dye, which can be described as colored substances that have an affinity to the substrates to which they are being applied. UV/visible spectrometry can be used for characterizing the color of dyes.

Based on applications, dyes can be classified based on the principal method adopted by the Colour Index (C.I.) [48]. Take C.I. reactive Red 22 as an example, it indicates the application type, color, and identifying number. The most important organic dyes and pigments, in roughly decreasing order of importance, belong to the azo ( $-N=N-$ ), carbonyl ( $C=O$ ) (including anthraquinones), phthalocyanine, arylcarbonium ion (including triphenylmethines), sulfur, polymethine, and nitro ( $NO_2$ ) chemical classes [43]. In section 2.3, azo and carbonyl dyes will be explicitly discussed.

Each class of dyes owes its color to the specific wavelength ranges in nm. However, human eyes are sensitive and correspond to radiation with a very narrow range of 360-780 nm. Beyond that range, there is the ultraviolet (UV) range (below 360 nm) and the infrared (IR) range (above

780 nm) [43]. To explain the visual effects of the dyes' colors, two laws will be introduced below: Planck's relationship and Beer–Lambert Law.

### **3.2.1. Planck's Relationship**

Absorption and scattering are used to explain the interaction between light with objects, in which absorption is the process by which radiant energy is utilized to raise molecules in the object to higher energy states. In contrast, scattering is the interaction by which light is redirected due to multiple refractions and reflections [43]. If only absorption is involved when light interacts with an object, then the object will appear transparent. The absorption of visible light energy by the molecule will promote electrons in the molecule from a ground state to a higher-energy excited state, where the dye molecule also undergoes an electronic transition during this excitation process. The energy difference,  $\Delta E$ , between the electronic ground state and the electronic higher-energy excited state of dye is given in Planck's relationship [43]:

$$\Delta E = h\nu = hc/\lambda \quad (14)$$

Where,

$h$  is the Planck's constant,  $\nu$  is the wavelength of light absorbed,  $c$  is the velocity of light absorbed (constant), and  $\lambda$  is the wavelength of light absorbed. Thus, the energy difference between the ground state and the excited state of dye ( $\Delta E$ ) is inversely correlated to the wavelength of light absorbed ( $\lambda$ ) [43].

### **3.2.2. Beer–Lambert Law**

The molar extinction coefficient ( $\epsilon$ ) at its  $\lambda_{\max}$  value (the wavelength of maximum absorbance) is a measurement of how strongly a substance absorbs light at a particular wavelength.

It is an intrinsic property of a substance that is dependent on its chemical compositions and structures. The SI units of  $\epsilon$  are  $\text{m}^2/\text{mol}$ , but in practice, they are usually taken as  $\text{M}^{-1}\cdot\text{cm}^{-1}$  or  $\text{L}\cdot\text{mol}^{-1}\cdot\text{cm}^{-1}$ . The molar extinction coefficient ( $\epsilon$ ) is frequently used in spectroscopy to measure a chemical's concentration in a solution [43]. The Beer–Lambert Law can be used to calculate a chemical species'  $\epsilon$  based on:

$$A = \epsilon cL \quad (15)$$

Where,

A is the dye's absorbance for a particular wavelength,  $\epsilon$  is the molar extinction coefficient at that wavelength, c is the dye's concentration, and L is the pathlength of the cell, commonly 1 cm, used for measurement of the spectrum.

The Beer–Lambert law can be applied for most dyes in solution at low concentrations, the color strength of the dye is positively correlated to the absorbance of the dye (area under the absorption band) but also depends on the shape of the absorption curve. But the qualitative relationship between the molar extinction coefficient ( $\epsilon$ ) and the color strength of dye should also be considered [43].

UV/Visible spectroscopy is used routinely to measure the color of opaque objects such as textile fabrics, paint films, and plastics for purposes such as color matching and dye and pigment recipe prediction. The technique can also be used to measure dye concentrations in solutions, which can be considered that, at the  $\lambda_{\text{max}}$  and  $\epsilon_{\text{max}}$  of dyes, the dye's absorbance is proportional to the concentration of that ideally.

### 3.3. Azo and Carbonyl Dyes

#### 3.3.1. Azo Dyes

As the name implied, azo dyes are compounds (Figure 18a) that contain azo groups linked to a methine or aromatic  $sp^2$ -hybridized C-atoms.

The first azo dyes were manufactured by Mène in 1861 (Aniline Yellow) and by Martius in 1863 (Bismark Brown) [49]. The original discovery of “covalent dyeing” is attributed to *Rattee* and *Stephen* in 1954 [47] when they found that dichlorotriazine-containing monoazo acid dyes react with the -OH groups of cellulosic fibers when the neutral dyebath is rendered alkaline [49].

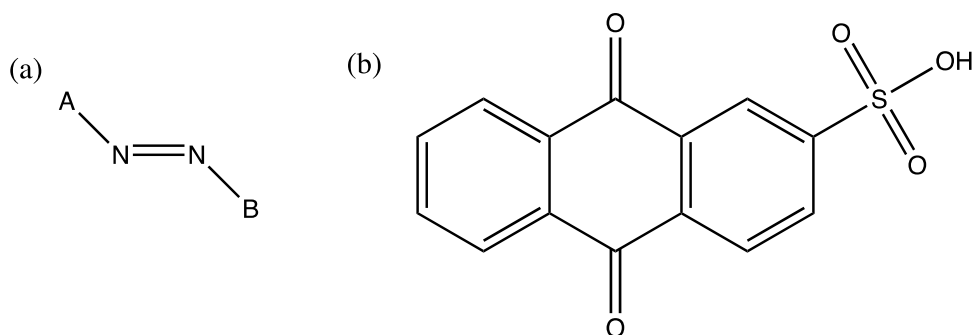


**Figure 18.** Example of an Azo Group Attached to Two Different Groups (a) and an Anthraquinone-1-sulfonic Acid Group (b)

Azo dyes almost represent 60% of the dyes used in traditional textile applications worldwide [43,47], including different types of dyes like disperse azo, azoic, cationic azo, metal-complex mono-azo, direct, and reactive azo dyes. Also, azo dyes are widely used in pharmaceutical, plastic, leather, paper, and printing industries [47], due to the following considerations: (1) simple synthetic procedures, (2) almost unlimited numbers of substituents, (3) generally high molar extinction coefficients, (4) can provide a high intensity of color (about twice that of the anthraquinones), and (5) medium-to-high fastness properties with respect to both light, heat, water and other solvents [49].

### **3.3.2. Carbonyl Dyes**

The most important synthetic carbonyl dyes are based on anthraquinone, particularly the higher-annulated anthraquinone derivatives [49]. Besides azo dyes, other classes of reactive dyes, such as anthraquinone dyes, are extensively used either as primary or secondary dyes in commercial trichromatic dyeing formulations [4].

The history of anthraquinone dyes can be traced back to the elucidation of alizarin structure, the basic compounds for Turkey Red [49]. They were one of the oldest types of dyes since they have been found in mummies' wrappings dating back over 4000 years. Anthraquinone constitutes the second most important class of textiles dyes after azo dyes [47]. The primary reason for the commercial importance of azo dyes is probably that they are the most cost-effective of all chemical classes of dyes [43]; The most complicated syntheses and lower tinctorial strengths of the anthraquinone dyes make the production costs higher compared to azo dyes [47].

Some 80 - 90% of all industrially produced anthraquinones are based on anthraquinone sulfonic acids, especially the derivatives of the corresponding anthraquinone-1-sulfonic acid [49], shown in Figure 18b. The anthraquinone dyes have essential advantages such as brightness and good fastness properties [47].

### **3.4. Reactive Dyes**

It took 100 years of dye chemistry to produce reactive dyes following W. H. Perkin's discovery of the first synthetic dyes, Mauvein, or Mauve in 1856 [2]. It was not until 1954 that Rattee & Stephenson at the Imperial Chemical Industry (ICI), Dyestuffs Division site in Bleckley, Manchester, UK, invented reactive dyes and made them first become commercial in 1956 [2]. The

first reactive dyes for cellulose fibers introduced by ICI in 1956 are dichlorotriazine reactive dyes [50].

With the development of the economy and technology, the public has become more sensitive to the protection of the environment. Synthetic dyes are extensively used in textiles, color photography, paper and pulp mills, cosmetic, food, and leather industries [9]. However, most dyes are toxic, mutagenic, and clastogenic to living organisms and highly resistant to degradation due to their complex chemical structures [9], which cause environmental problems (water and soil). Because reactive dyes based on azo and anthraquinone functional groups are the most commonly used dyes [51] and its excellent affinity to cotton fibers, reactive dyes were chosen as the subject of this experimental research related to their degradation products to have a better understanding of their potential harm to the environment.

Reactive dyes are anionic dyes, which are colored compounds that contain one or two groups capable of forming covalent bonds to a given substrate. Reactive dyes are a highly successful class of modern synthetic dyes because of the following advantages: their wide shade gamut and flexibility in applications [52]; high solubility and stability [53]; good diffusivity, levelness, dye permeability; and good light fastness (very stable electron arrangement and can protect the degrading effect of ultra-violet ray), good perspiration fastness [53], easy dyeing methods, and comparatively cheap. Thus, reactive dyes are widely used in the textile manufacturing industry with cotton, rayon, flax, wool and silk, polyamides, and acetate fibers [2].

The difference of reactive dyes from other dyestuffs is the reactive groups present in the molecule, which react chemically with the fiber's functional groups generate a covalent bond between the dyes and the fibers [2]. Usually, this covalent bonding occurs between a C- or P-

atoms of the dye and an O-, N-, or S- atoms of a hydroxyl, an amino, or a thiol group on the polymer that constitutes the fiber [49].

The development of reactive dyes for cellulosic materials had brought about a change of considerable magnitude in the research of dye chemistry and dye applications [54]. They also have been the most commonly used textile dyes for cotton fibers, considering their consumed tonnage and amount. It's reported that China uses approximately 10 million tons of reactive dyes annually in 2016 [2].

### ***3.4.1. Characteristic Structural Features of Reactive Dyes***

The general structure of a reactive dye can be represented as:



S is a solubilizing group (such as  $-\text{SO}_3\text{Na}$  or  $-\text{COONa}$  or a combination of both), which imparts solubility. Dyes for cellulose and protein fibers usually contain 1-4 sulfate groups.

D is a chromophoric group or chromogen, which is the reason why the dyes have colors. It gives different colors, brightness, fastness, and substantivity to the reactive dyes [2]. The chromophoric group for most reactive dyes is similar to that of acid dyes.

B is the bridging group, which attaches the reactive system Re to the chromogen D. The bridging group is usually  $-\text{NH}$ ,  $-\text{NHCO}$ -,  $-\text{OCH}_3$ ,  $-\text{SO}_3$ -,  $-\text{SO}_2\text{NH}$ -,  $-\text{O}$ -, and  $-\text{S}$ -. However  $-\text{O}$ - and  $-\text{S}$ - are not widely used because they are easy to hydrolyze and have a bad dye stability. Bridging groups have some key performance indicators like solubility, diffusivity, dye permeability, and safety. Re is a reactive group that reacts chemically to the fiber's functional group to form a covalent bond.

For C.I. Reactive Blue 19 (RB19), the four components are shown in different colors in Figure 19. The chromophoric group (D) is in red, the solubilizing group (S) is in blue, the bridging group (B) is in green, and the reactive group (Re) is in purple.

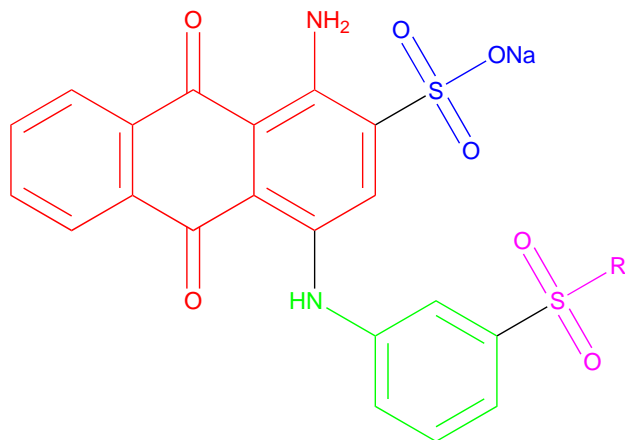


**Figure 19.** Structures of C. I. Reactive Blue 19 (RB19) and its Derivatives (D in red, S in blue, B in green, and Re in purple). R:  $-\text{CH}_2-\text{CH}_2-\text{SO}_3\text{Na}$ , dye; R:  $-\text{CH}=\text{CH}_2$ , vinyl sulfone; R:  $-\text{CH}_2-\text{CH}_2\text{OH}$ , hydroxylate.

In alkaline conditions, the sulfone precursor is converted to the vinyl sulfone, which in turn reacts either with the hydroxy groups of the substrate or hydroxide ions (Figure 19). This competitive reaction is why the relatively low fixation rates of reactive dyes [53]. This low fixation results in a typical mixture of the vinyl sulfone and the dye's hydrolyzed form on the wastewaters after manufacturing. The 70% of fixation rate and hydrolysis of dye are the main two disadvantages of conventional reactive dyes for cellulosic fibers [2]. Studies have shown that the two possible solutions to deal with these problems are to use a reactive group that is not easily hydrolyzed and the addition of one or more reactive groups in a dye molecule to increase the probability of fixation [2].

One of the most commonly used dyes in cotton dyeing, RB 19, is an anthraquinone based vinyl sulfone dye, which is difficult to degrade by chemical oxidation because its anthraquinone

structure is stabilized by resonance. RB19 has a 75-80% fixation efficiency on cellulose (cotton textiles), and the unfixed dye persists in the environment for long periods of time [51].

For RB19, the low dye absorption efficiency is due to the competition for cellulose in the dyeing solution between the native RB19 dye and the partially hydrolyzed RB19 dye (RB19-OH), which has no affinity for cellulose [51]. The sulfone would also continue to undergo alkaline hydrolysis as time goes. Thus, it is essential to analyze samples shortly after acquisition and neutralize the sample pH if necessary [53].

#### ***3.4.1.1. Chromophoric Groups/ Chromogen (D)***

In Section 3.3, azo and carbonyl dyes are introduced, which are the typical chromophoric groups in reactive dyes. The chromogen is responsible for the color, affinity, and diffusion of dye. Different types of chromogens are suitable for dyeing fibers. In general, metal-free mono-azo dyes result in yellow, orange, and red bright colors. Cupriforous mono- and bis- azo dyes result in violet, grey, ruby, and navy-blue dark colors. Anthraquinones derivatives (of phthalocyanine dyes) result in brilliant blue and green colors [2].

Chromogen is a chemical compound that is either colored or could be made colored by the attachment of a suitable substituent, which includes the chromophore and the auxochrome (see Figure 20 [47]). The chromophore is a covalently unsaturated group responsible for absorption in the UV or visible like  $C=C$ ,  $C\equiv C$ ,  $C=O$ ,  $C\equiv N$ ,  $N=N$ , or  $NO_2$ . While auxochrome ( $-NH_2$ ,  $-OH$  groups) is a covalently saturated substituent group that, when attached to a chromophore, changes both the wavelength and the intensity of the absorption maximum [47]. As previously explained in section 3.2.1 and section 3.2.2, as the energy of electronic transitions decreases, their probability

usually increases, so the  $\epsilon_{\max}$  increases. It is important to mention that the combination of chromophore and auxochrome behaves as a new chromophore with different  $\lambda_{\max}$  and  $\epsilon_{\max}$ .

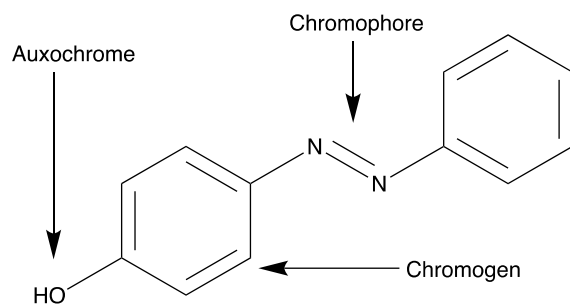


**Figure 20.** An Example of Chromogen with Chromophore and Auxochrome

### 3.4.1.2. Reactive Groups (*Re*)

Since the late 1960s, many mono- and di-functional dyes based on new reactive groups have been introduced [49]. The existence of *Re* in reactive dyes is the main difference compared to other dyes.

*Re* has the ability to form a new covalent bond with the cellulose fibers, aka reactivity. The reactivity affects the reaction speed between dyes and fibers and determines the degree of fixation of dyes on fibers to some degree. *Re* is also related to dyes' stability, solubility, and diffusivity. Therefore, the reactive system's choice is crucial for reactive dyes and restrictive on their application performance.

Typically, reactive groups can be classified into three different types: triazine (a), pyrimidine (b), and vinyl sulfone active groups (c) (see Figure 21).

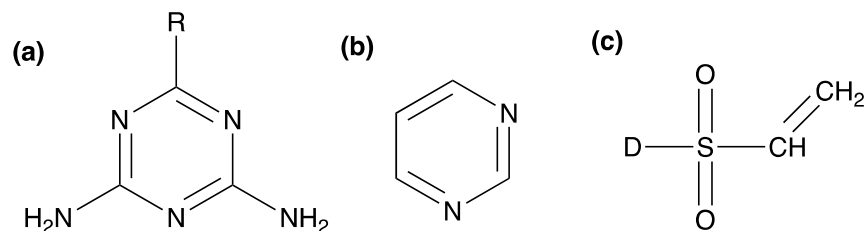


**Figure 21.** Three Basic Types of Reactive Groups

Triazine reactive dyes have the following advantages: (1) due to the electrophilic property of the cyanuric group, a wide range of chromophores having good fastness to light, perspiration-light, and chlorine can be selected; (2) the increase in substantivity resulting from the introduction of a triazine group to the dye molecule improves the degree of exhaustion and fixation of the dyes [50].

As one of the most important commercial dyes, vinyl sulfone reactive dyes are generated from the  $\beta$ -sulfato-ethylsulfone group under alkaline conditions [4]. The advantages of the vinyl sulfone reactive dyes include: (1) The chemical bonds between vinyl sulfone reactive dyes and cellulosic fibers are very stable to acid hydrolysis, so that these dyes have excellent stability on dyed goods on storage; (2) The substantivity of hydrolyzed byproducts produced during the dyeing process is very small so that the unfixed hydrolyzed dyes can be easily washed off [50]. It has a stable covalent bond with the fiber, whose reactivity is between triazine and pyrimidine.

For the pyrimidine active group, the carbon's electron density is higher than that of the active triazine group, making it a lower reaction reactivity but has higher stability (the structure is harder to hydrolysis). In general, the order of reaction activity can be sorted from high to low [43], which are dichloro- triazine (a), dichloroquinoxaline (b), vinyl sulfone (c), monochloro-triazine (d) and chloropyrimidine (e) (see Figure 22).

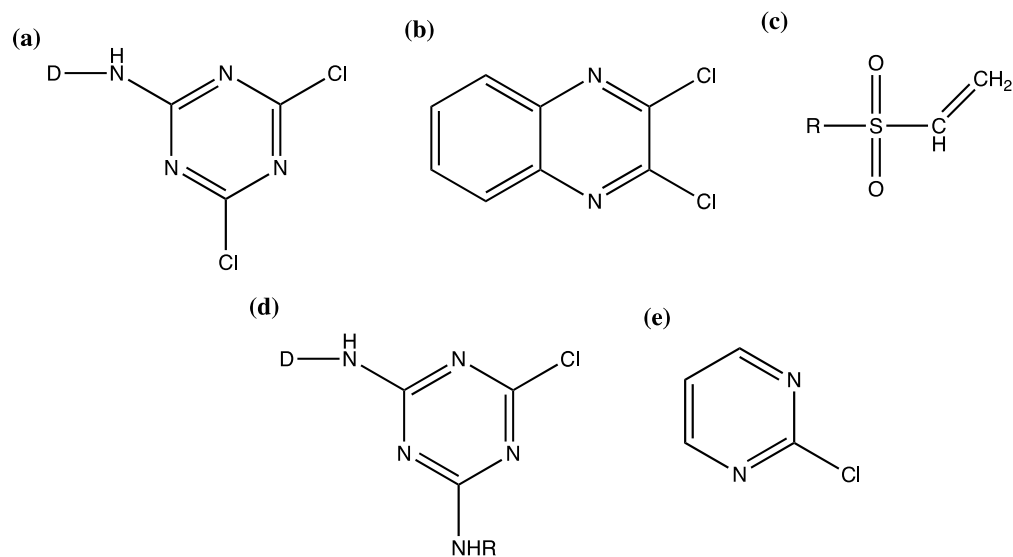


**Figure 22.** General Structures of Different Kinds of Basic Reactive Dyes Based on Reaction Activities

### 3.5. Dye-Fiber Chemical Reactions

During the dyeing process, the dye is partitioned between the two phases, the solid fiber phase (substrate) and the aqueous phase (dyeing bath) [49]. The distribution process between the dye and the substrate is called adsorption, this is when the dye is retained on the substrate's surface and sorption when entering it. Thus, when the fiber absorbs the dye, and the dye molecules penetrate into the fiber, a dyeing equilibrium (sorption and desorption) is reached. After dyeing, soaping is carried out to remove unreacted or hydrolyzed dyes that are not fixed to the fiber, improving the color's vividness.

There are interactions between the dye and fiber that prevent the dye molecules' desorption back into solution when the dye molecules penetrate the fiber. Three types of intermolecular forces should be considered in the process: Van der Waals forces, hydrogen bonding, and hydrophobic effects. Their relative strengths are listed in Table 6 [2]. Specifically, a qualitative relationship can be demonstrated between the sorption energy of a dye and its ability to form intermolecular H-

bonds. Take wool as an example, the –OH group of the dyes can form an intermolecular H-bond with the O-atom of the amide groups of wool. Some examples of H-bond donors and acceptors are listed in Table 7.

**Table 6.** Approximate Relative Strengths of Bonding Between Dye and Fiber [2]

Bond Type	Approximate relative strength
Covalent	30
Ionic	7
Hydrogen	3
Other intermolecular	1

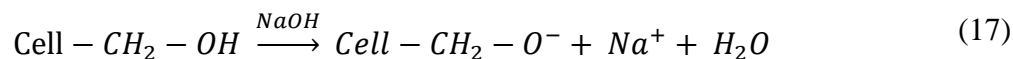
**Table 7.** Some H-bond Donors and Acceptors [55]

Donors	Acceptors
C-H	C=C, C≡C
N-H	N
P-H	P
O-H	O
S-H	S
Cl-H	Cl
Br-H	Br
I-H	I

In this research, cellulose (cotton) fibers and reactive dyes are studied as subjects. As described in section 3.4, the dyeing of reactive dyes for cotton fiber is a chemical reaction process, which is the covalent interaction between cellulose and reactive dye molecule [49]. More details about reactive dyes – cellulose fibers interactions will be discussed below.

### 3.5.1. Ionization of Cellulose Fibers

The reaction between a reactive dye and cellulose begins with the deprotonation of the cellulose hydroxyl groups. This is done under alkaline conditions, as described in equation 17.



### 3.5.2. Nucleophilic Substitution Reaction Between a Reactive Dye and a Fiber

On the periodic table, electronegativity generally increases as you move from left to right across a period and decreases as you move down a group. The nitrogen atom's electronegativity is stronger than that of the carbon atom on the aromatic heterocyclic ring of the reactive group. The electron density of the carbon atom on the heterocyclic ring is lower and partially positive. Similarly, the chlorine atom's electronegativity linked to the carbon atom is stronger, making this atom more electro-positive, which a nucleophile can easily attack.

By far the most important fiber-reactive groups that react by nucleophilic substitution contain six-membered aromatic heterocyclic ring with halogen as substituents (see Figure 23) [43]. A feature of nucleophilic substitution reaction is the requirement for a good, stable leaving group, such as the chloride anion [43].

Currently, both dichloro- and monochloro-triazinyl dyes have been commercialized. The first group of commercial reactive dyes, the Procion dyes, remains among the most important today, containing the 1,3,5-triazine (or s-triazine) ring six-membered ring of alternate carbon and nitrogen atoms. They have at least one chlorine (or fluorine) substituent and with the amino (–NH–) group as the bridging group [43]. The reaction of a chlorotriazinyl dye with a cellulose anion, is illustrated in Figure 23, in which dichlorotriazinyl dyes (a: X = Cl in Figure 23, marketed as Procion M) and the monochlorotriazinyl (b: X = –NHR, commonly amino (either primary or

secondary) or methoxy in Figure 23, marketed as Procion H) are shown. The difference between the electron-withdrawing group Cl and the electron-releasing group X can explain why the dichlorotriazinyl dyes are more reactive than the monochlorotriazinyl. The increase in the ring's electron density in the monochlorotriazinyl dyes lowers the reactivity towards nucleophilic attack. Dichlorotriazinyl dyes (Procion M, applied at around 40-60 °C) can react with cellulosic fibers at lower temperatures than monochlorotriazinyl dyes (Procion H, applied at around 80-90 °C).

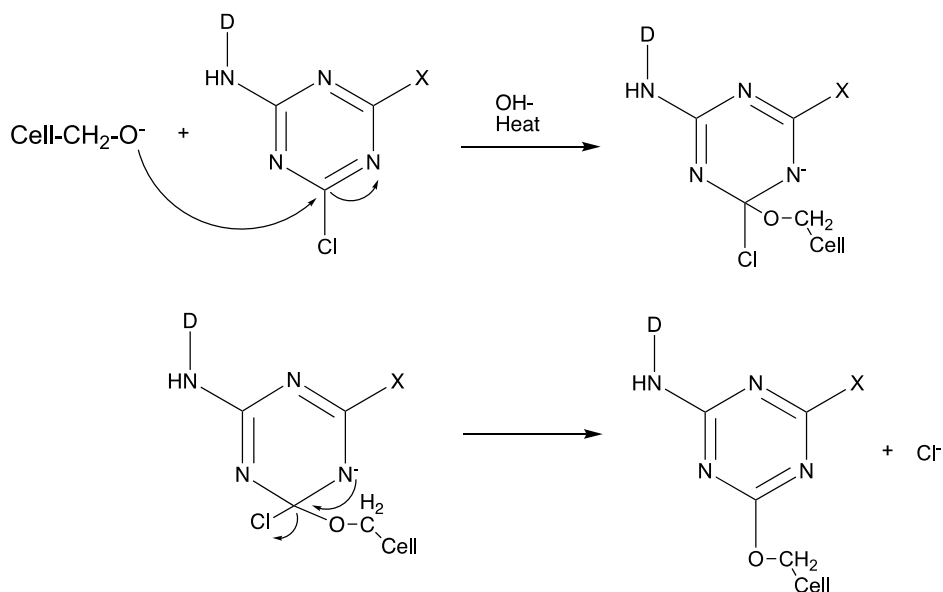


**Figure 23.** Diagram of the Nucleophilic Substitution Mechanism on Triazine Reactive Groups  
(a: X = Cl; b: X = -NHR.)

In general, a nucleophilic substitution reaction mainly occurs on the C atoms with very low electron densities. First, the larger the number of N atoms on the heterocycle decreases the carbon atom's electron density. Thus, the C atom on the mesazine has the lowest electron density, making the reactive group most reactive. Second, the introduction of electron-withdrawing groups (EWGs, such as Cl, F) on the heterocycle will also reduce the C atom's electron density to enhance the reactivity of the active group. Third, the position of the substituent also matters. The introduction of an electron-withdrawing group at the 6-position can significantly reduce the electron density of

the C atom (0.883 electrons per cubic ångström,  $e \text{ \AA}^{-3}$ ) at the 2-position because of the conjugation effect, so the nucleophilic substitution mainly occurs at the 2-position C atom. Last, the larger the leaving tendency the leaving group is, the faster the substitution reaction rate is. The stronger the electronegativity of the leaving group (electron-withdrawing atoms Cl, F), the easier it is to get the electrons to become anions and then leave. However, F has a smaller tendency to leave than Cl, it has a stronger electron-withdrawing ability and reduces the C electron cloud density ability, so the reactivity of the heterocyclic containing an F atom is higher than the one containing a Cl atom.

In this way, the C atom is more susceptible to being attacked by a nucleophile, thus causing a faster nucleophilic substitution reaction. During color fixing, the generated negative cellulose anions produced in an alkaline condition will undergo nucleophilic substitution reactions with the reactive dyes' active groups.

### 3.5.3. Nucleophilic Addition by Conjugate Addition

Alkenes are generally regarded as relatively reactive compounds. Their reactivity is attributable to the presence of the C=C double bond, which is usually formed during the dyeing process and can undergo nucleophilic addition reactions with nucleophiles (cellulose anions). Nucleophilic addition to substituted alkenes of this type is alternatively referred to as either conjugate addition or Michael addition [43,52].

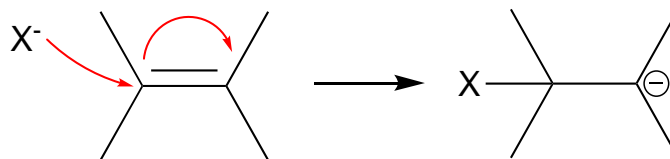


**Figure 24.** An Example of Nucleophilic Addition Reaction

In commercial applications, the most important reactive dyes reacted with cellulosic fibers in which the fiber-reactive groups react by nucleophilic addition processes are the Remazol

reactive dyes that are based on the vinyl sulfone reactive group. Soon after the Procion dyes launched the triazine system by Imperial Chemical Industries (ICI), the Remazol reactive dyes were then introduced by Hoechst [56].

The typical example of the nucleophilic addition process in which vinyl sulfone reactive dyes react with cellulose under alkaline conditions is illustrated in Figure 25. During dyeing under the action of alkali, the dye will generate vinyl sulfone groups with active double bonds ( $-\text{SO}_2\text{CH}=\text{CH}_2$ ), and due to the presence of the strongly electron-withdrawing group  $\text{SO}_2$ , will make the  $\beta$ -C atom more positive by inductive effects, thus facilitating the nucleophilic addition reactions with cellulose anions [43].

The addition reaction is completed by protonation [43], and the outcome is the permanent formation of a covalent dye–fiber (C–O) bond, as illustrated in Figure 25. However, in this reactive dyeing process, as with dyes that react by nucleophilic substitution, hydrolysis also occurs in competition with the dye–fiber reaction, thus resulting in hydrolyzed dye form (see Figure 25).

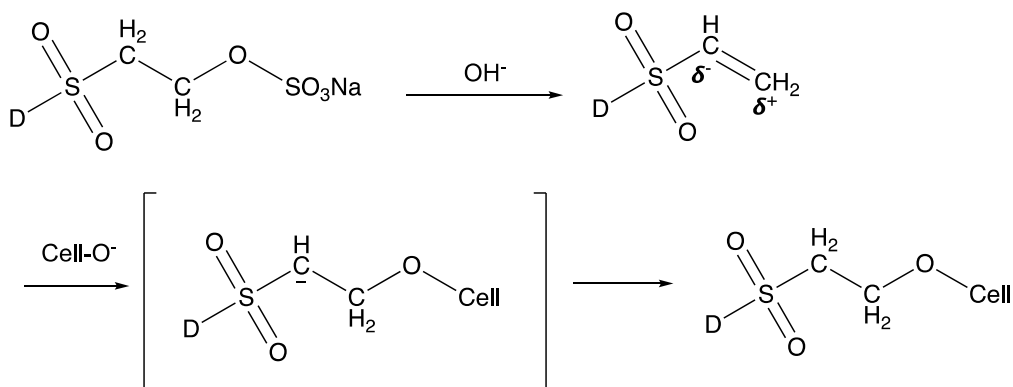


**Figure 25.** Diagram of the Nucleophilic Addition Mechanism on Vinyl Sulfone Reactive Dyes with Cellulose Fibers

#### 3.5.4. *Hydrolysis of Reactive Dyes*

Hydrolysis of a reactive dye happens when the dye reacts with the hydroxide ion from the dye bath's basic solution. This reaction will make the reactive dye not able to be bonded to cellulose [49]. When dyeing the cellulosic materials, maximum stability is reached at pH 6-7. Under more acidic or basic conditions, the rate of dye-fiber hydrolysis increased by a factor of ca. 10 per pH unit, which corresponds to a hydrolysis mechanism that proceeds under specific acid or base catalysis, respectively [49].

The dye-fiber linkage's stability, which largely determines the washing-fastness of reactive dyes, depends on their thermal and chemical resistance to alkaline or acid hydrolysis. Low wet-fastness properties are usually caused by hydrolyzed dye molecules that have not been completely washed out [49].

Take dichrolotriazine as an example, they can have different forms during the reaction with cellulose fibers when using different alkaline solutions. When using a mild alkaline solution such as  $\text{NaHCO}_3$  as the alkaline solution, the product is in Figure 26a; when using stronger alkaline such as  $\text{Na}_3\text{PO}_4$ , the product is in Figure 26b; when the reaction condition becomes more severe (1%  $\text{NaOH}$ , 100 °C), a ketone can be formed (see Figure 26c [49]). In alkaline conditions, the stabilities of covalent bonds between dyes and cellulose vary, the product in Figure 26b is the most stable one, while in Figure 26a is the most unstable. However, in acid conditions, the most unstable bonds are the products in Figure 26c.

Overall, dyes with triazine reactive groups have better alkaline tolerance, while dyes with vinyl sulfone reactive groups have better acid tolerance [49].

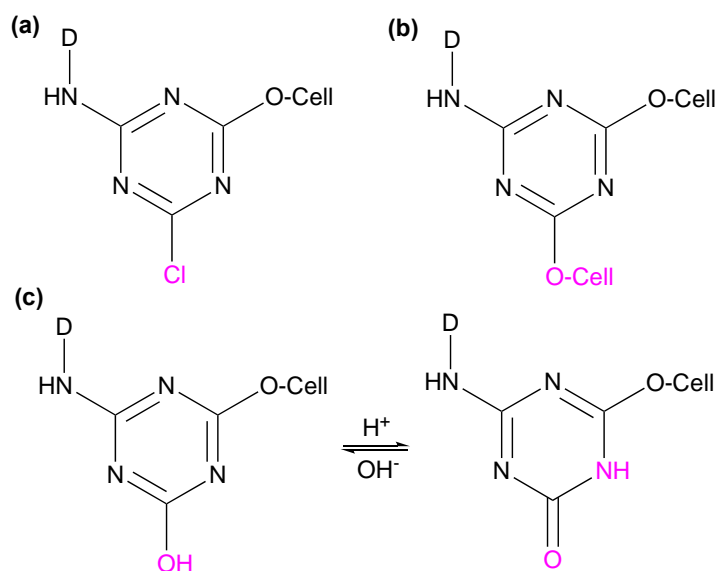


**Figure 26.** Different Reaction Products of Dichlorotriazine Reactive Groups under Different Alkaline Solutions [49]

The dyes' hydrolyzed form has a much lower affinity to the cellulose, which is so-called the fading of the reactive dyes on the textile fabrics. This is no doubt that this dye's significant weakness and will reduce the cost efficiency of the process, plus requires a thorough wash-off process, with the consequence of considerable dye residues being discharged to effluent.

As previously mentioned in section 3.4.1, the most successful approach to addressing this issue is to use a reactive group that is not easily hydrolyzed and incorporating more than two reactive groups in a dye molecule to increase the chance of fixation, which statistically improve the chances of dye–fiber bond formation. Typical the dye used for the second approach can be called bifunctional dye, which is defined as a dye molecule having two independent reactive systems [50]. There are two types of bifunctional dyes, one having two or more reactive systems of the same type (homo-bifunctional dyes) and another having two or more reactive systems of different types (hetero-bifunctional dyes). The typical example of the homo-bifunctional dyes is the Procion H-E range [43], which contains two monochlorotriazinyl reactive groups (Figure 27a)

and some dyes of the Remazol range that contain two  $\beta$ -sulfo-ethyl-sulfone groups. Another example of the hetero-bifunctional dye, which includes a monochlorotriazinyl and a  $\beta$ -sulfo-ethyl-sulfone group [50] (see Figure 27b). Because of the two groups' differing reactivities, hetero-bifunctional dyes have greater flexibility in performance, for example, reducing sensitivity to temperature and to pH variation [43].

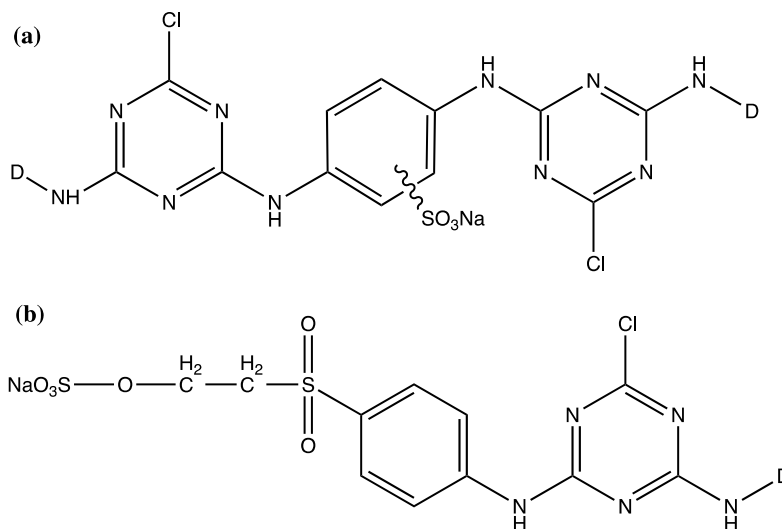


**Figure 27.** Typical Examples of Homo-bifunctional (a) and Hetero-bifunctional (b) Reactive Dyes [43]

Besides bifunctional dyes, there are a few commercial examples of trifunctional reactive dyes, such as the Cibacron and Remazol ranges [43]. Logically, the fixation efficiency might be improved further by incorporating even more reactive groups into the dye molecules. However, there are opposing effects associated with the increase in molecular size as more groups are added that can inhibit migration leading to reduced fixation and low color build up [43]. In the current chemistry industry, it's still a big challenge and needs more effort, to develop a practical reactive dye system that is entirely free of the problems associated with hydrolysis or incomplete dye-fiber reactions.

### 3.5.4.1. Hydrolysis of RB19

RB 19 reacts with cellulose fibers by addition to the sulfur-oxygen double bond. In the aqueous solution, reactive dyes can undergo hydrolysis of the sulfone, making it unreactive to the cellulose. This means that unreacted dye, if not washed off properly, will remain on the fabric's surface, leaving an apparent color that will wash out over time [2].

For the subject of this research, the hydrolysis path of RB19 is predicted in Figure 28. Commercial RB19 is stored under a stable state of the  $\beta$ -sulfato-ethyl-sulfone structure (a), under alkali conditions, the vinyl sulfone dye (b) will be formed. Then, in a short time under alkali conditions, the vinyl sulfone yields a  $\beta$ -hydroxyethyl sulfone dye (c) after adding water. The etherification reaction of vinyl sulfone dye (a) and  $\beta$ -hydroxyethyl sulfone dye (c) can then generate an ether dye (d), which is inactive in the dye solution. Treatment under the hot strong alkali condition can then facilitate the cleavage of ether dyes (d) to yield  $\beta$ -hydroxyethyl sulfone dye (c) in turn.

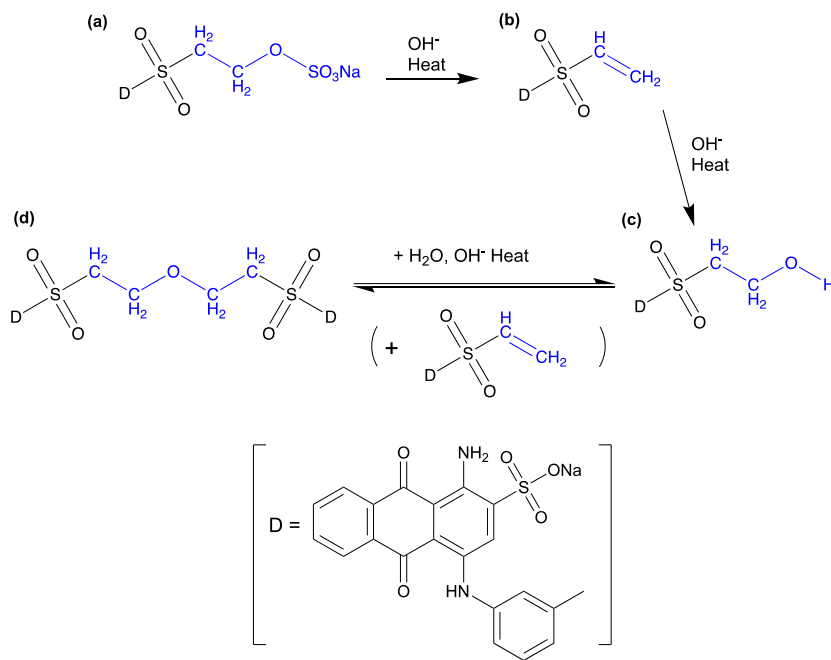


**Figure 28.** Hydrolysis Route of RB19

### 3.6. Acid Dyes

Acid dyes are generally small to medium-sized planar molecules [43], and they are applied in the presence of organic and inorganic acid in dye bath solutions [2]. In a sequence of importance, acid dyes are commercially applied mainly on the natural protein (wool and silk), synthetic polyamide (nylon), and to a small extent to acrylic and blends of these materials. However, not suitable for cellulosic because they have no affinity for cotton cellulose [2]. Their colors are generally bright; depending on the chemical structures of the dyestuff, the fastness to light and washing range from poor to excellent [47].

The chemistry of acid dyes is quite complex, which are normally large aromatic molecules consisting of many linked rings. A characteristic feature of acid dyes for protein and polyamide fibers is the presence of one or more sulfonate ( $-\text{SO}_3^-$ ) groups, usually present as the sodium ( $\text{Na}^+$ ) salt, which can either provide solubility in water or ensure the dyes can carry negative charges [43].

Easily, acid dyes can be classified as acid leveling and acid milling types based on the requirement of acid added to the dyebath when dyeing protein fibers [43]. Briefly speaking, acid leveling dyes are a group of dyes that show only moderate affinity. In contrast, acid milling dyes are a group of dyes that offer a much stronger affinity for the protein fibers [43]. For acid leveling dyes, because the intermolecular forces between the dye and the fibers are not strong, these dyes can migrate through the fiber and thus produce a level dyeing. Differently, because of the superior strength of the intermolecular forces between the dye and the fiber molecules, the acid milling dyes have less migration capabilities through the fibers but superior fastness to washing, because which appropriate processing conditions have to be adopted to ensure that level dyeing is achieved [43].

Besides protein fibers, polyamides are also commonly dyed using acid dyes. These are attracted to the fibers by a mechanism similar to the acid dyeing of wool, involving the attraction of the dye anions to amino groups, which are present for example, at the end of the polyamide chains that are protonated under acidic conditions [43].

Based on their structures, acid dyes are mainly confined to three chemical classes: azo (a), anthraquinone (b), triphenylmethane (c), and the corresponding examples are illustrated in Figure 29. Their market proportion are 65%, 15%, and 12%, respectively [2]. Generally, the azo class provides most of the yellows, oranges and reds, while the anthraquinone class (developed in the 1990s) mainly provides bright blues [43]. Triphenylmethane group provides brilliant blues, greens and violets; as the oldest class, its first member Nicholson Blue was firstly made in 1862 [2].

An example of an azo acid dye is C.I. Acid Orange 7 (Figure 29a), which illustrates the effects of intramolecular hydrogen bonding. The hydrogen bonding also makes it possible for significantly improved fastness to alkaline washing and lightfastness. C.I. Acid Blue 1 is an example of a triphenylmethane acid dye (Figure 29c) [43]. Even though the nitrogen atoms carry a formal single delocalized positive charge, however, the presence of two sulfonate groups still make sure that the acid dye is anionic. As presented in Figure 29b, many blue dyes have the structure as their basic shape; C.I. Acid Blue 25 (AB25) is an anionic anthraquinone dye, which has an empirical formula of  $C_{20}H_{13}N_2NaO_5S$ , the molecular weight of 416.38 g/mol, chemical index (CI) of 62055.

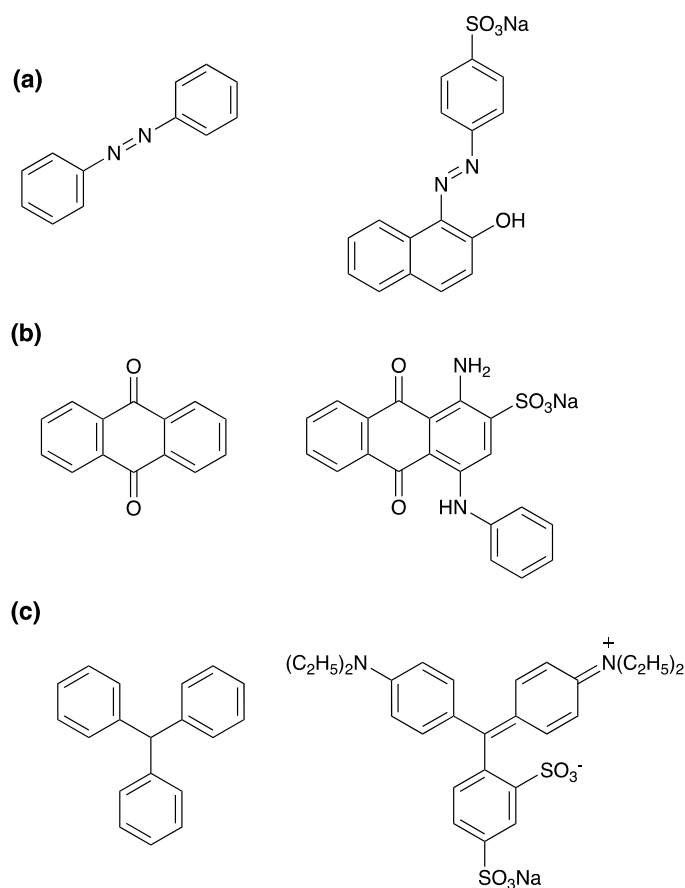


**Figure 29.** Three basic acid dyes types and typical examples. (a) Azo, C.I. Acid Orange 7; (b) Anthraquinone, C.I. Acid Blue 25; (c) Triphenylmethane, C.I. Acid Blue 1.

Acid dyes are thought to be attached to fibers by ionic bonds, hydrogen bonds, and Vander Waals forces. They are generally sold as a sodium salt; thus, they are in the form of anions in solution. Because protein and polyamide fibers contain many cationic sites, an anionic dye molecule is attracted to a cationic site on the fiber [2]. A diagram showing the affinity mechanism between AB25 and protein fiber is shown in Figure 30.

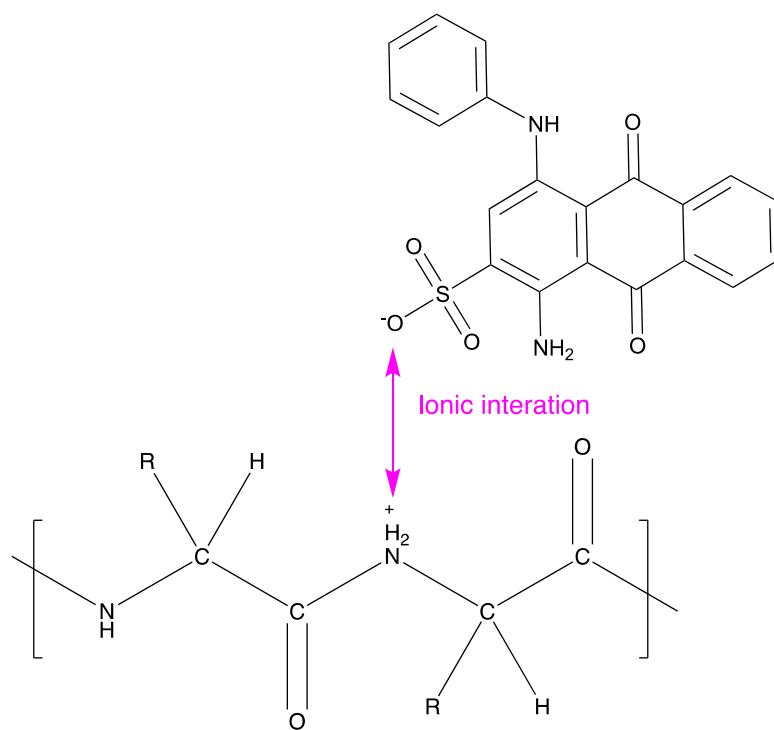


**Figure 30.** Affinity Mechanism Between AB25 and Protein Fiber

## CHAPTER 4. Soil and QuEChERS Method

### 4.1. Main Compositions of Soil

As a major part of the cycling elements on the earth's surface, the soil is a heterogeneous and complex matrix composed of minerals, organic matter, air, and water [57, 58].

Minerals are made up of two parts: one is abundant primary mineral, such as  $\text{SiO}_2$  and feldspars ( $\text{MAlSi}_3\text{O}_8$ , M is a combination of  $\text{Na}^+$ ,  $\text{K}^+$ ,  $\text{Ca}^+$ ); the second is the secondary mineral, such as silicates, carbonates ( $\text{CaCO}_3$ ), aluminum ( $\text{Al}(\text{OH})_3$ ), iron hydroxides ( $\text{Fe}(\text{OH})_3$ ), and sulfur-containing compounds. Organic matters include plant or animal residues in various breakdown stages (decomposition), detritus, and stable soil organic matter referred to as humus [59]. Furthermore, in pore space, a good mixture of macropores (serve as pathways for the movement of air, water, and organisms, including plant roots through the soil) and micropores (serve as a storage point for water in the soil) [59] is important in the soil.

“Ideal” soil is about 45% minerals and 5% organic matter, and 50% pore space (half water and half air by volume), illustrated in Figure 31 [59]. In this “ideal” balance, enough minerals provide nutrition; enough organic matters promote important soil physical, chemical, and biological properties and processes, affecting soil fertility and productivity. Adequate water and air support important biological activities [59]. It is known that one gram of soil can contain up to 108 different microorganisms [7]. However, in the real world, because soil water and air levels fluctuate constantly throughout the year, and organic matter levels fluctuate overtime periods of years to decades [59] in response to human soil management, “ideal” balance are hard to be achieved.

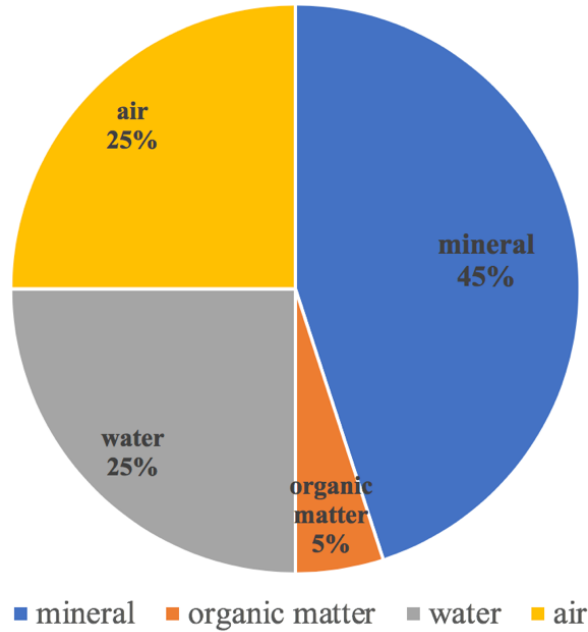


**Figure 31.** Components in "Ideal" Soil with 50% Solid Material and 50% Pore Space [59]

In summary, the soil is a biologically balanced system and plays an important role in developing life. Any drastic change in the soil can also affect the microbial community structure, and the biochemical processes carried out [60]. Because of its enormous surface area and microbial catalytic activity, soil degrades most wastes quickly and returns the components to their natural cycles, thereby minimizing environmental disturbance [57].

#### 4.2. Textile Wastes to Landfills

Solid waste issues have attracted more attention to human civilization, even before the water and air pollution issues [61]. Solid wastes are called so because large parts of the waste are generally solid, and they are useless, unwanted, but can be reused, such as textiles fabrics. Because the main disposal methods for solid waste are open dumping and sanitary landfill [61], improper waste management would largely result in environmental pollution to human and animal health [59]. Among numerous environmental challenges, one of them being the increasing pollution is in

the atmosphere and landfills [7]. When considering the landfill sites, soil plays a significant role and needs to be evaluated, whose degradation process will also be affected by the physicochemical properties of soil and chemicals under consideration. Soil has been recognized as a potentially important medium of exposure.

Soil is often subject to intense chemical pollution, which is the diversion of chemical elements from the natural biogeochemical cycles. Its contamination is a serious environmental problem for both industrialized and non-industrialized nations. Once released into the air or water, organic pollutants will someday end up in the soil [62]. For example, the carbon, nitrogen, and phosphate in municipal water released to streams and lakes are removed from the soil-plant cycle, which is the nitrogen source and much of the phosphate [57]. A large body of evidence has shown the risks of adverse health effects with the exposure of humans to contaminated soil, such as pesticides for agricultural products [62], coal burning, motor vehicle emissions, waste dumping, and textile wastes [10].

In summary, soil contamination is a naturally occurring problem where anthropogenic organic and inorganic chemicals can become a serious environmental problem [58]. Thus, focusing the attention on reducing existing environmental pollution, green chemistry, and environmental remediation is important. Because of the complex chemical structures of reactive dyes, their degradation in soil could result in possible hazardous compounds, including such as benzidine, azobenzene, and other aromatic compounds [9,10,63]. Therefore, the disposal of cotton fabrics with reactive dye is a complex phenomenon when considering soil's complex properties and a serious challenge to waste management. To study and extract the studied textile dyes from the soil, QuEChERS, which stands for Quick Easy Cheap Effective Rugged Safe approach, will be introduced in section 4.4.

### 4.3. Separation Practicalities

Based on the differences of samples (volatile or non-volatile) and matrices (solid or liquid), different sample separation methods can be used, such as gas-phase extraction, liquid-liquid extraction (LLE), liquid extraction from solid matrices, and solid-phase extraction (SPE) [20]. The different sample extraction procedures commonly used are illustrated in Table 8.

**Table 8.** Different Sample Extraction Procedures Commonly Used [36]

	Matrix	
	Solid	Liquid
Sample	Gas-phase extraction	Gas-phase extraction
	Solid-phase microextraction (SPME)	Solid-phase microextraction (SPME)
	Supercritical fluid extraction (SFE)	Supercritical fluid extraction (SFE)
	Solid-liquid extraction	Liquid-liquid extraction (LLE)
Non-volatile	Supercritical fluid extraction (SFE)	Solid-phase extraction (SPE)
		Solid-phase microextraction (SPME)

#### 4.3.1. Liquid-Liquid Extraction (LLE)

Liquid-liquid extraction (LLE) can be used to extract dyes from aqueous solutions, in the situation of a non-volatile sample and a liquid matrix. To explain the principle, a target compound, typically a desired product of a chemical synthesis process or a target analyte in a liquid A matrix, is mixed with a second liquid B that is immiscible with its original liquid A. The target compound

is then transferred from its original liquid A to liquid B, with a high degree of selectivity as possible [20].

For the desorption procedure towards the target compounds, the desorption solvent's polarity must approximately equal the compounds' polarity considering the 'like dissolves like' principle [64]. The properties of common solvents used in extractions are shown in Table 9 [65].

**Table 9.** The Properties of Common Solvents used in Extractions [65]

Solvents	Polarity Index	Dielectric Constant <sup>a</sup>	Viscosity ( $mN s^{-1} m^{-2}$ )	Density <sup>b</sup> ( $g mL^{-1}$ )	Solubility in Water (%w/w)
Hexane	0	1.89	0.313	0.659	0.001
Ethyl Acetate	4.4	6.02	0.455	0.901	8.7
Acetone	5.1	20.7	0.337	0.791	100
Methanol	5.1	32.7	0.544	0.791	100
Ethanol	5.2	24.55	1.08	0.789	100
Acetonitrile	5.8	37.5	0.375	0.786	100
Water	9	78.3	0.890	0.998	--

<sup>a</sup>At 25 °C

<sup>b</sup>At 20 °C

An example of LLE is a new, fast and efficient ionic liquid-based dispersive liquid-liquid extraction (IL-DLLE) method [66], which has been applied to extract and remove Congo dyes from aqueous solutions, such as textile effluents that are causing both environmental and economic issues [66]. A binary solution containing the extraction solvent (1-hexyl-3 methylimidazolium bis(trifluoromethylsulfonyl)imid,  $C_{12}H_{19}F_6N_3O_4S_2$ ) and a suitable disperser solvent is injected into a water sample with Congo dyes (CR). After obtaining a cloudy solution, most of the dye molecules are then extracted into fine ionic liquid droplets and removed from the aqueous phase,

thus potentially providing a method of minimizing pollutions of textile effluents. Except for Congo dyes, other dyes such as acid dyes, reactive dyes can be extracted from aqueous solutions as well [67], by adjusting the different parameters (choice of extraction solvents, pH of aqueous solutions, sample volume, extraction time) [66].

However, because many polar analytes are often partly soluble in water and cannot be extracted with good recoveries whatever the organic solvents selected [68]. Another method, solid-phase extraction (SPE), has virtually displaced LLE in water methods due to its greater versatility, convenience, solvent reduction, and sample volume capacity [65]. Furthermore, because soil is a complex matrix composing of minerals that are also soluble in water, the extraction solution will be a mixture of both reactive dye degradation products and some salts, thus affecting the analysis of MS instruments due to ion suppression. Also, it will make LLE not appropriate for the extraction of reactive dyes degradation products from soil due to the high solubility of these dyes in water.

#### ***4.3.2. Solid Phase Extraction (SPE)***

Solid-phase extraction (SPE), sometimes referred to as liquid-solid extraction, is a reliable, efficient, and cost-effective sample preparation technique for the extraction of analytes from a complex matrix, often achieving higher recovery of analyte than other methods of sample preparation because of its selectivity [68, 69].

The analyte dispersion in SPE is between a liquid (sample medium or MP) and a solid phase (sorbent or SP). SPE can separate a mixture into the desired of interest and undesired components, according to the affinities of solutes dissolved or suspended in a liquid (sample medium or MP) for a solid particle (sorbent or SP) through which the sample is passed. Therefore, either the desired compound of interest or the undesired compounds are retained on the sorbent.

With SPE development, there are larger SPE sorbents choices: polar particles such as silica, Florisil, or alumina for normal-phase separations; and nonpolar bonded silica phases or polymers for reversed-phase separations. One of the most widely used types of SPE columns is packed with nonpolar octadecylsilylated-derivatized silica, or C18 [65]. Thus, when liquids such as water, plasma, or milk, are eluted through C18 SPE solid columns, nonpolar organic compounds such as pesticides, drugs, or some industrial pollutants will be adsorbed on it, whose adsorbed organic compounds can be later eluted from the column with organic solvent [65]. In many cases, the choice of solvent, pH and SPE phase provides clean-up of matrix components during the extraction processes.

The advantages of SPE include rapid process (usually less than 30 minutes), easy to perform, and can be automated. Currently, SPE is typically used to isolate analytes of interest from a wide variety of matrices, including water, urine, blood, beverages, food samples, animal tissue, and soil [68]. There are some classic applications for SPE, including trace enrichment of organic pollutants, extraction of insecticides and pesticides from soil, explosives residues in groundwater, soil and grease analysis in the environmental market; extraction of pesticides in fruits and vegetables, caffeine in beverages, sodium benzoate in colas and fruit juice in food market; purification and fractionation of proteins and peptides, purification of DNA from microbial broths in biotechnology market; drug analysis from serum, plasma, and urine in pharmaceutical dosage forms; and analysis of lipids, vitamins and steroids in serum, and drugs in tissues [69].

One of the SPE variations that significantly decreases the time and simplifies the extraction process is dispersive SPE (dSPE) [70], whose extraction process is conducted in the liquid sample using dispersed material instead of using SPE column, disk, or cartridge. In the dSPE process, the mass of the sample and the solvents are important. The sample's mass will affect the extraction

process's efficiency, although the solvent containing the sample is key to ensuring the retention of compounds on the adsorbent [70].

#### **4.4. Quick, Easy, Cheap, Effective, Rugged, and Safe (QuEChERS) Method**

To extract pesticide residues from fruits and vegetables, a new method was developed between 2000 and 2002 and was first reported in 2003 by M. Anastassiades et al. [71]. This method is rapid, simple, inexpensive (less than 1 US dollar for a 10g sample), effective, safe, rugged, and uses minimal amounts of solvents, needs no special equipment, avoids glassware (and cleaning/storage thereof), and provides high-quality results for a wide range of pesticides in foods [71]. Therefore, the method is proposed to be called “QuEChERS,” which stands for Quick, Easy, Cheap, Effective, Rugged, and Safe.

The general procedures in the original QuEChERS extraction method are illustrated in Figure 32 [71]. Where, a- sieving, b-T tube with soil sample, c-addition of the extraction solvent and hand mix, d-addition of the QuEChERS content, e-vortex, f-centrifugation step for 5 minutes at 5000 rotations per minute (rpm), g-aliquot of the supernatant, h-filtration with a syringe filter, and i-vial with the extract for analysis.

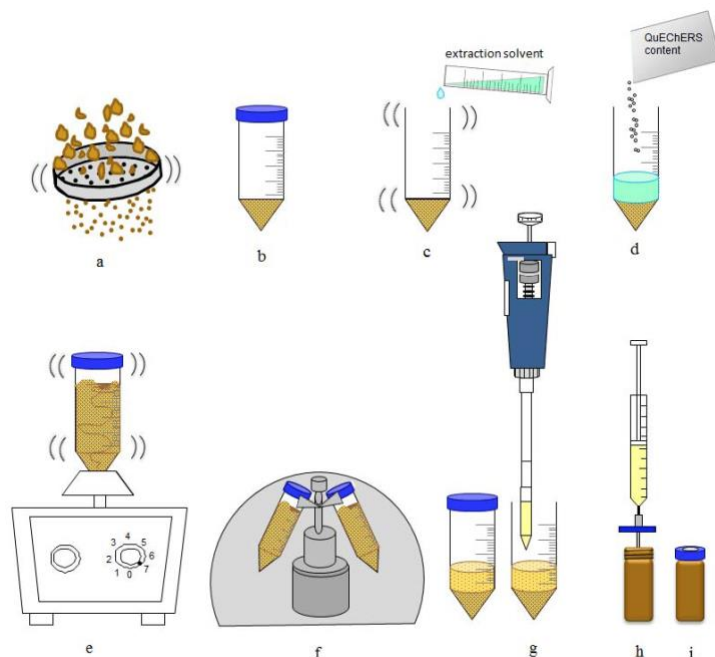


**Figure 32.** Main Steps in QuEChERS Extraction Method for Pesticides Extractions [58]

In the original method, the extraction solvents used were acetonitrile. The QuEChERS contents used were salts, including  $\text{MgSO}_4$  and  $\text{NaCl}$ . After the final centrifuging to separate solids from the solution for 1 minute, an aliquot of the final extract is taken for MS analysis. This method had been approved to be effective for pesticides. However, we still need to investigate its applications' possibilities to reactive dyed cotton fabrics in soil with appropriate modifications to the original method.

## **CHAPTER 5. Modifications of QuEChERS Extraction Method and its Application to the Extraction of Reactive Dyes from Blank Soil**

### **5.1. Introduction**

As discussed in Chapter 3, synthetic dyes are essential and commonly used in all sorts of materials and critical needs, which have wide applications, such as textiles, paper printing, food, color photography, cosmetics, coating, and leather industries [9]. Some of these dyes will have detrimental effects on the health of humans, plants, and earth after being released into the air, water, and soil. Paper and pulp mills, textiles, and dyestuff industries will mostly release large amounts of highly colored wastewaters worldwide annually. Many scientific works are discussing the decolorization and treatment of dye wastewater; however, there are only few studies that focus on the degradation of dyes in soil [72].

One of this chapter's aims is to develop a new method for extracting dyes from a complex matrix such as water and soil. Some common sample preparation techniques like ultrasonication, SPE [73], and QuEChERS methods are used for water, sediment, or soil samples.

Developed initially to extract pesticides (such as dichlorvos, acephate, diazinon, metalaxyl, and folpet) residues from fruits and vegetables, the QuEChERS method was developed by M. Anastassiades et al. in 2003 [71,74]. Currently, there are only a few studies related to the extraction of synthetic dyes using this method. For example, the extraction of triphenylmethane dyes from fish tissues [75], extraction of Sudan dyes (a group of harmful and carcinogenic azo dyes) from chili pepper or other foods [76], which provides a potential effectiveness of the QuEChERS method in the extractions of synthetic dyes. However, compared with the subject in this study, reactive dyes, the triphenylmethane dyes have a much lower polarity and higher hydrophobicity. Moreover, the differences of reactive dyes from other synthetic dyes include reactive groups

capable of forming a covalent bond with cellulosic fabrics and several solubilizing groups, making these dyes more hydrophilic and water-soluble. QuEChERS has not been used on reactive dyes due to the differences in chemical structures/properties and polarities between reactive dyes and pesticides.

In this study, the textile industry commonly used a reactive dye to give navy blue shade, C.I. Reactive Blue 19 (RB19, trade name Ramazol Brilliant Blue R, RBBR), an anthraquinone dye with a vinyl sulfone reactive group, was chosen for this research. To explore the possibility of extraction of reactive dyes from soils. Several modifications were made on the original QuEChERS method for improving the recoveries and effectiveness, such as the choices of extraction solvents, QuEChERS content (different salts), and agitation modes. Both the standard RB19 dye solutions and RB19 extracted from blank soil were analyzed using Quadrupole Time-of-Flight (Q-TOF) mass spectrometry and Velos Pro Dual-Pressure Linear Ion Trap (LTQ) mass spectrometer. The method was proven to have good linearity ( $R^2 = 0.9997 \pm 0.0002$ ), good sensitivity (LLOQ was evaluated to be  $3.4329 \pm 1.0287 \mu\text{g/mL}$ , and LOD was  $1.0299 \pm 0.2920 \mu\text{g/mL}$ ). Both accuracy and precision were within the acceptable range  $\pm 12\%$  for all seven concentrations ranging from 1, 3, 5, 10, 30, 50, to 70  $\mu\text{g/mL}$  and two quality controls (QCs).

## **5.2. Materials**

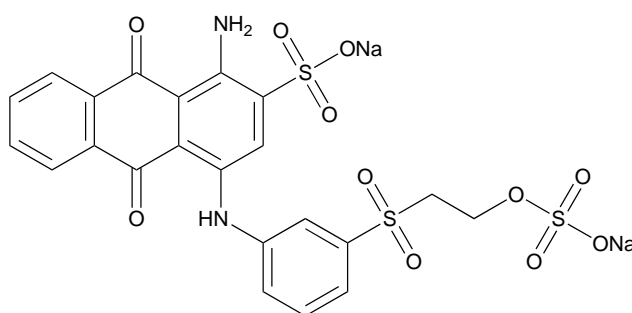
### **5.2.1. Solvents**

Acetonitrile (LC-MS grade, 99.9%) and methanol (LC-MS grade,  $\geq 99.9\%$ ) for QuEChERS extraction were purchased from Sigma-Aldrich (Sigma-Aldrich, MO, USA) and used without any further purification. HPLC grade water was acquired using a Pure Lab Ultra water purification system from ELGA Lab Water (ELGA Lab Water, High Wycombe, UK).

### 5.2.2. Chemicals and Dyes

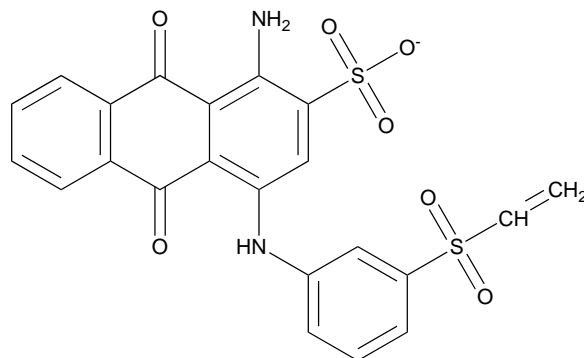
Magnesium sulfate (ReagentPlus<sup>®</sup>,  $\geq 99.5\%$ ) was purchased from Sigma-Aldrich, USA. C.I. Reactive Blue 19 (RB19, CAS no. 2580-78-1, molecular formula  $C_{22}H_{16}N_2Na_2O_{11}S_3$ , molecular weight 626.5325 g/mol, dye content 50%) was purchased from Sigma-Aldrich, USA. The structures of C.I. Reactive Blue 19 in sulfatoethylsulfone (SES) form and vinyl sulfone (VS) form are shown in Figure 33a and Figure 33b, respectively.

(a) C.I. Reactive Blue 19 - SES Form



Chemical Formula:  $C_{22}H_{16}N_2Na_2O_{11}S_3$   
Exact Mass: 625.9712  
Molecular Weight: 626.5325

(b) C.I. Reactive Blue 19 - VS Form



Chemical Formula:  $C_{22}H_{15}N_2O_7S_2^-$   
Exact Mass: 483.0326

**Figure 33.** Structures of C.I. Reactive Blue 19 in SES Form (a) and VS Form (b)

### ***5.2.3. Other Supplies***

Disposable Luer-slip plastic syringes (1 mL) were purchased from Sigma-Aldrich, MO, USA. PTFE 0.2  $\mu\text{m}$  Non-Sterile Syringe Filters were purchased from Fisher Scientific, PA, USA. Snap-Cap™ Flat-Top Graduated Microcentrifuge Tubes were purchased from Fisher Scientific, PA, USA. 2 mL Amber Glass Screw Vials for HPLC were purchased from Fisher Scientific, PA, USA.

### ***5.2.4. Blank Compost Soil for Analysis***

The blank compost soil was purchased from Lowes and provided by Cotton Incorporated. It contained a blend of composted manure, wood compost, and sand; and was sieved to a particle size of less than 2 mm and stored at 4 °C for 7 days to achieve homogeneous conditions before use. Additionally, preliminary tests such as determination of pH, moisture content, and elemental composition were conducted to ensure an appropriate composition.

## **5.3. Experimental and Instrumentation**

### ***5.3.1. Sample Preparation***

Firstly, the RB19 1000  $\mu\text{g}/\text{mL}$  stock solutions were made from the C.I. Reactive Blue 19 powder purchased from Sigma-Aldrich, USA. By diluting the 1000  $\mu\text{g}/\text{mL}$  stock solution, seven different concentrations of solutions were made for further analysis, ranging from 1, 3, 5, 10, 30, 50, to 70  $\mu\text{g}/\text{mL}$  (see Figure 34).

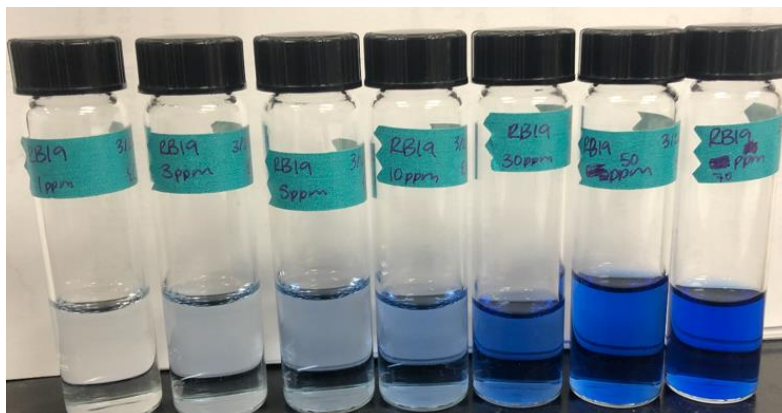


**Figure 34.** C.I. Reactive Blue 19 Solutions for Analysis (seven concentrations ranging from 1, 3, 5, 10, 30, 50, to 70  $\mu\text{g/mL}$ )

### ***5.3.2. Modifications to Original QuEChERS Extraction Method***

By comparing the computed properties (see Table 10, from PubChem [77, 78]) between the five pesticides used in the original QuEChERS method, ibuprofen, two mentioned dyes in the introduction and RB19, the polarity (represented by topological polar surface area) and hydrophobicity (represented by XlogP) of the samples can be explained. Different from the eight samples that have been tested to be effective using the QuEChERS method, RB19 has a much higher polarity and MW, and relatively high hydrophobicity. Therefore, modifications to the original QuEChERS method are quite necessary for this study.

**Table 10.** Molecular Weight, Topological Polar Surface Area and XlogP for Typical Samples (Pesticides, Ibuprofen and Dyes) used in QuEChERS Extraction Method [77, 78]

Samples	Molecular weight	Topological polar surface	XlogP
	(g/mol)	area (Å <sup>2</sup> )	
Dichlorvos	220.97	44.8	1.4
Acephate	183.17	80.7	-0.8
Diazinon	304.35	85.6	3.8
Metalaxyl	279.33	55.8	1.6
Folpet	296.6	62.7	2.8
Ibuprofen	206.28	37.3	3.5
Triphenylmethane	244.3	0	5.3
Sudan I	248.28	45	4.1
RB19	626.5	255	3.3

### 5.3.2.1. Modifications to Extraction Solvents

In the extraction process, the extraction solvents' selection is one of the most crucial factors, which can improve the efficiency of the analytes and minimize interferences from the soil. Many factors need to be considered when selecting the extraction solvents, such as the ability to cover the desired analytical spectrum (polar or non-polar compounds), amenability to chromatographic separation techniques, safety, cost, and environmental impacts [58]. In the original extractions process, the extraction solvent is acetonitrile (ACN), which is tested to be the most selective and the most advantageous extraction solvents because of its ability to separate easily from water when applying appropriate salts [71]. Other polar co-solvents can also be employed if ACN cannot

provide adequate recoveries, such as methanol (MeOH). In 2012, Bragança et al. conducted a study using different solvents and changing the ratios, and the results showed that the solvent mixtures of ACN and MeOH could get better results when trying to extract ibuprofen from soils [79].

At the beginning of this study, ACN was used as the extraction solvent for extractions of reactive dyes from soils. However, the recoveries were proven to be not ideal. In the modification processes, after trying different ratios of ACN and MeOH, the ratio of 9:1 was tested to achieve excellent recoveries for the extractions of RB19 from blank soils. All solvents used in the modified QuEChERS extraction method are summarized in Table 11.

**Table 11.** Solvents Used in Modified QuEChERS Extraction Method

Solvents	Polarity Index	Dielectric Constant <sup>a</sup>	Viscosity ( $mN s^{-1} m^{-2}$ )	Density <sup>b</sup> ( $g mL^{-1}$ )	Solubility in Water (%w/w)
Acetonitrile	5.8	37.5	0.375	0.786	100
Methanol	5.1	32.7	0.544	0.791	100
Water	9	78.3	0.890	0.998	--

<sup>a</sup>At 25 °C.

<sup>b</sup>At 20 °C.

### 5.3.2.2. Modifications to QuEChERS Contents

In the extraction process, after the initial single-phase solvent extractions, salts were added to induce phase separation. The addition of salts is not only conveniently fast, cheap, and easy but also can control the percentage of water in the organic phase (and vice versa for organic solvent in the water phase), thus making it possible for the adjustment in the polarity of the phases to some degree [71], which is also important because the partitioning of analytes between the two phases depends on the polarity differences of the upper and lower phases. Furthermore, it has the

advantages of not increasing the volume of the extracts (thereby reducing or avoiding the need for post-extraction solvent evaporation steps) and not instilling excessively nonpolar solvent properties (thereby reducing the need for post-extraction cleanup) [71]. In the original method, a salt mixture of magnesium sulfate ( $\text{MgSO}_4$ ) and sodium chloride ( $\text{NaCl}$ ) was used in the method based on pesticides' recoveries. For different samples, the choice for different salts was also possible. For example, the use of only  $\text{NaCl}$  for extraction was applied for procymidone analysis [80], the use of only  $\text{MgSO}_4$  was applied for five herbicides analysis.

Studies indicate that the recoveries decreased more than 20% for more polar compounds when 1 g of  $\text{NaCl}$  was added [58]. Accordingly, reactive dyes have higher polarity than pesticides, pure  $\text{MgSO}_4$  is chosen as the QuEChERS content due to good recoveries obtained and simplifying the new approach.  $\text{MgSO}_4$  also can bind large amounts of water and thus significantly reduce the water phase, which would promote the partitioning of pesticides into the organic layer [71]. Furthermore, the hydration of  $\text{MgSO}_4$  is a highly exothermic process, causing the sample extract to get hot during the extraction/partitioning step, reaching temperatures as high as 40 - 45 °C, in which heat is believed to be beneficial for extractions.

### ***5.3.2.3. Modifications to Agitation Modes***

There are several choices in agitation modes in the method, such as blending, vortex mixing, sonication. Blending has some significant disadvantages: the sample is under the exposure of the active metal surfaces of the blender; the cleaning of the blender jar/probe is needed between different samples; possible frictional heat will be generated during blending, especially after adding salts. Differently, shaking/vortex mixing is a better method compared with blending, with the following advantages: easier to be performed, less cost and noise; a batch of samples can be

extracted more easily in parallel; the vial used in shaking is a closed vessel that is safer [71]. In the original method, there are one step of vortex mixing and one centrifuge step. However, due to the strong binding characteristics of soil, stronger agitation modes are needed. Also, the time spent on blending and shaking steps and the number of repetitions can affect the extraction process's efficiency. In our modified method, another two steps of vortex mixing, and two steps of sonication were added to obtain better recoveries.

### ***5.3.3. The Final Decision of Modified QuEChERS Method and Its Application to the Extraction of RB19 from Blank Soils***

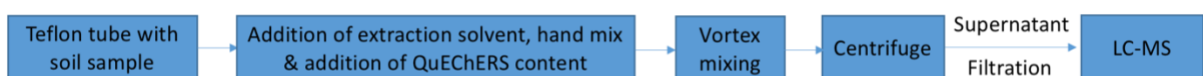
After exploring different methods, the QuEChERS extraction method was selected to be used to extract reactive dyes from soils which can provide satisfactory and reliable results and only required little labor, solvents, and materials, thus meeting the requirements of “green chemistry.”

Compared with the original method, two more vortex mixing, and sonication steps were added. The volumes and types of QuEChERS content (salts) and extraction solvents were modified to achieve high enough recoveries and adequate selectivity in the modified method. The extraction of RB19 was performed on the blank soil provided by Cotton Inc. First, 100  $\mu\text{L}$  of RB19 dye solution in seven different concentrations (ranging from 1, 3, 5, 10, 30, 50, to 70  $\mu\text{g}/\text{mL}$ ) were added into a microcentrifuge tube containing  $100 \pm 1$  mg of soil. The soil was extracted following a QuEChERS extraction standard operation procedure (SOP) demonstrated in Figure 35b. The centrifuge tube loaded with soil was then stirred using a VWR vortex mixer for 15 seconds at 2500 rpm and sonicated for 10 minutes before adding 400  $\mu\text{L}$  of QuEChERS extraction solvent mixture, which was composed of acetonitrile and methanol (both HPLC grade) at a ratio of 9:1, and QuEChERS contents ( $80 \pm 0.8$  mg of ACS grade magnesium sulfate powder). The tube was

vortexed and sonicated again before centrifugation using a VWR mini centrifuge for 5 minutes at 8500 rpm.

The supernatant liquid was then taken and filtered using a PVDF syringe before being analyzed by HPLC-DAD-MS. Except for the supernatant solutions obtained from QuEChERS extraction methods, the standard AB25 dye solutions with the same concentrations were also analyzed using LC-MS.

**(a) Original Method**



**(b) Modified Method**

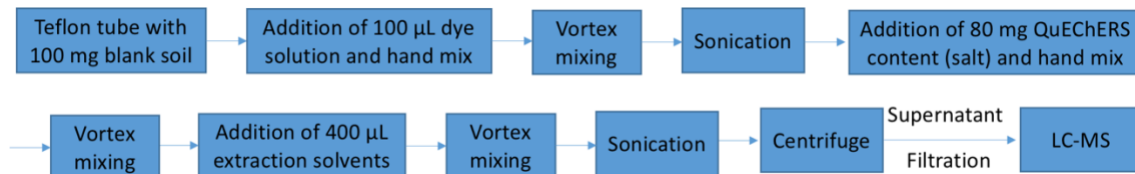


**Figure 35.** Original QuEChERS Extraction Method (a) and Modified QuEChERS Extraction Method (b) for Extractions of Reactive Blue 19 from Blank Soils (QuEChERS content was 80 mg MgSO<sub>4</sub>, extraction solvent was made up by HPLC Grade ACN and MeOH with the ratio of 9:1)

### 5.3.4. Instrumentation

#### 5.3.4.1. Q-TOF MS

After the QuEChERS extraction process, the filtered supernatant solutions were transferred to a 2-mL Agilent amber screw-top glass LC vials (Part number: 5188-6535) and then performed on an Agilent Technologies 1260 High-Performance Liquid Chromatography (HPLC) system coupled with an Agilent 6520 Q-TOF mass spectrometer (Agilent Technologies, CA, USA). An Agilent ZORBAX SB-C18 (3.0 x 150mm, 3.5 µm) reverse-phase column was used as the

stationary phase for the separation. The flow rate of the HPLC was set to 0.5 mL/min. For separation, a gradient elution composed of water and acetonitrile (%B) was chosen. Starting at 5% solvent B for 1 min during the pre-run, 5-80% solvent B from 0 min to 4 min, hold at 80% for half min, and then 80-5% solvent B from 4.5 min to 5 min; the total run time was 5 minutes. Ionization was performed via ESI and was carried out in negative mode with the following parameters: gas temperature of 350 °C, drying gas of 6 liters per minute, nebulizer of 30 psi,  $V_{\text{cap}}$  voltage of 3500 V, and fragmentor voltage of 175 V.

#### **5.3.4.2. Linear Ion Trap MS (LTQ)**

An Ultimate 3000 UHPLC system with a diode array detector (DAD) and Velos Pro Dual-Pressure Linear Ion Trap mass spectrometer (LTQ) from ThermoFisher Scientific were used for further analysis. The DAD was used for the detection of any spectral absorption of the reactive dyes. The mass spectrometer was used to detect the mass-to-charge ratio ( $m/z$ ) of degradation products. Due to soil complexity, a ZORBAX SB- C18, 3.5  $\mu\text{m}$ , 3.0 x 100 mm reverse- phase HPLC column was used as the stationary phase to separate the dye from the soil matrix. In ion trap MS, the mobile phase was composed of water (solvent A) and acetonitrile (solvent B) via a gradient elution. The flow rate and injection volume were set to 0.5 mL/min and 2  $\mu\text{L}$ , respectively, using the following gradient method: holding at 20% solvent B for 1 min during the pre-run, 20-65% solvent B from 0 min to 2 min, and 65-20% solvent B from 2 min to 3 min; the total run time was 3 min. The column temperature was set to 40 °C during all sample analyses. The detection wavelength in the DAD was set to 593 nm based on the maximum absorption wavelength ( $\lambda_{\text{max}}$ ) of RB19. Ionization in the mass spectrometer was conducted via ESI source in negative mode. The parameters from the ESI source were set to the following parameters: heater temperature of 40 °C,

sheath gas flow rate of 10 arbitrary (arb.) units, auxiliary gas flow rate of 4 arb, spray voltage of 4000 V, capillary temperature of 350 °C, and S-lens RF level of 68.2%.

## 5.4. Results and Discussion

### 5.4.1. Detection of Standard Dye RB19 Solutions

Before using modified the QuEChERS extraction method, the RB19 dye solutions with concentrations ranging from 1, 3, 5, 10, 30, 50, to 70 µg/mL, were analyzed using the Q-TOF mass spectrometer. The mass spectra of detected signals are shown in Figure 36, with a typical isotopic distribution of singly charged ions. MassHunter software was used to generate this formula, which is matchable to the VS structure of RB19 in Figure 33b. The ppm error was calculated to be 3.49, where the experimental  $m/z$  value was 483.0343, and the calculated  $m/z$  value was 483.0326.

The response from DAD (green line) and extracted ion chromatogram (EIC, purple line) were also shown in Figure 36. EIC refers to data that has been drawn from the total ion current chromatogram (TIC), and it is a chromatogram for a particular  $m/z$  value, in this case, the ions of  $m/z$  483.0205 and 483.0652. The response from DAD showed a maximum absorption wavelength ( $\lambda_{\max}$ ) of 593 nm at a retention time of 4.11 min; because of a delay of 0.1 min between DAD and EIC, the acquisition time of EIC is detected to be 4.21 min.

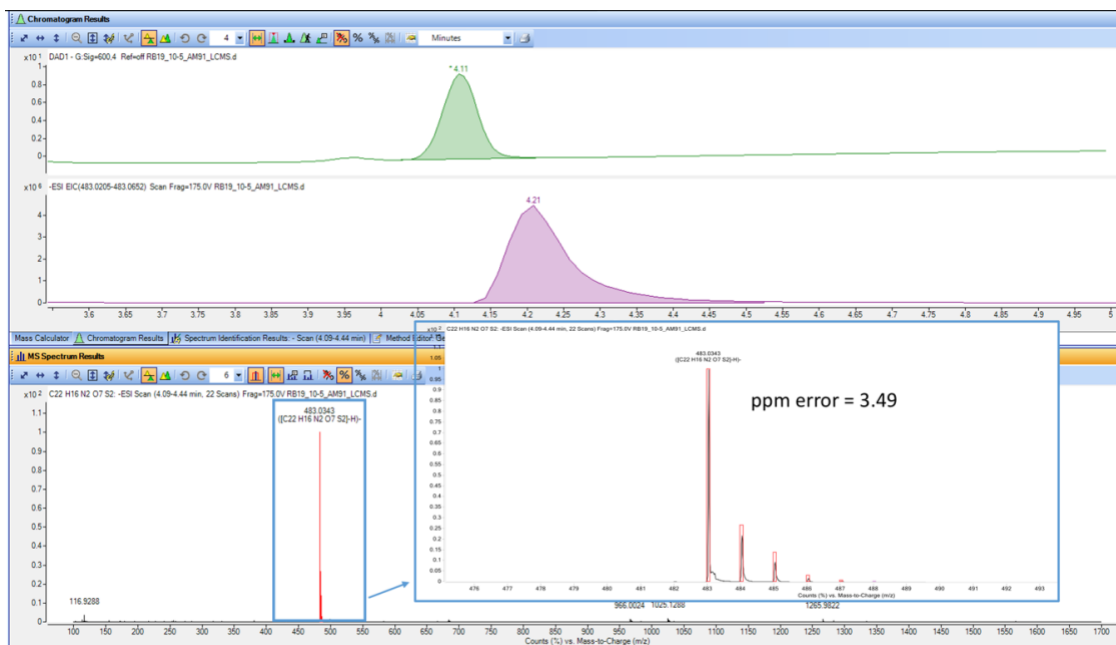


**Figure 36.** Response from DAD, EIC, and Mass Spectra of Standard Dye RB19 Solutions Detected by LC-DAD-MS

The calibration curve (Figure 37) is built according to the relationship between detected DAD area and corresponding dye solution concentrations based on Beer-Lambert Law, using linear ion trap MS. Usually, the Beer-Lambert law can be applied for most dyes in solution at low concentrations. The dye's color strength is positively correlated to the absorbance of the dye (area under the absorption band) and depends on the shape of the absorption curve. When the sample is pure deionized water without any dye solutions, the response from DAD is zero under no interference, so the intercept of the calibration curve is set to zero.

In Figure 37, The x-axis represents the concentrations ( $\mu\text{g/mL}$ ) of RB19 dye solutions, and the y-axis represents the DAD area (mAu, the response from the DAD device). In addition to the seven concentrations, two quality controls (QC, 7 and 40  $\mu\text{g/mL}$ ) samples were used to give more quality to the work (Figure 37). The calculated dye concentrations based on the calibration curve were  $6.92 \pm 0.27 \mu\text{g/mL}$  (for QC 7  $\mu\text{g/mL}$ ) and  $40.16 \pm 1.52 \mu\text{g/mL}$  (for QC 40  $\mu\text{g/mL}$ ),

respectively. In summary, the quantification of pure dye RB19 solution is acceptable with an  $R^2$  of  $0.9997 \pm 0.0002$ .

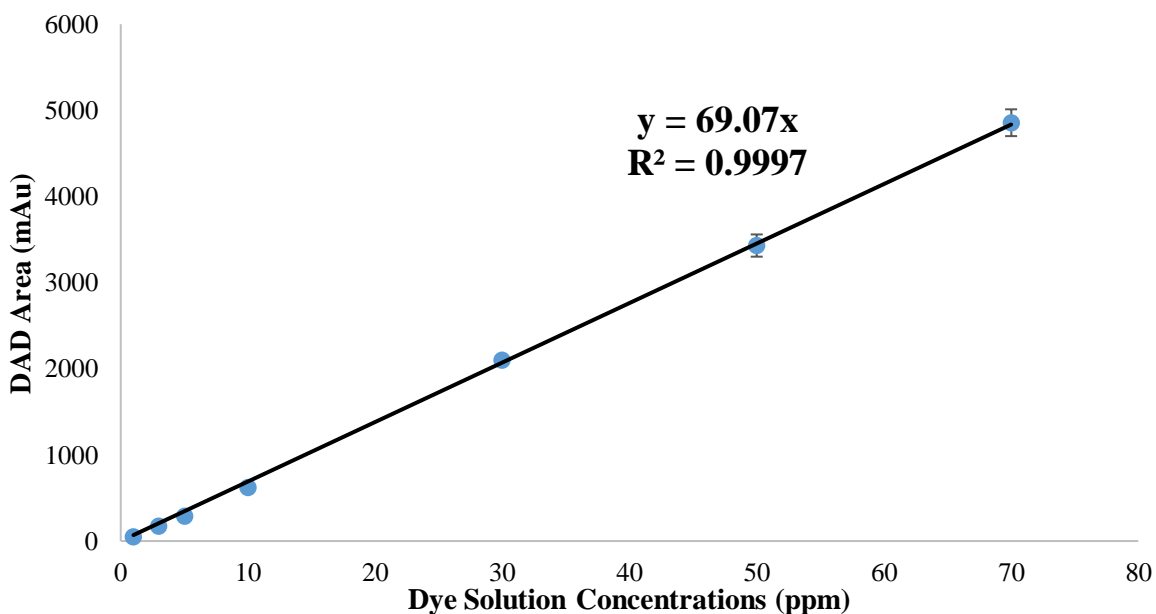


**Figure 37.** Calibration Curve for Pure Dye RB19 Solutions (Standard deviations were calculated based on three repeated runs)

#### 5.4.2. Detection of Reactive Dyes Extracted from Blank Soils

After multiple tests, the modified QuEChERS method was effective for extracting RB19 from blank soils. The recoveries of reactive dyes were also tested to be good enough under certain conditions. The addition of sonication steps can make smaller particles of soil; thus, the extraction solvents can have a more significant contact area to interact with the RB19, which organic solvents can extract. Also, the results proved that the QuEChERS extraction method is more effective by adding sonication steps and two more times of vortex mixing. The finalized modified QuEChERS method was summarized in Figure 35b and Table 12.

**Table 12.** Modifications to QuEChERS Extraction Method

Modifications	Original method	Modified method
QuEChERS content (salt)	MgSO <sub>4</sub> and NaCl	MgSO <sub>4</sub>
Extraction solvent	Acetonitrile	Acetonitrile and methanol
Agitation modes		
Vortex mixing	One time	Three times
Sonication	N/A	Two times
Centrifuge	One time	One time

Using the modified QuEChERS extraction method, the RB19 dye solutions with seven concentrations ranging from 1, 3, 5, 10, 30, 50, to 70 µg/mL were used to extract the dye from blank soil samples. The mass spectra of detected signals ( $m/z$  483.0336) and isotopic distributions of the targeted signals are shown in Figure 38. From the mass spectra of pure dye solutions (Figure 36) and RB19 extracted from blank soils (Figure 38), the ions of  $m/z$  966.0017 and  $m/z$  1265.9802 were observed, which were from backgrounds. Based on HR-MS, a potential molecular formula of the ion of  $m/z$  483.0336 to be  $C_{22}H_{15}N_2O_7S_2^-$ . The experimental parameters of standard dye RB19 solutions and RB19 extracted from blank soil (ions generated, mass-to-charge ratios of theoretical and experimental, and ppm error) are listed in Table 13. The calculated ppm errors for both cases were smaller than 5 ppm, an acceptable value for characterization of known and unknown compounds.

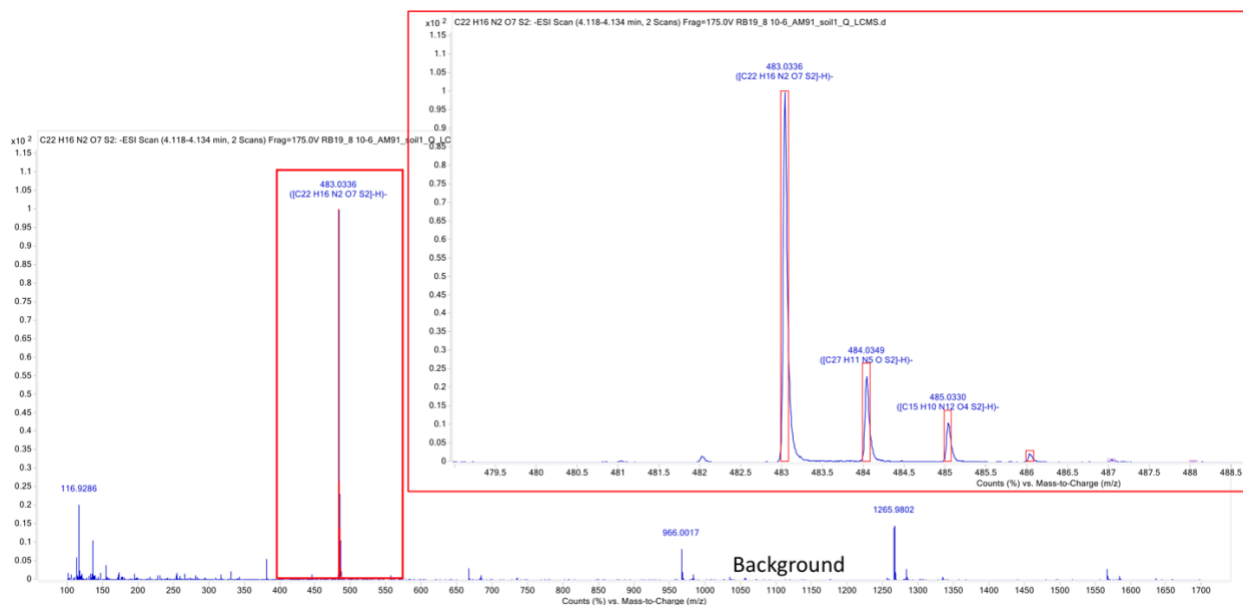


**Figure 38.** Mass Spectra of RB19 Extracted from Blank Soils

**Table 13.** Experimental Parameters for Standard Dye RB19 Solutions and RB19 Extracted from Blank Soil (ions generated, mass-to-charge ratios of theoretical and experimental, ppm error)

Samples	Ion generated	m/z (theo.)	m/z (exp.)	ppm error
Standard Dye RB19 Solutions	$C_{22}H_{15}N_2O_7S_2^-$	483.0326	483.0343	3.49
RB19 Extracted from Blank Soil	$C_{22}H_{15}N_2O_7S_2^-$	483.0326	483.0336	2.04

Note: m/z = mass-to-charge ratio, theo. = theoretical (based on structures in Figure 33), exp. = experimental

Same with the standard dye RB19 solutions, the samples extracted from blank soils were later analyzed using linear ion trap MS for LC-DAD-MS analysis. The samples with seven concentrations (1, 3, 5, 10, 30, 50, and 70  $\mu\text{g/mL}$ ) and two extra QCs (7 and 40  $\mu\text{g/mL}$ ) were repeated three times, respectively. A total of 27 samples were extracted by the QuEChERS extraction method and analyzed by LC-MS. For QCs, the calculated dye concentrations based on the calibration curve (see Figure 39) were  $7.06 \pm 0.15 \mu\text{g/mL}$  (for QC 7  $\mu\text{g/mL}$ ) and  $41.22 \pm 2.23 \mu\text{g/mL}$  (for QC 40  $\mu\text{g/mL}$ ), respectively. According to Beer-Lambert law, the detected DAD area has a linear relationship with the concentrations of dye solutions used for the QuEChERS

extraction method. In the calibration curve build for RB19 extracted from blank soils using my modified QuEChERS method (Figure 39), the x-axis represents the dye solution concentrations ( $\mu\text{g/mL}$ ), and the y-axis represents DAD area (mAu, response from DAD device). Also, due to soils' complexity, the response from DAD might not be zero even when only deionized water (concentration is zero) was used.

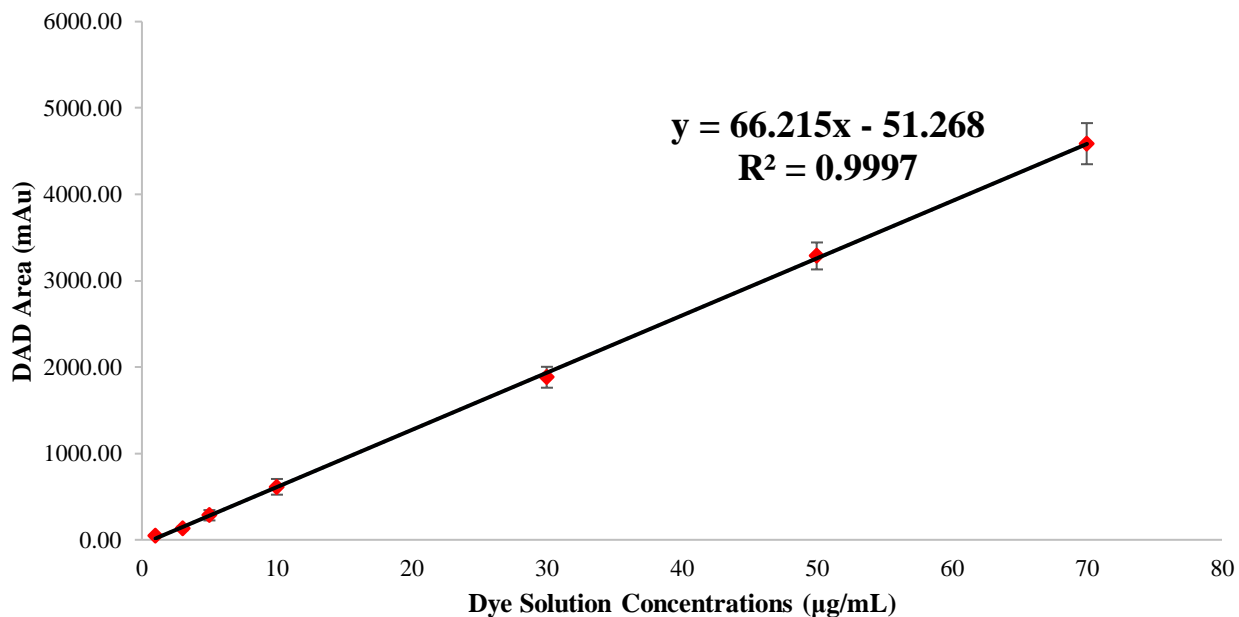


**Figure 39.** Calibration Curve for RB19 Extracted from Blank Soils

#### 5.4.3. Validation of Quantification Method

As shown in Figure 39, the calibration curve's linearity was excellent for all runs with  $R^2$  of  $0.9997 \pm 0.0002$ , indicating a consistent and robust correlation between the DAD area and the dye concentrations. The method was further evaluated based on sensitivity, accuracy, and precision (Table 14). Sensitivity was assessed by evaluating the average limit-of-detection (LOD) and lower limit-of-quantification (LLOQ), in which they were calculated using the following equations:  $\text{LOD} = 3 \times \text{SD} / b$  and  $\text{LLOQ} = 10 \times \text{SD} / b$ , where SD is the standard deviation of the response, which

can be estimated by the standard deviation of the y-intercepts of the regression line, and b is the slope of the calibration curve [81]. LLOQ was evaluated to be  $3.4329 \pm 1.0287 \mu\text{g/mL}$ , and LOD was  $1.0299 \pm 0.2920 \mu\text{g/mL}$ .

Experiments were repeated in triplicate on three non-consecutive days, and accuracy and precision were assessed across 3 days (inter-day). Accuracy was evaluated by comparing experimental values to theoretical values and reported as percent error (% error). Precision was assessed based on variations across runs and reported as the coefficient of variation (% CV). Except for the concentration of  $1 \mu\text{g/mL}$ , all concentrations' precision and accuracy were within 9%.

**Table 14.** Overall Validation Parameters

<b>Validation Parameters</b>	<b>Average <math>\pm</math> SD</b>
<b>Average Linearity (<math>R^2</math>)</b>	$0.9997 \pm 0.0002$
<b>Sensitivity</b>	
LLOQ	$3.4329 \pm 1.0287 \mu\text{g/mL}$
LOD	$1.0299 \pm 0.2920 \mu\text{g/mL}$
<b>Precision (mean % CV)</b>	$5.5057 \pm 3.7297$
<b>Accuracy (mean % error)</b>	$0.8253 \pm 5.0672$

Note: SD: standard deviation; Linearity, LOQ, and LLOQ were the averages across all runs.

**Table 15.** The Results of Inter-day Precision and Accuracy of Each Concentration Points of RB19 Extracted from Blank Soils

<b>Concentration (<math>\mu\text{g/mL}</math>)</b>	<b>Inter-day Precision (% CV)</b>	<b>Inter-day Accuracy (% error)</b>
1	11.76	11.00 (1.11 $\mu\text{g/mL}$ )
3	8.47	-5.33 (2.84 $\mu\text{g/mL}$ )
5	6.32	1.40 (5.07 $\mu\text{g/mL}$ )
10	5.49	0.40 (10.04 $\mu\text{g/mL}$ )
30	1.86	-2.57 (29.23 $\mu\text{g/mL}$ )
50	3.13	0.82 (50.41 $\mu\text{g/mL}$ )
70	1.51	0.06 (70.04 $\mu\text{g/mL}$ )

### 5.5. Summary

Due to the difference in polarity and hydrophobicity between pesticides and RB19, the original QuEChERS method's modifications are necessary. Based on the results, it could be concluded that all changes to the original QuEChERS method were ideal, and the modified QuEChERS method was efficient in extractions of RB19 from blank soils. The overall experiment results showed that the combination of LC-DAD-MS with the modified QuEChERS extraction method would greatly facilitate the study of RB19 leached into the soil. The calibration curved built using the modified QuEChERS extraction method was also validated to be useful. Both accuracy and precision were within the acceptable range  $\pm 12\%$  for all concentrations. The calibration curves' linearity was excellent for all runs with  $R^2$  of  $0.9997 \pm 0.0002$ , indicating a strong and consistent correlation between the DAD area and the dye concentrations. The successful application of the QuEChERS method and quantification of RB19 from blank soil gives us an idea that the QuEChERS method is applicable to the degradation studies of reactive dyes in complex

matrices such as soil. More details will be discussed in the following two chapters to investigate the real soil samples with RB19 dyed cotton fabrics after 90-day degradation processes.

## **CHAPTER 6. Detection and Structural Elucidation of C.I. Reactive Blue 19 Degradation**

### **Products from soil**

#### **6.1. Introduction**

In the process of landfills, soil plays an extremely important role. Soil is a biologically balanced system, any drastic change in soil can affect the microbial community structure and the biochemical processes that are carried out [60]. In this sense, reactive dyes' complex chemical structures can undergo degradation in soil, which could result in possible hazardous compounds, such as benzidine, azobenzene, and other aromatic compounds [10]. Thus, the disposal of dyed cotton fabrics with reactive dye can be considered a potential source of pollution if these dyes undergo degradation into more harmful compounds. The majority of the work of dye degradation is focused on wastewater treatments. These studies involve the biodegradation of reactive dyes via different fungi, bacteria, yeasts, and algae, with promising results for these contaminated wastewaters [9]. However, few studies are carried out on the degradation of dyes and their pollutants in soil. At this time, there is no assessment of the biodegradation fate of reactive dyes on fabrics during landfill disposal. Even though cotton fibers have been identified as one major natural fiber in soil, their effects and possible degradation processes in soils are still unknown. Thus, to evaluate the impact of landfilled textiles into the ground, two questions arise: 1) What happens during the biodegradation of dyed cotton fabrics in soil?; and 2) What has leached to the soil?

In this study, in the simulated degradation process of Reactive Blue 19 (RB19) dyed cotton fabrics, the RB19 dyed fabrics were obtained by dyeing a single-knit 28 cut jersey fabric (100% cotton ring-spun yarn) with 2% on the weight of goods (owg). Then 2 x 2 cm dyed fabrics with RB19 were then placed into the compost soil (sieved to a particle size below or equal 2 mm) for

90-day simulated degradation. After this time interval, the soil was taken out and stored in a refrigerator prior to further analysis. For the soil samples analysis after 90-day simulated degradation processes, the combination of modified QuEChERS extraction method and LC-DAD-MS were used. The present study aims to find, detect any possible RB19 degraded products in soil. Using high resolution MS, the possible degraded product was identified and elucidated to be Acid Blue 25 (AB25).

## **6.2. Materials**

### **6.2.1. Solvents and Chemicals**

Acetonitrile (LC-MS grade, 99.9%) and methanol (LC-MS grade,  $\geq$  99.9%) for QuEChERS extraction were purchased from Sigma-Aldrich (Sigma-Aldrich, MO, USA) and used without any further purification. HPLC grade water was acquired using a Pure Lab Ultra water purification system from ELGA Lab Water (ELGA Lab Water, High Wycombe, UK). Magnesium sulfate (ReagentPlus<sup>®</sup>,  $\geq$  99.5%) was purchased from Sigma-Aldrich, MO, USA.

### **6.2.2. Dyes**

C.I. Reactive Blue 19 (RB19, CAS no. 2580-78-1, molecular formula  $C_{22}H_{16}N_2Na_2O_{11}S_3$ , molecular weight 626.5325 g/mol, dye purity 50%) was used for dyeing cotton fabrics. Standard C.I. Acid Blue 25 (AB25, CAS no. 6408-78-2, molecular formula  $C_{20}H_{13}N_2NaO_5S$ , molecular weight 416.3828 g/mol, dye purity 45%) was purchased from Sigma-Aldrich, USA. Both of the structures were illustrated in Figure 40.

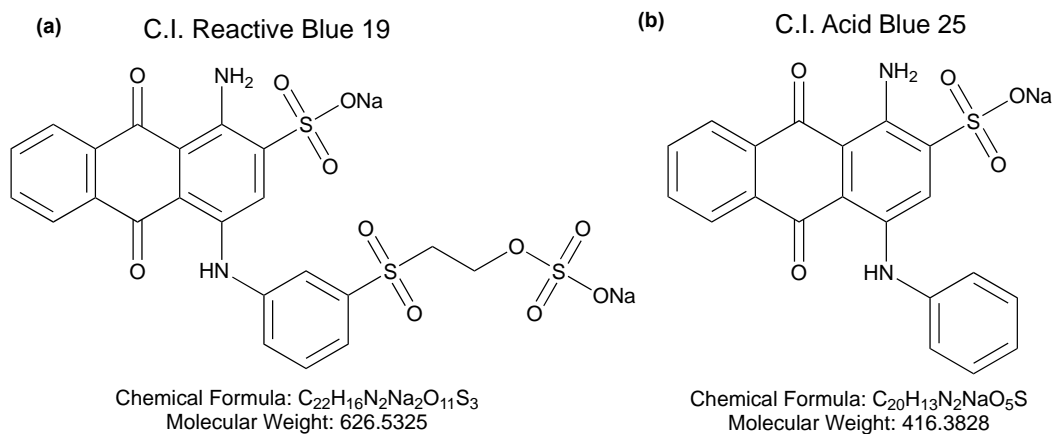


**Figure 40.** Chemical Structures of RB19 in SES Form (a) and AB25 (b)

### 6.2.3. Other Supplies

Disposable Luer-slip plastic syringes (1 mL) were purchased from Sigma-Aldrich, MO, USA. PTFE 0.2  $\mu$ m Non-Sterile Syringe Filters were purchased from Fisher Scientific, PA, USA. Snap-Cap™ Flat-Top Graduated Microcentrifuge Tubes were purchased from Fisher Scientific, PA, USA. 2 mL Amber Glass Screw Vials for HPLC were purchased from Fisher Scientific, PA, USA.

### 6.2.4. RB19 Dyed Cotton Fabrics

The RB19 dyed fabrics were obtained by dyeing a single-knit 28 cut jersey fabric (100% cotton ring-spun yarn) with 2% on the weight of goods (owg). The dyeing was performed at the Dyeing and Finishing Application Laboratory at Cotton Incorporated, Cary, NC, USA. In brief, the dyeing process was performed by following these steps: 1370 g of fabric were loaded into an OptiLab dyeing machine at a 15:1 liquor ratio. The salt (sodium sulfate) was then added at a rate of 55 g/L (1130 g salt for a total of 21 liters) and circulated for 5 min at 37.8 °C. Next, 27.4 g of dye at 2.0 % owg was added and circulated for 15 min at 60 °C, followed by the addition of 267 g

of soda ash (sodium carbonate) at a rate of 13 g/L and circulated for 45 min; 10 g of acetic acid at a rate of 0.5 g/L was added and circulated for 10 min after decreasing the temperature to 48.9 °C. The fabric was circulated for 10 min after increasing the temperature to 93.3 °C. Lastly, the fabric was cooled to 82.2 °C. The solution was drained, the machine was filled with cold water, and circulated for 2 minutes [82].

### **6.3. Experimental**

#### ***6.3.1. Simulated Compost Degradation and Sample Preparation***

The biodegradation of the dyed cotton fabrics in the soil was performed at the Department of Fiber Science and Apparel Design, Cornell University, under controlled laboratory conditions, according to the ASTM D 5988-18 standard test method [83]. For the biodegradation process, Garden Scape Cow Manure, which is a soil blend containing manure, wood compost, and sand, was purchased from Lowes, USA. The soil was sieved to a particle size below or equal to 2 mm and had an average pH value of 7.71 (measured using a Fisher Science Education™ Laboratory Benchtop pH Meter). To perform the degradation, 380.2 g of soil, 72.6 g of diammonium hydrogen phosphate ((NH<sub>4</sub>)<sub>2</sub>HPO<sub>4</sub>) solution (4.72 g/L in water), and 47.2 g of purified water were mixed and placed into a desiccator (150 mm nominal diameter). The 2 x 2 cm dyed cotton fabrics with RB19 were placed into the soil for 90 days. After this time interval, the soil samples were then collected and stored in a refrigerator prior to further analysis.

### 6.3.2. QuEChERS Extraction of RB19 Degradation Products from Soil Samples After Simulated Compost Soil Degradation

The extraction of RB19 degradation product from the soil samples was performed. First, 100  $\mu$ L HPLC grade water was added into a microcentrifuge tube containing  $100 \pm 1$  mg of soil obtained from simulated compost soil degradation. The soil was extracted following a modified QuEChERS extraction SOP demonstrated in Figure 41. The centrifuge tube loaded with soil was then stirred using a VWR vortex mixer for 15 seconds at 2500 rpm and sonicated for 10 minutes before adding 400  $\mu$ L of QuEChERS extraction solvent mixture, which was composed of HPLC grade acetonitrile and methanol at a ratio of 9:1, and  $80 \pm 0.8$  mg of ACS grade magnesium sulfate powder. The tube was vortexed and sonicated again before centrifugation using a VWR mini centrifuge for 5 minutes at 8500 rpm. The supernatant liquid was then taken and filtered using a PVDF syringe filter before being analyzed by HPLC-DAD-MS. The diagram showing the modified QuEChERS extraction method's workflow after simulated compost degradation is shown in Figure 41.

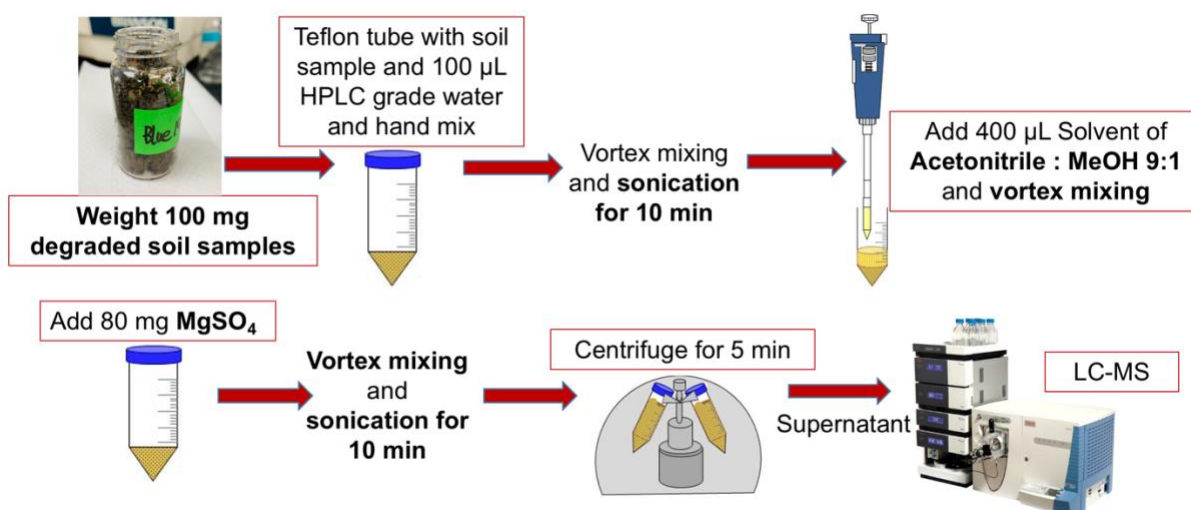


**Figure 41.** Diagrams of QuEChERS Extraction on the Soil Samples after Simulated Compost 90-Day Degradation

### ***6.3.3. Detection and Structural Elucidation of RB19 Degradation Products from Degradated Soil using LC-MS***

#### ***6.3.3.1. Detection of RB19 Degradation Products from Soil (Linear Ion Trap MS)***

The detection of RB19 degradation products in soil after 90 days was performed on an Ultimate 3000 UHPLC system from ThermoFisher Scientific with a diode array detector (DAD) and Velos Pro Dual-Pressure Linear Ion Trap mass spectrometer from ThermoFisher Scientific. The DAD was used to detect any spectral absorption of the reactive dye, and the detection wavelength in the DAD was set to 593 nm. The mass spectrometer was used to detect the mass-to-charge ratio ( $m/z$ ) of any potential RB19 degradation products. Due to soil complexity, a ZORBAX SB- C18, 3.5  $\mu\text{m}$ , 3.0 x 100 mm reverse-phase HPLC column was used as the stationary phase to separate the dye from the soil matrix. The flow rate and injection volume were set to 0.5 mL/min and 2  $\mu\text{L}$ , respectively. To separate the potential degradation products from the soil matrix, a gradient elution (see Figure 42) composed of water (solvent A) and acetonitrile (solvent B) was chosen. Starting at 20% solvent B for 1 min during the pre-run, 20-65% B from 0 min to 2 min, and 65-20% solvent B from 2 min to 3 min; the total run time was 3 min. Ionization in the mass spectrometer was conducted by a heated electrospray ionization (HESI) source in negative mode. The parameters from the HESI source were set to the following parameters: heater temperature of 40  $^{\circ}\text{C}$ , sheath gas flow rate of 10 arbitrary (arb.) units, auxiliary gas flow rate of 4 arb, spray voltage of 4000 V, capillary temperature of 260  $^{\circ}\text{C}$ , and S-lens RF level of 68.2%.

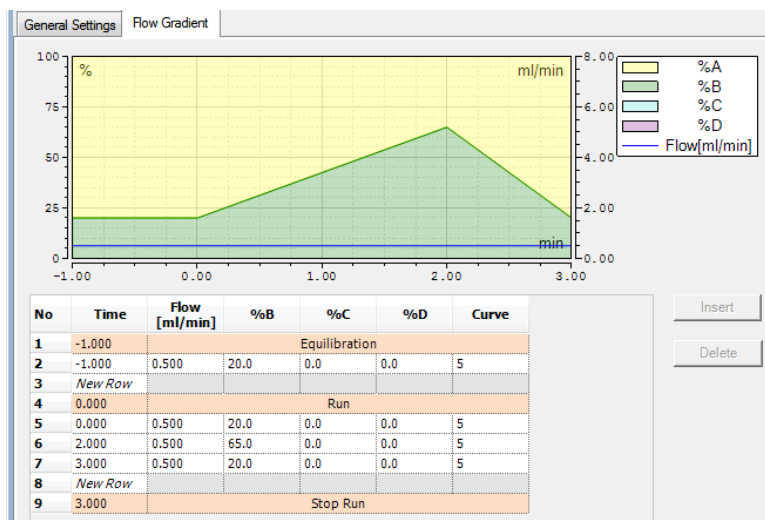


**Figure 42.** Gradient Method used in Software “XCalibur” for Ion Trap MS (water as solvent A and acetonitrile as solvent B)

### 6.3.3.2. Structural Elucidation of RB19 Degradation Products from Soil (Q-TOF MS)

After detecting RB19 degradation products in the ion trap mass spectrometer, the supernatant solutions from QuEChERS extractions were then transferred to 2 mL Agilent amber screw-top glass LC vials (Part number: 5188-6535). The structural elucidation by exact mass and tandem mass spectrometry (MS/MS) of RB19 derivatives was performed on an Agilent Technologies 1260 HPLC system coupled with an Agilent 6520 Quadrupole Time-Of-Flight (Q-TOF) mass spectrometer. An isocratic mobile phase composed of water (solvent A) and acetonitrile (solvent B) at a ratio of 6:4 was performed. An Agilent ZORBAX SB-Aq (3.0 x 150mm, 3.5  $\mu$ m) column was used as the stationary phase for the separation. The flow rate was set to 0.5 mL/min, and the total run time for each sample was 6 minutes. Ionization was performed via ESI and was carried out in negative mode with the following parameters: gas temperature of 350  $^{\circ}$ C, drying gas rate of 5 liters per minute, nebulizer pressure of 50 psi,  $V_{cap}$  voltage of 3500 V, and fragmentor voltage of 185 V.

MS/MS analysis was performed by collision-induced dissociation (CID) using nitrogen gas as the collision gas. The collision energy was set to 40 eV in MassHunter™ software, and the isolation window was set to narrow (1.3 m/z).

## **6.4. Results and Discussion**

### ***6.4.1. Detection of RB19 Degradation Products from Degraded Soil***

As described in the experimental section 6.3.1, the cotton fabrics with 2 cm x 2 cm size were randomly placed into the soil for degradation processes for 90 days. However, in the simulated degradation process, not all soils could have contacted the cotton fabrics, and a sample of only 0.1 g was taken for analysis each time.

Based on the results, three out of thirty samples (10 percent) can be detected for the degradation products using LC-MS; twenty-seven samples (90 percent) cannot be detected for any degradation products. The TIC (x-axis of time and y-axis of signal intensity) and response from DAD for those 90 percent samples are shown in Figure 43. The TIC chromatogram represents the summed intensity across the entire range of masses detected at every point in the analysis. The range is typically several hundred mass-to-charge units or more. In complex samples, the TIC chromatogram often provides limited information as multiple analytes elute simultaneously, obscuring individual species. Usually, the hyphenation of LC-MS and the resulting TIC chromatogram can provide the information required for characterization. The TIC chromatogram (Figure 43a) indicates no observed products in the samples during the total running time of 3 mins. In addition, there has no response from the DAD device (Figure 43b); the peaks at 0.75 min and 0.83 min in DAD are from the solvents when running LC-MS.

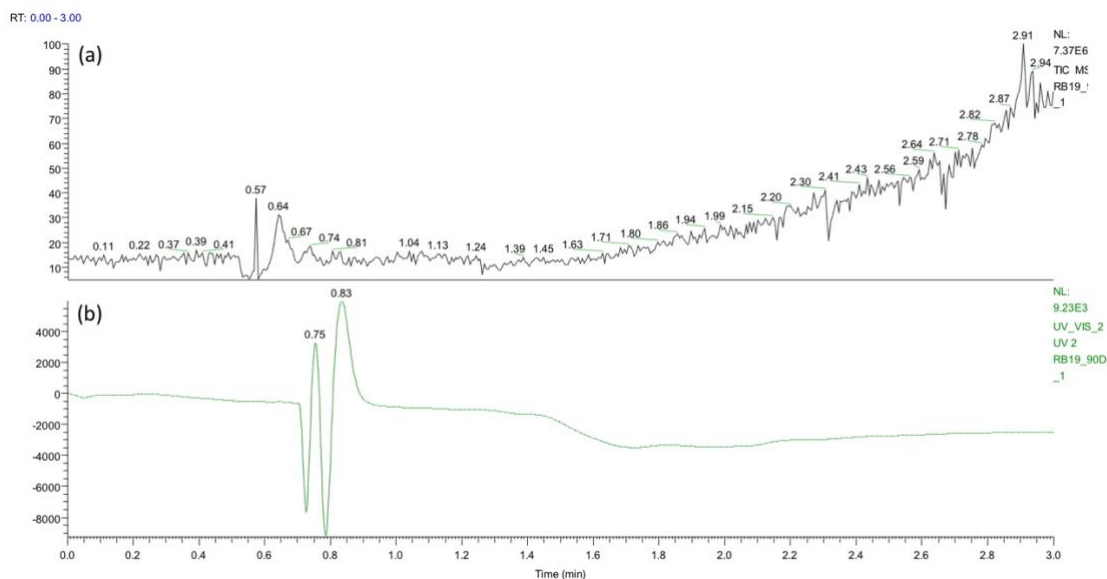


**Figure 43.** TIC Chromatogram and Response from DAD for Degraded Soil Samples Detected with no Signals

However, only 10% of those samples can be detected with unknown signals; and EIC (m/z 392.58-393.59, RT of 2.40 min, intensity vs. time) and DAD response of the unknown signals are shown in Figure 44. Compared with Figure 43, it is evident that a signal was detected, shown in Figure 44, and it has an obvious response from the DAD device. After the extraction and LC-MS analysis in the linear ion trap MS, an ion with an m/z of 393 (see Figure 45, relative abundance (%) vs. m/z), a retention time of 2.39 min, and a lambda max ( $\lambda_{\max}$ ) of 624 nm were found. This unknown ion has a lower m/z than RB19 in terms of mass spectrometry results, and it should have a similar chromophore as that of RB19. However, the ion trap results were not enough to identify the structure of this unknown degradation product. For this reason, the same samples were then characterized using the Q-TOF mass spectrometer for high-resolution measurements and tandem mass spectrometry analysis in the following section.

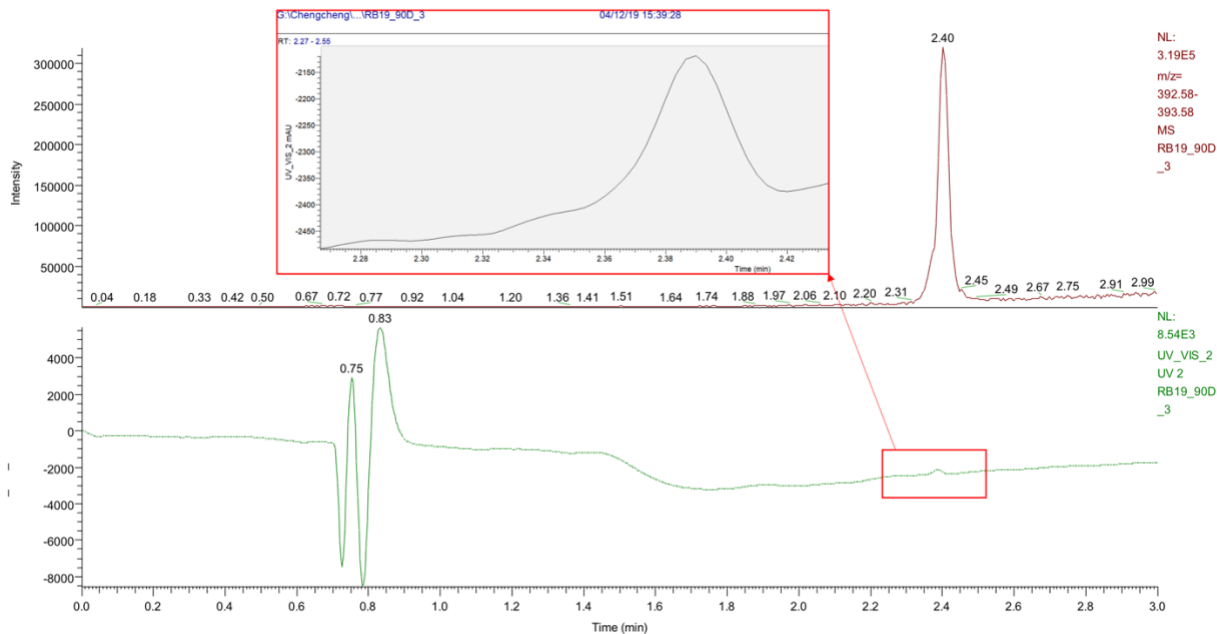


**Figure 44.** EIC and DAD Response of the Unknown Signal from Degraded Soil Samples

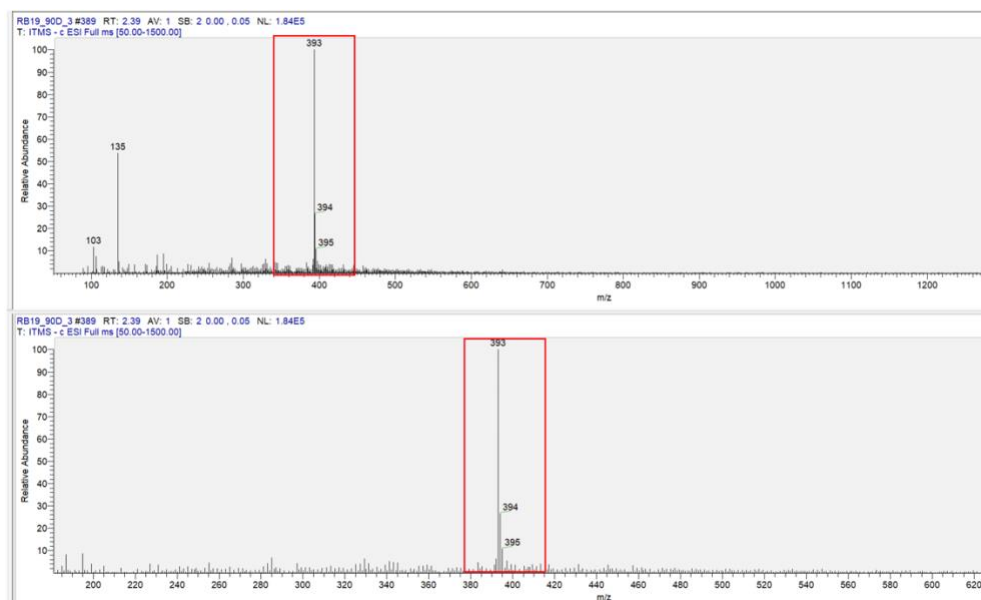


**Figure 45.** Mass Spectra of the Unknown Signal from Degraded Soil Samples

#### 6.4.2. Structural Elucidation of RB19 Degradation Products from Degraded Soil

The high-resolution mass spectrum (relative abundance (%) vs. m/z) gathered from Q-TOF was shown in Figure 46. The degradation product has an m/z of 393.0551, and by using the formula

generation function in MassHunter™ qualitative analysis software, a series of chemical formulas were generated by evaluating their isotopic distribution (the decrease of M+2 peak indicates the loss of one sulfur by comparing the isotopic distributions in mass spectrum of RB19 and Figure 46), degree of double bond equivalent (DBE, also called unsaturation number), and mass measurement accuracy (MMA, represented by ppm error).

Based on this analysis, the chemical formula for the degradation product in soil of  $[\text{C}_{20}\text{H}_{14}\text{N}_2\text{O}_5\text{S}]\text{-H}^-$  was selected from all options, because of its reasonable DBE (DBE = 15) and appropriate MMA (ppm error = -0.41). Although the chemical formula of this product was selected; however, its structure still has not been confirmed. From the structure of RB19 (see Figure 40a) and the mass spectrometry result, the loss of one sulfur atom was noticed based on the decrease of the M+2 isotopic peak after performing MS/MS. Furthermore, for the unknown degraded product, the loss of  $\text{SO}_2$  (63.9619 Da) was found using MS/MS in Figure 47. It was very likely that the vinyl sulfone reactive group was removed instead of the sulfonate group based on mass difference. If this hypothesis is correct, the structure of the RB19 derivative after degradation could be the same as that of AB25 (chemical structure in Figure 40b).

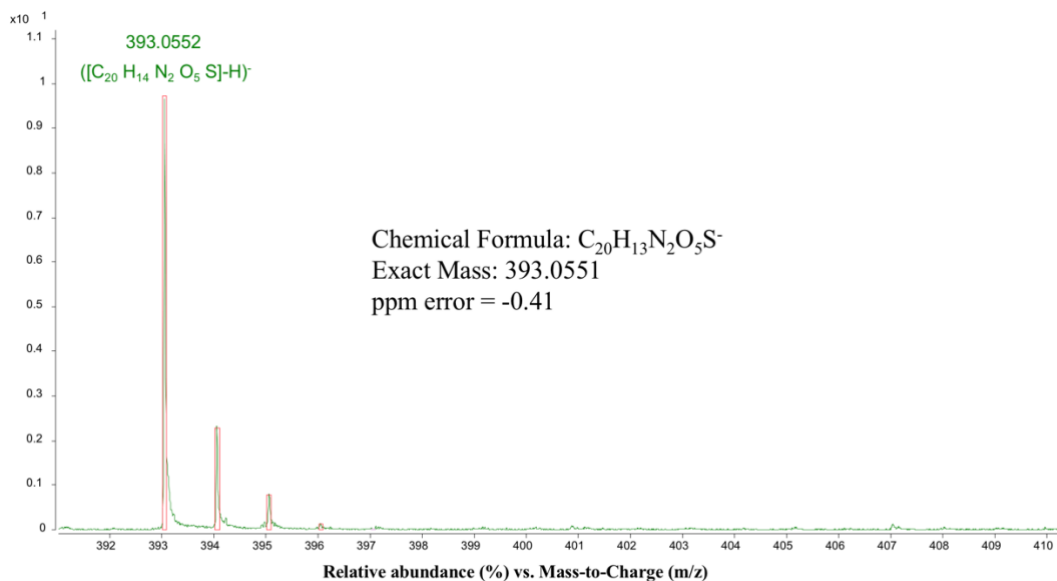


**Figure 46.** Q-TOF MS Spectrum (Relative Abundance (%) vs. Mass-to-Charge Ratio) Showing the Detection of RB19 Degradation Product from Soil with 90-Day Interval

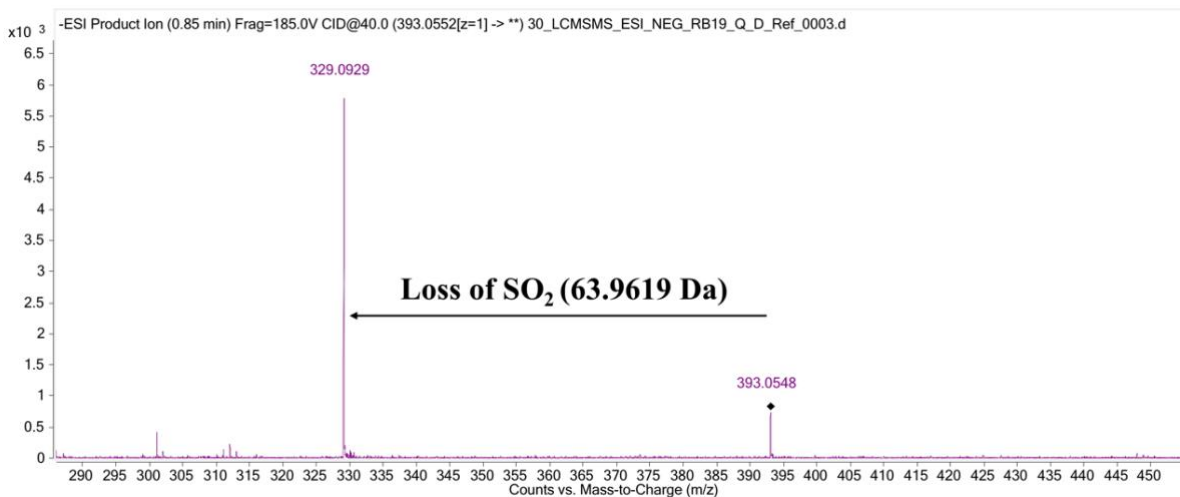


**Figure 47.** MS/MS of RB19 Degradation Product from Soils with 90-Day Interval

The ability to identify unknown samples is one of the most powerful uses of a mass spectrometer. Because of the hypothesis that the degradation product is likely to be AB25, a commercial dye standard AB25 (chemical structure in Figure 40b) was used to compare with the unknown degradation product extracted from the soil using LC-MS/MS analysis under the same CID conditions (collision gas of N<sub>2</sub>, collision energy of 40 eV, isolation window of narrow).

As is shown in the bottom mass spectra in Figure 48, the isolation of deprotonated AB25 ( $m/z$  393.06) and its fragmentation show the formation of a stable phenoxide ion after the sulfonate group rearranges to have a loss of 64 Da. MS/MS experiments observed the same fragmentation pathway for the unknown degradation product found in the 90-day degradation soil of RB19 (see upper mass spectra in Figure 48). Hence, based on exact mass measurements, isotopic distribution, chemical formula, and MS/MS experiments, the unknown degradation product found in soil can be concluded to be AB25.

The successful identification of the RB19 degradation product suggests a different pathway of degradation compared to another study by Sultana et al., where it was found a loss of the sulfonate group from RB19 [84]. Furthermore, according to existing studies, this degradation pathway observed with RB19 is not uncommon, as the reactive group's dissociation after soil degradation has also been reported with C.I. Reactive Black 5 and C.I Reactive Red 198 [82].

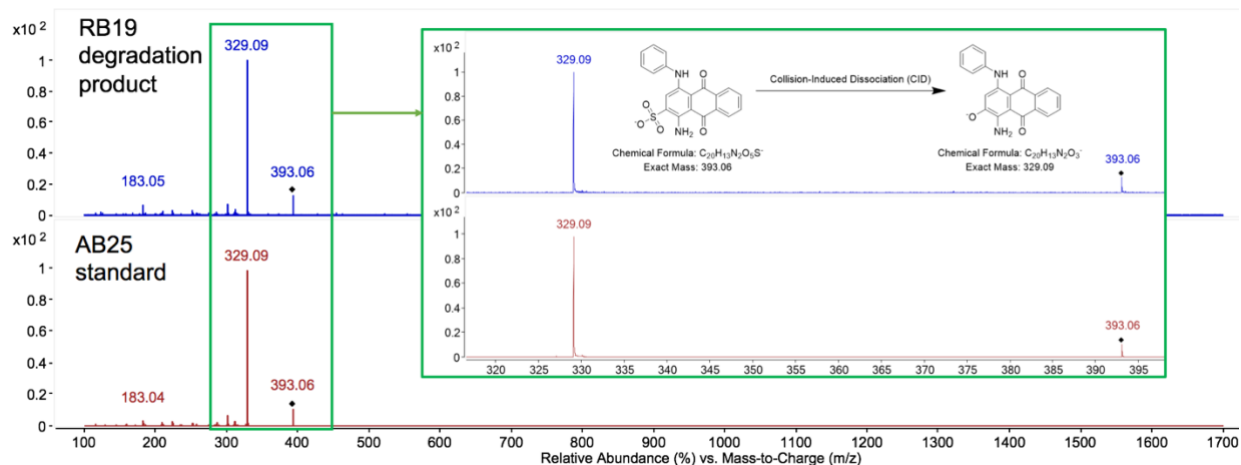


**Figure 48.** MS/MS Spectra from QTOF-MS of RB19 Degradation Product from Soil with 90-Day Interval and AB25 Standard Dye

## 6.5. Summary

A systematic analytical approach was successfully carried out to study the biodegradation of RB19 after 90 days in compost soil. Based on the experiments, an unknown degradation product has been proven to exist in the soil containing degraded RB19-dyed cotton fabrics using linear ion trap MS. The degradation product was confirmed to have an  $m/z$  of 393.0551, and by using the formula generation function in MassHunter<sup>TM</sup> qualitative analysis software from Q-TOF MS, a series of chemical formulas were generated by evaluating their isotopic distribution (the decrease of  $M+2$  peak indicates the loss of one sulfur), DBE (unsaturation number), and MMA (represented by ppm error). By using the combination of the modified QuEChERS extraction method and HPLC system coupled with QTOF-MS in both LC-MS and LC-MS/MS modes, the chemical formula for the degradation product in soil of  $[C_{20}H_{14}N_2O_5S]-H^-$  was selected from all options because of its reasonable DBE (DBE = 15) and appropriate MMA (ppm error = -0.41). The structure was elucidated, and the degradation product was concluded to be AB25. In the next chapter, the quantification analysis of this degradation product (AB25) will be performed, and a calibration curve will be further established and validated.

## CHAPTER 7. Quantification of C.I. Reactive Blue 19 Degradation Products from Soil

### 7.1. Introduction

As discussed in Chapter 6, an unknown degradation product (signal of  $m/z$  of 393.0551) found in the degraded soil was characterized and confirmed to be C.I. Acid Blue 25 (AB25) via high-resolution MS and Tandem MS. The next logical step is the quantification of the dye present in soil samples. Generally, an adequate quantification method requires combining an effective analyte extraction method and a sensitive analytical technique [85]. In this study, a quantitation method was established using the QuEChERS method and HPLC-DAD-MS so that it can be applied to quantify and measure the concentration of dyes in soil after simulated compost degradation of RB19 dyed cotton fabrics.

After the establishment of this quantification method, the quantification method was then validated. After evaluation, the quantitation method provided excellent linearity ( $R^2 = 0.9990 \pm 0.0006$ ), accuracy (mean % error =  $5.17 \pm 1.88$ ), precision (mean % CV =  $4.73 \pm 4.16$ ), and sensitivity (lower limit of quantitation LLOQ =  $1.2949 \pm 0.4770 \mu\text{g/mL}$ , lower limit of detection LOD =  $0.3884 \pm 0.1431 \mu\text{g/mL}$ ) for nine concentrations ranging from 0.5 to 40  $\mu\text{g/mL}$ . These parameters were obtained from the inter- and intra-day measurements for both calibration and the quality control sample. Using the calibration curve, the concentrations of the degraded samples extracted from simulated compost degradation of cotton fabrics were measured to be  $1.43 \pm 0.02 \mu\text{g/mL}$  with good precision. Understanding the complex processes governing the biodegradation of reactive dyes in the soil is also the key to solving the contamination problems. The successful development of this quantification method could also deepen the understanding of textile dyes in environmental complex matrices such as soil and benefit future studies of reactive dyes contaminations in soil.

## 7.2. Materials

### 7.2.1. Solvents and Chemicals

Acetonitrile (LC-MS grade, 99.9%) and methanol (LC-MS grade,  $\geq 99.9\%$ ) for QuEChERS extraction were purchased from Sigma-Aldrich (Sigma-Aldrich, MO, USA) and used without any further purification. HPLC grade water was acquired using a Pure Lab Ultra water purification system from ELGA Lab Water (ELGA Lab Water, High Wycombe, UK). Magnesium sulfate (ReagentPlus<sup>®</sup>,  $\geq 99.5\%$ ) was purchased from Sigma-Aldrich, MO, USA.

### 7.2.2. Dyes

Standard C.I. Acid Blue 25 (AB25, CAS no. 6408-78-2, molecular formula  $C_{20}H_{13}N_2NaO_5S$ , molecular weight 416.3828 g/mol, dye purity 45%) was purchased from Sigma-Aldrich, USA. The chemical structure of AB25 is shown in Figure 49.

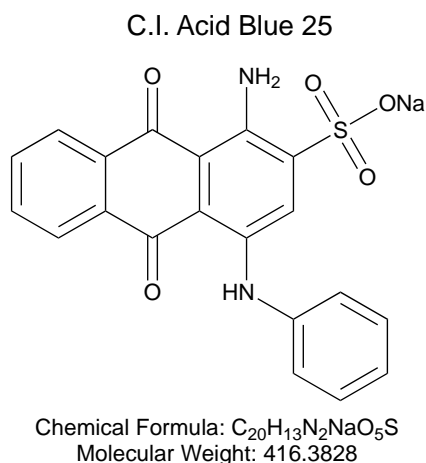


**Figure 49.** Chemical Structure of C.I. Acid Blue 25

### **7.2.3. Other Supplies**

Disposable Luer-slip plastic syringes (1 mL) were purchased from Sigma-Aldrich, MO, USA. PTFE 0.2  $\mu\text{m}$  Non-Sterile Syringe Filters were purchased from Fisher Scientific, PA, USA. Snap-Cap™ Flat-Top Graduated Microcentrifuge Tubes were purchased from Fisher Scientific, PA, USA. 2 mL Amber Glass Screw Vials for HPLC were purchased from Fisher Scientific, PA, USA.

## **7.3. Experimental**

### **7.3.1. Sample Preparation of Stock Solution for Standard AB25 Dye Solutions**

Firstly, the AB25 1000  $\mu\text{g}/\text{mL}$  stock solutions were made from the C.I. Acid Blue 25 powder purchased from Sigma-Aldrich, USA. By diluting the 1000  $\mu\text{g}/\text{mL}$  stock solution, nine different concentrations of solutions were made for further analysis, ranging from 0.5, 0.6, 0.8, 1, 3, 5, 10, 30, to 40  $\mu\text{g}/\text{mL}$ .

### **7.3.2. Extraction of Standard AB25 from Blank Soil Using Modified QuEChERS Extraction**

#### ***Method and Establishment of Calibration Curve***

To establish a calibration system for the RB19 degradation product (AB25), the modified QuEChERS extraction method was used on blank soils spiked with nine different concentrations of AB25 pure dye solutions. After preparing the nine calibration solutions ranging from 0.5 to 40  $\mu\text{g}/\text{mL}$ , 100  $\mu\text{L}$  of spiking solution was spiked into 100 mg of blank soil obtained from Cotton Incorporated (Cary, NC). The spiked soil was extracted following the same modified QuEChERS extraction method (see Figure 50). Unlike the method used in section 5.3.3, every step remains the same except that the dye solution was replaced with standard AB25 instead of RB19. After adding

100  $\mu\text{L}$  AB25 solutions into the centrifuge tube loaded with spiked soil, it was hand mixed, stirred using a VWR vortex mixer for 15 seconds at 2500 rpm, and sonicated for 10 minutes. The 400  $\mu\text{L}$  of QuEChERS extraction mixture composed of HPLC grade methanol and HPLC grade acetonitrile at a ratio of 1:9 and 80 mg of ACS grade magnesium sulfate powder were added into the system. The tube was vortexed and sonicated again before centrifugation using a VWR mini centrifuge for 5 minutes at 8500 rpm. The supernatant liquid was then taken and filtered using a PVDF syringe filter before being analyzed by HPLC-DAD-MS. The quantification trials were performed on a Velos Pro Linear Ion Trap Mass Spectrometer (LTQ-MS) from Thermo Fisher Scientific, PA, USA, where LC-DAD-MS measured all calibration samples and QC samples to create a calibration curve.

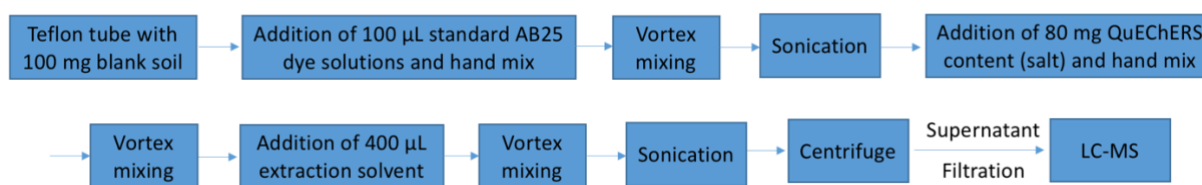


**Figure 50.** Modified QuEChERS Extraction Method SOP for Extraction of AB25 from Blank Soil

### 7.3.3. Method Validation for the Quantification System

Following the calibration system's establishment, this quantification method was then validated by evaluating linearity, sensitivity, accuracy, precision, and recovery rate. To facilitate the calibration curve's reproductivity, the preparation of calibration solutions and quantification were repeated multiple times on the same day (intra-day repeats) and different days (inter-day repeats). Linearity is represented by the coefficient of determination ( $R^2$ ) obtained from intra-day and inter-day repeats. Sensitivity is evaluated by the limit of detection (LOD) and the lowest limit

of quantification (LLOQ). Accuracy is assessed by the mean percent error of calibration standard and QC standard against their nominal concentration from intra-day and inter-day repeats. Precision is evaluated by the mean coefficient of variance (% CV) from the performed replications.

#### ***7.3.4. Instrumentation – Linear Ion Trap MS (LTQ)***

The instrumentation used for further analysis included the Ultimate 3000 UHPLC system from ThermoFisher Scientific with a diode array detector (DAD) and Velos Pro Dual-Pressure Linear Ion Trap mass spectrometer from ThermoFisher Scientific. The DAD device was used to detect any spectral absorption of AB25, and the detection wavelength in the DAD was set to 624 nm based on the maximum absorption wavelength ( $\lambda_{\max}$ ) of AB25. A ZORBAX SB- C18, 3.5  $\mu\text{m}$ , 3.0 x 100 mm reverse-phase HPLC column was used as the stationary phase to separate the dye from the soil matrix. In the linear ion trap MS, the flow rate and injection volume were set to 0.5 mL/min and 2  $\mu\text{L}$ , respectively. The mobile phase was composed of water (solvent A) and acetonitrile (solvent B) via the following gradient elution: holding at 20% solvent B for 1 min during the pre-run, 20-65% solvent B from 0 min to 2 min, and 65-20% solvent B from 2 min to 3 min; the total run time was 3 min. Ionization in the mass spectrometer was conducted via ESI source in negative mode. The parameters from the ESI source were set to the following parameters: heater temperature of 40  $^{\circ}\text{C}$ , sheath gas flow rate of 10 arbitrary (arb.) units, auxiliary gas flow rate of 4 arb, spray voltage of 4000 V, capillary temperature of 350  $^{\circ}\text{C}$ , and S-lens RF level of 68.2%. Except for the supernatant solutions gotten from QuEChERS extraction methods, the pure RB19 dye solutions with the same levels of concentrations were also analyzed using LC-MS.

## 7.4. Results and Discussion

### 7.4.1. Detection of Standard AB25 Dye Solutions using LC-DAD-MS

After confirming the unknown product (AB25) in the degraded soil, the standard AB25 dye solutions were then analyzed. Same to Chapter 5, the detection of standard dye solutions was performed using LC-DAD-MS. The response from DAD and mass spectra for standard AB25 dye solutions (the example of 10  $\mu\text{g/mL}$ ) were shown in Figure 51. As is shown in the mass spectra, the signal ion was detected with  $m/z$  of 393, the same as the structure ( $[\text{M-Na}]^{-1}$ ,  $\text{C}_{20}\text{H}_{13}\text{N}_2\text{O}_5\text{S}^{-}$ ) shown in Figure 51. Even though the linear ion trap MS has a lower mass resolution than the Q-TOF, the pure dye solutions can still be detected without further noise disturbance.

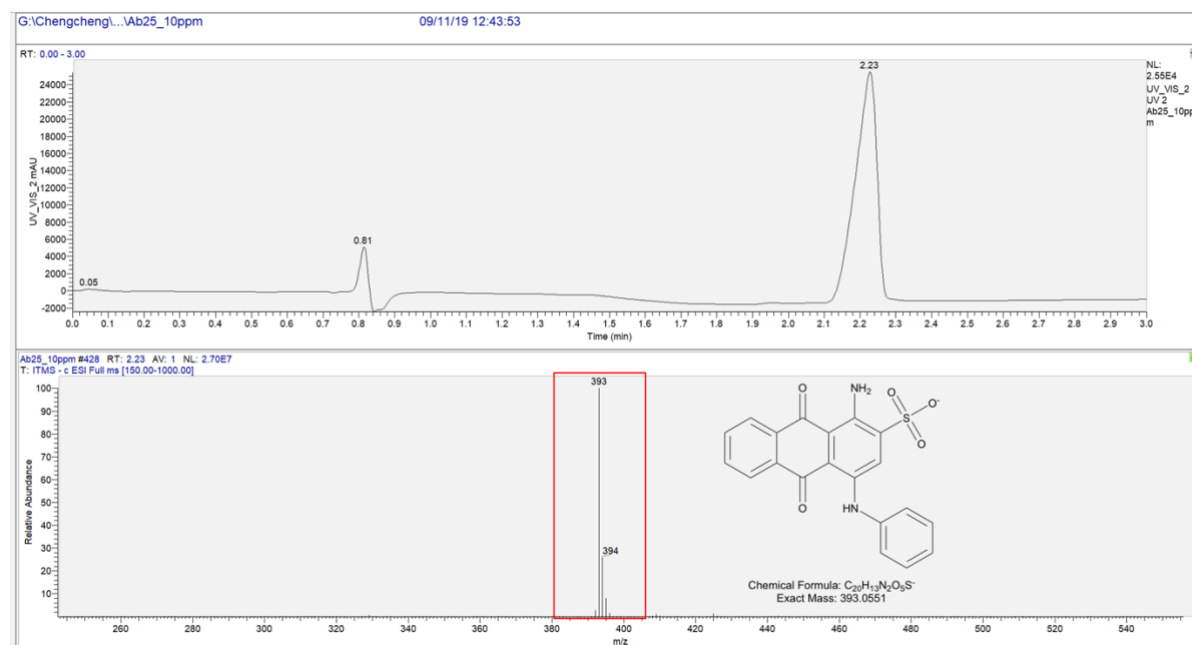


**Figure 51.** Response from DAD and Mass Spectra of Standard AB25 Dye Solutions

The calibration curve represents the ideal Beer-Lambert's Law scenario, where the absorption of the dye solution is directly proportional to the concentration of dye in solution under certain measurement conditions. The quantification of AB25 was achieved down to a concentration of 0.5  $\mu\text{g/mL}$ . A total of nine concentration points were used to build the calibration

curve. These included 0.5, 0.6, 0.8, 1, 3, 5, 10, 30, and 40  $\mu\text{g/mL}$ . Calibration curves were obtained by monitoring the area (mAu unit) under the DAD chromatogram at 624 nm for each concentration of AB25. As is shown in Figure 52, the good linearity (mean coefficient of determination,  $R^2 = 0.9997 \pm 0.0002$ ) of this curve also provides a good starting point for quantification, as the calibration curve in soil was developed based on these dye solutions.

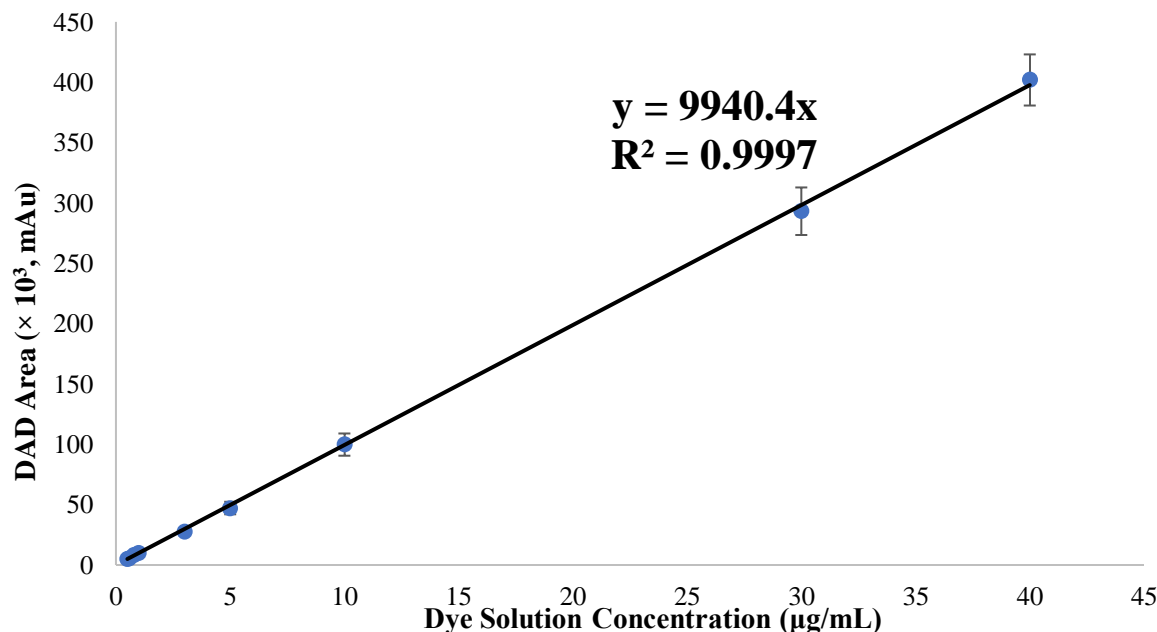


**Figure 52.** Calibration Curve for Standard AB25 Dye Solutions

#### ***7.4.2. Extraction of AB25 from Blank Soil and Establishment of Calibration System***

Then the standard AB25 dye solutions were used for extractions from blank soils using the same SOP (see Figure 50). Same concentrations to section 7.4.1, ranging from 0.5, 0.6, 0.8, 1, 3, 5, 10, 30, to 40  $\mu\text{g/mL}$ , were used for the QuEChERS extraction analysis from blank soils. The DAD response and mass spectra (relative abundance vs.  $m/z$ ) for AB25 extracted from blank soils are shown in Figure 53.

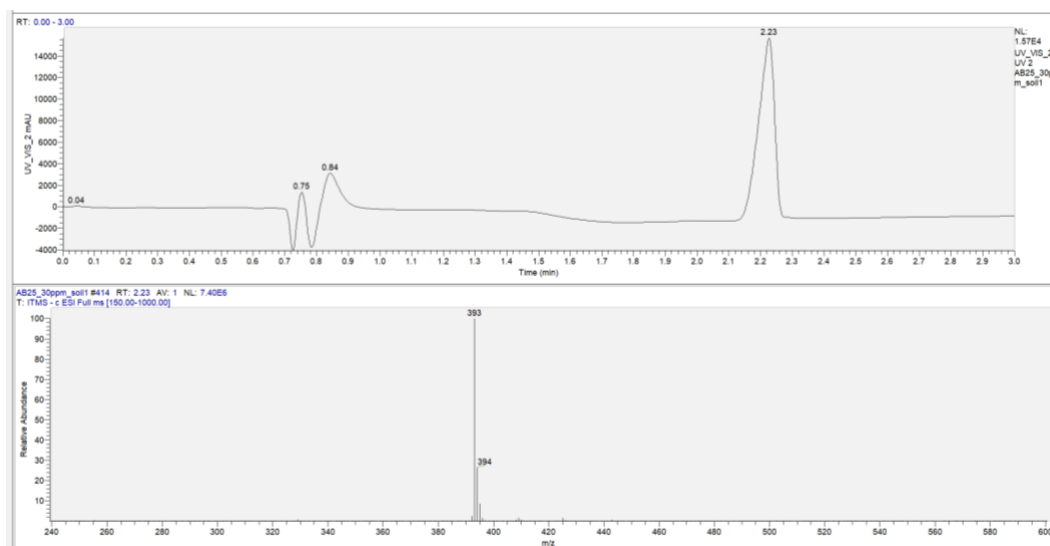


**Figure 53.** Response from DAD and Mass Spectra of AB25 Extracted from Blank Soil

By evaluating the relationship between dye concentrations and DAD area (mAu unit) under DAD chromatogram at 624 nm, the calibration curve obtained from soil extraction samples can be summarized in Figure 54 (red line). As is shown in this plot, the linearity of the AB25 calibration curve obtained from the samples in 90-day degraded soil showed is almost as good as the calibration curve obtained from the pure dye solutions. In addition, the RT for all runs (mean  $\pm$  SD) is  $2.22 \pm 0.02$  min, which also indicates that this method is stable and reliable for both intraday and inter-day trials.

### 7.4.3. Validation of Calibration Curve

The average value of the recovery rate was also calculated to be  $18.0390 \pm 0.0076\%$  by comparing the average DAD areas (mAu unit) observed in pure AB25 standard dye solutions (blue line in Figure 54), and AB25 extracted from blank soils (red line in Figure 54).

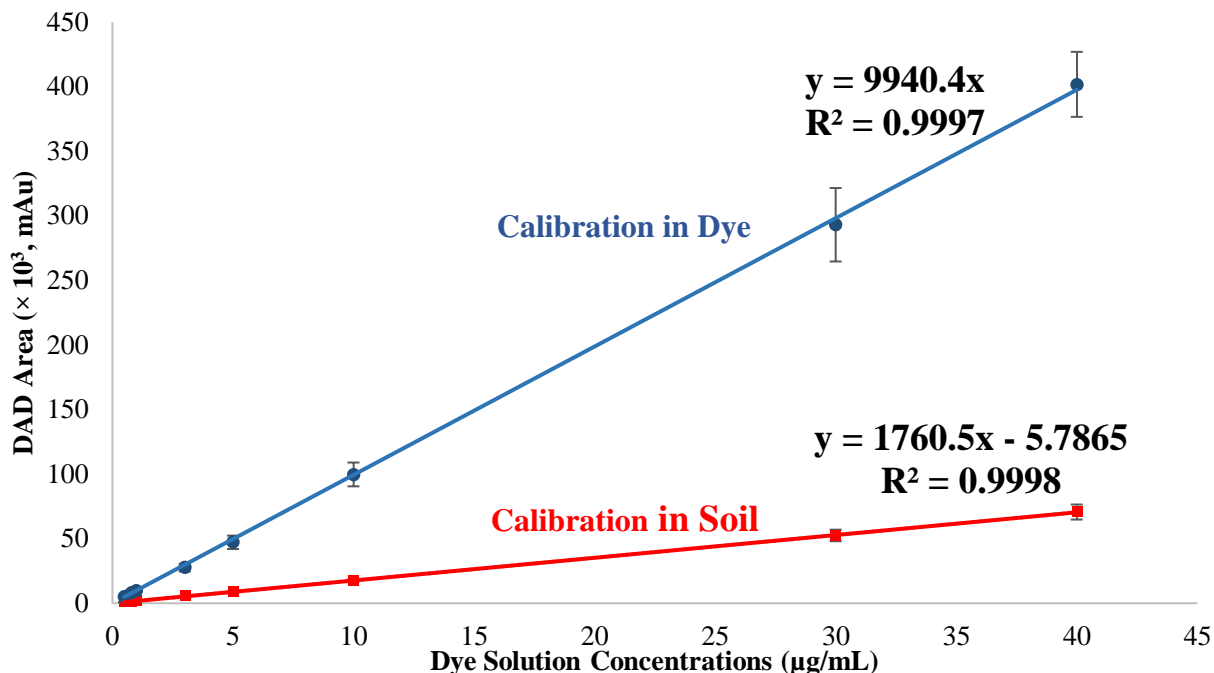


**Figure 54.** The Linearity Assessments for Quantitative Analysis of Pure AB25 Standard Dye Solutions (blue line) and AB25 Extracted from Blank Soils (red line), respectively, via LC-DAD-MS. Each point in the calibration curve shows the average across all runs (n=9).

Nine linear regression models were generated in Table 16, which summarized the linear calibration data obtained from MS/MS quantification, and the mean coefficient of determination ( $R^2$ ) was  $0.9990 \pm 0.0006$  with high linearity. This value also suggests that under these experimental conditions, the dye concentrations' change is highly proportional to the DAD area.

**Table 16.** Linear Regression Data from MS/MS Calibration Curves for AB25 Extracted from Blank Soils

<b>Trials</b>	<b>R<sup>2</sup></b>
<b>Day 1</b>	0.9982
	0.9994
	0.9991
<b>Day 2</b>	0.9989
	0.9989
	0.9997
<b>Day 3</b>	0.9994
	0.9979
	0.9994
<b>Mean Value</b>	0.9990
<b>Standard Error</b>	0.0006

Except for linearity, the method was further evaluated based on sensitivity, accuracy, and precision. The summary of validation parameters obtained from both intra-day and inter-day repeats are shown in Table 17. Sensitivity was assessed by evaluating the average limit-of-detection (LOD) and lower limit-of-quantification (LLOQ), in which they were calculated using the following equations:  $LOD = 3 \times SD / b$  and  $LLOQ = 10 \times SD / b$ . SD is the standard deviation of the response, which can be estimated by the standard deviation of the y-intercepts of the regression line, and b is the slope of the calibration curve [81]. Based on the two equations, the LLOQ of this quantification method was determined to be  $1.2949 \pm 0.4770 \mu\text{g/mL}$ , and LOD was determined to be  $0.3884 \pm 0.1431 \mu\text{g/mL}$  for all repeats.

**Table 17.** Summary of Validation Parameters on AB25 QuEChERS Quantification Method

<b>Validation Parameters</b>	<b>Average <math>\pm</math> SD</b>
<b>Linearity (<math>R^2</math>)</b>	0.9990 $\pm$ 0.0006
<b>LOD (<math>\mu\text{g/mL}</math>)</b>	0.3884 $\pm$ 0.1431
<b>LLOQ (<math>\mu\text{g/mL}</math>)</b>	1.2949 $\pm$ 0.4770
<b>Accuracy (mean % error)</b>	
<b>Intra-day</b>	4.26 $\pm$ 3.57
<b>Inter-day</b>	5.17 $\pm$ 1.88
<b>Precision (mean % CV)</b>	
<b>Intra-day</b>	6.36 $\pm$ 3.80
<b>Inter-day</b>	4.73 $\pm$ 4.16

SD, standard, linearity, LOD, and LLOQ were the averages across all runs; accuracy and precision data are noted as the average across all quantitation standards.

Experiments were repeated in triplicate on three non-consecutive days. Accuracy and precision were assessed across one day (intra-day) and three days (inter-day), except for evaluating the linearity and sensitivity. The results for both intra-day and inter-day are summarized in Table 18. Precision was assessed based on variations across runs and reported as the coefficient of variation in percentage (% CV). Accuracy was evaluated by comparing experimental values to theoretical values and reported as percent error (% error).

Both precision and accuracy were within the acceptable range  $\pm 12\%$  for all concentrations. For precision, lower concentrations (0.5, 0.6, 0.8, and 1  $\mu\text{g/mL}$ , around LLOQ) showed a relatively high % CV, but still lower than a threshold of 12%; and the % CV for higher concentrations was much lower. In terms of accuracy, all quantification standards showed a % error lower than 9%; also, the % error was lower than 2% for higher concentrations (3, 5, 10, 30, and 40  $\mu\text{g/mL}$ ),

suggesting that this quantification method has good accuracy and consistency. The lower precision and accuracy at high concentrations could be explained that measurements at lower concentrations are more susceptible to instrumental fluctuation and errors from QuEChERS extractions.

**Table 18.** Results of Intra-day and Inter-day Accuracy and Precision of Each Concentration Point of Standard AB25 Dye Solutions Evaluated by the LC-DAD-MS Method

Concentrations ( $\mu\text{g/mL}$ )	Intra-day		Inter-day	
	Precision	Accuracy	Precision	Accuracy
	(% CV)	(% error)	(% CV)	(% error)
<b>0.5</b>	6.44	0.29 (0.50 $\mu\text{g/mL}$ )	11.24	-3.96 (0.48 $\mu\text{g/mL}$ )
<b>0.6</b>	10.77	2.10 (0.61 $\mu\text{g/mL}$ )	0.15	8.33 (0.65 $\mu\text{g/mL}$ )
<b>0.8</b>	8.41	-1.12 (0.79 $\mu\text{g/mL}$ )	3.22	6.25 (0.84 $\mu\text{g/mL}$ )
<b>1</b>	6.39	3.36 (1.03 $\mu\text{g/mL}$ )	11.67	-0.24 (0.99 $\mu\text{g/mL}$ )
<b>3</b>	4.06	0.64 (3.01 $\mu\text{g/mL}$ )	7.29	1.60 (3.04 $\mu\text{g/mL}$ )
<b>5</b>	2.21	-0.96 (4.95 $\mu\text{g/mL}$ )	5.68	1.58 (5.07 $\mu\text{g/mL}$ )
<b>10</b>	6.23	-1.91 (9.80 $\mu\text{g/mL}$ )	2.65	0.63 (10.06 $\mu\text{g/mL}$ )
<b>30</b>	3.80	-0.47 (29.85 $\mu\text{g/mL}$ )	0.78	-0.51 (29.84 $\mu\text{g/mL}$ )
<b>40</b>	2.14	-0.14 (39.94 $\mu\text{g/mL}$ )	0.48	0.05 (40.02 $\mu\text{g/mL}$ )

Values reported with two decimal points; CV, coefficient of variation.

After validating the quantification method, it can be concluded that the method is successful and can be applied for the quantification of the unknown product from the biodegraded soil samples. Based on the calibration curve (red line in Figure 54, equation  $y = 1760.5x - 5.7865$ ), the concentration of original RB19 on 90-day biodegraded fabrics was determined to be  $1.43 \pm$

0.02  $\mu\text{g/mL}$ . Furthermore, the measured concentration is higher than LLOQ and three times higher than LOD. It is obvious the degradation has happened in this study.

## 7.5. Summary

The quantification study of RB19 degradation product in soil has never been studied in previous studies. As the pioneer, to solve this problem, a novel analytical measurement method based on tandem mass spectrometry and modified QuEChERS extraction was successfully developed to quantify the concentration of degradation product in soil. The modified QuEChERS extraction method was also proven useful in the extraction of AB25 from blank soils.

After building the calibration curve, method validation was performed where the accuracy and precision of this method were evaluated based on intra-day and inter-day repeats. The average value of the recovery rate was also calculated to be  $18.0390 \pm 0.0076\%$ . Besides, by performing intraday and inter-day repetitions, the quantification method based on LC-DAD-MS showed excellent linearity ( $R^2 > 0.9990$ ), good accuracy (mean % error less than 12%), good precision (mean % CV less than 9%), good sensitivity (the LLOQ of this quantification method was  $1.2949 \pm 0.4770 \mu\text{g/mL}$  and LOD was  $0.3884 \pm 0.1431 \mu\text{g/mL}$ ), and good recovery rate. Furthermore, based on the calibration curve (red line Figure 54, equation  $y = 1760.5x - 5.7865$ ), the concentration of original RB19 on 90-day biodegraded fabrics was determined to be  $1.43 \pm 0.02 \mu\text{g/mL}$ .

This quantification method would greatly benefit both the textile and environmental fields as the combination of QuEChERS extraction and LC-DAD-MS quantification provides an accurate and precise measurement of RB19 degradation product (AB25) quantification in soil.

## CHAPTER 8. Conclusion and Future Aspects

### 8.1. Conclusions

In this dissertation, a QuEChERS method, developed initially to extract pesticides from fruits and vegetables, was modified to extract reactive dyes from the soil. In this research, RB19 was chosen as the subject. Due to the complexity of soils, there are many aspects needed to be considered in the modifications of the extraction method, including QuEChERS content (salt), extraction solvent, and agitation modes. After developing the new extraction method, the extraction of RB19 from blank soil was performed using the modified QuEChERS method and LC-MS.

To understand how the cotton fabrics and reactive dyes that we usually use in daily life can become sources of pollution to nature and the fundamentals of what is happening, a simulated compost soil degradation was then performed on RB19 dyed cotton fabrics for 90 days. The modified QuEChERS method was applied on the degraded soil to detect and elucidate RB19 degradation product in soil via LC-MS/MS approach. The structural elucidation of an RB19 degradation product from soil was confirmed to be AB25 using qualitative and quantitative tandem mass spectrometry.

After the elucidation of the unknown degradation product, a quantification method was developed to measure the concentration of this degradation product in soil using LC-DAD-MS. After the establishment of this quantification method, it was then validated and the results suggested that it has very good linearity ( $R^2 > 0.9990$ ), good accuracy (mean % error less than 12%), good precision (mean % CV less than 9%), good sensitivity (the LLOQ of this quantification method was  $1.2949 \pm 0.4770 \mu\text{g/mL}$  and LOD was  $0.3884 \pm 0.1431 \mu\text{g/mL}$ ) and satisfying recovery rate. Also, the RB19 degradation product (AB25) concentration extracted from the

degraded soil was confirmed to be  $1.43 \pm 0.02 \mu\text{g/mL}$ , which is higher than LLOQ and 3 times higher than LOD. Because these chemicals from those unwanted disposed textiles could also be leaching out and degraded under the soils' decomposition process, the established calibration curve could potentially give an idea to both academia and the textile industry. More work still to be conducted to understand the fundamentals of the degradation of these chemicals in soils.

## **8.2. Recommendations for Future Works**

In this soil degradation study, the finishing on the cotton fabrics was applied for RB19 dyeing only; but both finishing and dyes are commonly used for cotton fabrics in a real scenario. In future steps, it is necessary to study the degradation of cotton fabrics with reactive dyes and finishing in soil and investigate their interactions with each other during the degradation process. Additionally, the toxicity should be evaluated on the obtained fabrics and soil from the simulated degradation processes.

In another aspect, being as a commonly used tool for the biological tissue imaging analysis, desorption electrospray ionization (DESI) can also be a strong tool for the study of the textile surfaces, such as the comparison between degraded and undegraded samples, especially the cotton fabrics samples after degradation process of soil, water, or light.

## REFERENCES

- [1] T Townsend, Natural Fibres and the World Economy, July 2019. <https://news.bio-based.eu/natural-fibres-and-the-world-economy-july-2019/>. Accessed July 20, 2020.
- [2] NN Mahapatra, *Textile dyes*, Woodhead Publishing India, New Delhi; Boca Raton, FL, 2016.
- [3] C Pearce. The removal of colour from textile wastewater using whole bacterial cells: a review, *Dyes and Pigments*. 58 (2003) 179-196.
- [4] W EPOLITO, Y LEE, L BOTTOMLEY, S PAVLOSTATHIS. Characterization of the textile anthraquinone dye Reactive Blue 4, *Dyes and Pigments*. 67 (2005) 35-46.
- [5] Grass Graham, Australia recycles paper and plastics. So why does clothing end up in landfill? (2019). <https://www.theguardian.com/commentisfree/2019/aug/27/australia-recycles-paper-and-plastics-so-why-does-clothing-end-up-in-landfill>. Accessed July 20, 2020.
- [6] United States Environmental Protection Agency – EPA. Textiles: Material-Specific Data, 2017. <https://www.epa.gov/facts-and-figures-about-materials-waste-and-recycling/textiles-material-specific-data>. Accessed October 15, 2019.
- [7] K Arshad, M Skrifvars, V Vivod, J Valh, B Voncina. Biodegradation of natural textile materials in soil, *Tekstilec*. 57 (2014) 118–132
- [8] JM Hawley. Digging for Diamonds: A Conceptual Framework for Understanding Reclaimed Textile Products, *Clothing and Textiles Research Journal*. 24 (2006) 262-275.
- [9] H Ali. Biodegradation of Synthetic Dyes—A Review, *Water, Air, & Soil Pollution*. 213 (2010) 251-273.
- [10] S Khan, A Malik. Toxicity evaluation of textile effluents and role of native soil bacterium in biodegradation of a textile dye, *Environmental Science and Pollution Research*. 25 (2018) 4446-4458.
- [11] CH Arnaud. Mass Spec’s Century of Change, *Chemical & Engineering News*. 91 (2013) 30-31.
- [12] I Falconer. Corpuscles, Electrons and Cathode Rays: J. J. Thomson and the 'Discovery of the Electron', *The British Journal for the History of Science*. 20 (1987) 241-276.
- [13] J Griffiths. A Brief History of Mass Spectrometry, *Analytical Chemistry*. 80 (2008) 5678-5683.
- [14] C Dass, *Fundamentals of contemporary mass spectrometry*, John Wiley & Sons 2007.

- [15] M Guilhaus. Principles and Instrumentation in Time-of-flight Mass Spectrometry - Physical and Instrumental Concepts, *Journal of Mass Spectrometry*. 30 (1995) 1519-1532.
- [16] JH Gross. Chhabil Dass: Fundamentals of contemporary mass spectrometry, *Analytical and Bioanalytical Chemistry*. 389 (2007) 675-676.
- [17] M Tswett. Physikalisch-chemische Studien über das chlorophyll. Die Adsorptionen, *Berichte der Deutschen botanischen Gesellschaft*. 24 (1906) 20.
- [18] MH Abraham. 100 years of chromatography—or is it 171? *Journal of Chromatography A*. 1061 (2004) 113-114.
- [19] B Boyd, C Basic, R Bethem, *Trace quantitative analysis by mass spectrometry*, 1. Aufl.; 1st ed., John Wiley & Sons, Hoboken, N.J; Chichester, West Sussex, England, 2008.
- [20] LS Ettre. Csaba Horvath and the development of the first modern high performance liquid chromatograph, *LC GC North America*. 23 (2005) 486.
- [21] K Shoykhet, K Broeckhoven, MW Dong. Modern HPLC Pumps: Perspectives, Principles, and Practices, *LC GC North America*. 37 (2019) 384.
- [22] WF Ho, B Stuart, ER Prichard, *High performance liquid chromatography*, Royal Society of Chemistry, Cambridge, 2003.
- [23] J Mizell, Diode-Array Detection can be used to identify unknown peaks observed in chromatography. <https://www.metricscontractservices.com/resource/diode-array-detection-used-to-identify-peaks-in-chromatography/>. Accessed July 20, 2020.
- [24] Principle and Feature of Various Detection Methods - Diode Array Detector. <https://www.hitachi-hightech.com/global/products/science/tech/ana/lc/basic/course7.html>. Accessed July 20, 2020.
- [25] M Dole, LL Mack, RL Hines, RC Mobley, LD Ferguson, MB Alice. Molecular beams of macroions, *The Journal of Chemical Physics*. 49 (1968) 2240-2249.
- [26] C Barner-Kowollik, C Barner-Kowollik, T Gruending, J Falkenhagen, S Weidner, *Mass Spectrometry in Polymer Chemistry*, Wiley-VCH, DE, 2012.
- [27] RB Cole, *Electrospray and MALDI mass spectrometry: fundamentals, instrumentation, practicalities, and biological applications*, John Wiley & Sons 2011.
- [28] P Kebarle, UH Verkerk. Electrospray: From ions in solution to ions in the gas phase, what we know now, *Mass Spectrometry Reviews*. 28 (2009) 898-917.

- [29] KK Murray, RK Boyd, MN Eberlin, GJ Langley, L Li, Y Naito. Definitions of terms relating to mass spectrometry (IUPAC Recommendations 2013), *Pure and Applied Chemistry*. 85 (2013) 1515-1609.
- [30] C Barner-Kowollik editor, *Mass spectrometry in polymer chemistry*, Wiley-VCH, Weinheim, 2011.
- [31] WE Stephens. A Pulsed Mass Spectrometer with Time Dispersion, *Physical Review*. 69 (1946) 691.
- [32] RJ Cotter. Time-of-Flight Mass Spectrometry for the Structural Analysis of Biological Molecules, *Analytical Chemistry*. 64 (1992) A1027-A1039.
- [33] BA Mamyrin. Laser assisted reflectron time-of-flight mass spectrometry, *International Journal of Mass Spectrometry and Ion Processes*. 131 (1994) 1-19.
- [34] J Dawson, M Guilhaus. Orthogonal-acceleration time-of-flight mass spectrometer, *Rapid communications in Mass Spectrometry*. 3 (1989) 155-159.
- [35] IV Chernushevich, AV Loboda, BA Thomson. An introduction to quadrupole–time-of-flight mass spectrometry, *Journal of Mass Spectrometry*. 36 (2001) 849-865.
- [36] I Lavagnini, I NetLibrary, *Quantitative applications of mass spectrometry*, 1. Aufl. ed., John Wiley, Chichester, England; Hoboken, NJ, 2006.
- [37] L Sleno, DA Volmer. Ion activation methods for tandem mass spectrometry, *Journal of Mass Spectrometry*. 39 (2004) 1091-1112.
- [38] A Westman-Brinkmalm, G Brinkmalm, *Tandem Mass Spectrometry*, John Wiley & Sons, Inc, Hoboken, NJ, USA, 2008, pp. 89-103.
- [39] DJ Douglas, AJ Frank, D Mao. Linear ion traps in mass spectrometry, *Mass Spectrometry Reviews*. 24 (2005) 1-29.
- [40] RE March, JFJ Todd, *Quadrupole ion trap mass spectrometry*, J. Wiley, Hoboken, N.J, 2005.
- [41] WE Morton, JWS Hearle, *Physical properties of textile fibres*, 4th ed., Woodhead Publishing in association with the Textile Institute, Boca Raton, FL; Cambridge, England, 2008.
- [42] RM Kozlowski, *Handbook of natural fibres: types, properties and factors affecting breeding and cultivation / Volumes 1*, Woodhead Publishing, Cambridge, England, 2012.
- [43] RM Christie, *Colour chemistry*, Royal Society of Chemistry, Cambridge, England, 2015.
- [44] RS Blackburn, *Biodegradable and sustainable fibres*, Woodhead Pub. in association with the Textile Institute, Boca Raton; Cambridge, England, 2005.

- [45] RR Mather, RH Wardman author, *The chemistry of textile fibres*, Royal Society of Chemistry, Cambridge, 2015.
- [46] T Kamppuri, M Vehviläinen, A Puolakka, M Honkanen, M Vippola, M Rissanen. Characterisation of novel regenerated cellulosic, viscose, and cotton fibres and the dyeing properties of fabrics, *Coloration Technology*. 131 (2015) 396-402.
- [47] A Gürses, Metin Açıkyıldız, Kübra Güneş, M. Sadi Gürses, *Dyes and pigments*, Cham, Switzerland: Springer, 2016.
- [48] USE and ASSESSMENT OF MARKER DYES USED WITH HERBICIDES, (1997). [https://www.fs.fed.us/foresthealth/pesticide/pdfs/091602\\_markerdyes.pdf](https://www.fs.fed.us/foresthealth/pesticide/pdfs/091602_markerdyes.pdf). Accessed July 20, 2020.
- [49] Zollinger Heinrich, *Color chemistry : syntheses, properties, and applications of organic dyes and pigments*, 3rd ed., Zürich: Verlag Helvetica Chimica Acta; Weinheim: Wiley-VCH 2003.
- [50] S Fujioka, S Abeta. Development of novel reactive dyes with a mixed bifunctional reactive system, *Dyes and Pigments*. 3 (1982) 281-294.
- [51] CR Holkar, H Arora, D Halder, DV Pinjari. Biodegradation of reactive blue 19 with simultaneous electricity generation by the newly isolated electrogenic *Klebsiella* sp. C NCIM 5546 bacterium in a microbial fuel cell, *International Biodeterioration & Biodegradation*. 133 (2018) 194-201.
- [52] DM Lewis. Developments in the chemistry of reactive dyes and their application processes, *Coloration technology*. 130 (2014) 382-412.
- [53] SR Camp, PE Sturrock. The identification of the derivatives of CI Reactive Blue 19 in textile wastewater, *Water Research*. 24 (1990) 1275-1278.
- [54] ID Rattee. Reactive dyes in the coloration of cellulosic materials, *Journal of the Society of Dyers and Colourists*. 85 (1969) 23-31.
- [55] CB Aakeröy, KR Seddon. The hydrogen bond and crystal engineering, *Chemical Society Reviews*. 22 (1993) 397-407.
- [56] AHM Renfrew, *Reactive dyes for textile fibres: the chemistry of activated [pi]-bonds as reactive groups and miscellaneous topics*, Society of Dyers and Colourists, Bradford, 1999.
- [57] HL Bohn, BL McNeal, GA O'Connor, *Soil chemistry*, 3rd ed., Wiley, New York, 2001.
- [58] J Vera, L Correia-Sá, P Paíga, I Bragança, VC Fernandes, VF Domingues, et al. QuEChERS and soil analysis. An Overview. *Sample Preparation*. 1 (2013) 54-77.

- [59] EC Brevik, LC Burgess, *Soils and human health*, CRC Press 2012.
- [60] M Imran, B Shaharoon, DE Crowley, A Khalid, S Hussain, M Arshad. The stability of textile azo dyes in soil and their impact on microbial phospholipid fatty acid profiles, *Ecotoxicology and Environmental Safety*. 120 (2015) 163-168.
- [61] R Chandrappa, DB Das, *Solid Waste and Livelihood*, Springer Berlin Heidelberg, Berlin, Heidelberg, 2012, pp. 373-387.
- [62] LC Burgess. Organic pollutants in soil, *Soils and human health*. (2013) 83-106.
- [63] L Lu, M Zhao, S Liang, L Zhao, D Li, B Zhang. Production and synthetic dyes decolourization capacity of a recombinant laccase from *Pichia pastoris*, *Journal of Applied Microbiology*. 107 (2009) 1149-1156.
- [64] I Montes, C Lai, D Sanabria. Like Dissolves Like: A Guided Inquiry Experiment for Organic Chemistry, *Journal of Chemical Education*. 80 (2003) 447.
- [65] SJ Lehotay, FJ Schenck, *MULTIRESIDUE METHODS: EXTRACTION*, in: Wilson ID (Ed.), *Encyclopedia of Separation Science*, Academic Press, Oxford, 2000, pp. 3409-3415.
- [66] M Gharehbaghi, F Shemirani. A Novel Method for Dye Removal: Ionic Liquid-Based Dispersive Liquid-Liquid Extraction (IL-DLLE), *Clean : soil, air, water*. 40 (2012) 290-297.
- [67] R Vijayaraghavan, N Vedaraman, M Surianarayanan, DR MacFarlane. Extraction and recovery of azo dyes into an ionic liquid, *Talanta (Oxford)*. 69 (2006) 1059-1062.
- [68] M Hennion. Solid-phase extraction: method development, sorbents, and coupling with liquid chromatography, *Journal of Chromatography A*. 856 (1999) 3-54.
- [69] DA Wells, *Solid-Phase Extraction with Cartridges*, *Reference Module in Chemistry, Molecular Sciences and Chemical Engineering*, Elsevier, 2013.
- [70] S Büyüktiryaki, R Keçili, CM Hussain. Functionalized nanomaterials in dispersive solid phase extraction: Advances & prospects, *TrAC, Trends in analytical chemistry*. 127 (2020) 115893.
- [71] M Anastassiades, SJ Lehotay, D Štajnbaher, FJ Schenck. Fast and easy multiresidue method employing acetonitrile extraction/partitioning and “dispersive solid-phase extraction” for the determination of pesticide residues in produce, *Journal of AOAC International*. 86 (2003) 412-431.
- [72] X Sui, C Feng, Y Chen, N Sultana, M Ankeny, NR Vinueza. Detection of Reactive Dyes from Dyed Fabrics after soil degradation via QuEChERS extraction and Mass Spectrometry, *Analytical Methods*. 12 (2020) 179-187.

- [73] P Payá, M Anastassiades, D Mack, I Sigalova, B Tasdelen, J Oliva, et al. Analysis of pesticide residues using the Quick Easy Cheap Effective Rugged and Safe (QuEChERS) pesticide multiresidue method in combination with gas and liquid chromatography and tandem mass spectrometric detection, *Analytical and Bioanalytical Chemistry*. 389 (2007) 1697-1714.
- [74] V Giaccone, G Cammilleri, A Macaluso, N Cicero, A Pulvirenti, A Vella, et al. A LC-HRMS After QuEChERS cleanup method for the rapid determination of dye residues in fish products, *Food analytical methods*. 11 (2018) 625-634.
- [75] JK Adjei, V Ahormegah, AK Boateng, HK Megbenu, S Owusu. *Fast, easy, cheap, robust and safe method of analysis of Sudan dyes in chilli pepper powder*, *Heliyon*. 6 (2020) e05243.
- [76] PubChem Compound Summary for CID 17409, *Reactive Blue 19*. 2021.
- [77] PubChem Compound Summary for CID 3039, *Dichlorvos*. 2021.
- [78] I Bragança, A Plácido, P Paíga, VF Domingues, C Delerue-Matos. QuEChERS: A new sample preparation approach for the determination of ibuprofen and its metabolites in soils, *Science of the Total Environment*. 433 (2012) 281-289.
- [79] L Chen, X Li, Z Wang, C Pan, R Jin. Residue dynamics of procymidone in leeks and soil in greenhouses by smoke generator application, *Ecotoxicology and Environmental Safety*. 73 (2010) 73-77.
- [80] A Shrivastava, VB Gupta. Methods for the determination of limit of detection and limit of quantitation of the analytical methods, *Chronicles of young scientists*. 2 (2011) 21.
- [81] C Feng, N Sultana, X Sui, Y Chen, E Brooks, MA Ankeny, et al. High-Resolution Mass Spectrometry Analysis of Reactive Dye Derivatives Removed from Biodegraded Dyed Cotton by Chemical and Enzymatic Methods, *AATCC Journal of Research*. 7 (2020) 9-18.
- [82] ASTM International. *D5988-18 Standard Test Method for Determining Aerobic Biodegradation of Plastic Materials in Soil*. West Conshohocken, PA; ASTM International, 2018.
- [83] N Sultana, K Williams, M Ankeny, NR Vinueza. Degradation studies of CI Reactive Blue 19 on biodegraded cellulosic fabrics via liquid chromatography-photodiode array detection coupled to high resolution mass spectrometry, *Coloration Technology*. (2019) 475-483.
- [84] C Feng, X Sui, MA Ankeny, NR Vinueza. Identification and quantification of CI Reactive Blue 19 dye degradation product in soil, *Coloration Technology*. (2021).